

**AN EXPERIMENTAL STUDY OF ALUMINUM BORIDE PARTICLES
DISTRIBUTION IN CENTRIFUGALLY CAST Al/AIB_x COMPOSITES**

By
Tunde Kingsley Adelakin

A thesis submitted in partial fulfillment of the requirements for the degree of

MASTER OF SCIENCE
In
MECHANICAL ENGINEERING

UNIVERSITY OF PUERTO RICO, MAYAGÜEZ CAMPUS
2009

Approved by:

Oscar Marcelo Suárez, PhD
President, Graduate Committee

Date

Gustavo Gutiérrez, PhD
Member, Graduate Committee

Date

Ricky Valentín, PhD
Member, Graduate Committee

Date

Paul Castillo, PhD
Representative of Graduate Studies

Date

Pablo Caceres, PhD
Chairperson of the Department

Date

ABSTRACT

In this research, centrifugal casting has been used to investigate the influence of casting parameters and chemical composition on the manufacturing of functionally graded Al-2 wt. %B-6 wt. %Mg and Al-2 wt. %B-6 wt. %Cu composites reinforced with aluminum boride particles. The resulting microstructure of the cast specimens were characterized both quantitatively and qualitatively via image J analysis to study the distribution of the reinforcement particles. An evaluation of the composite hardness was also conducted through the use of superficial Rockwell hardness and Vickers microhardness.

The microstructure analysis revealed the strong effect of varying centrifugal casting parameters on the redistribution of the reinforcement particles along the cylindrical casting axis, which was parallel to the centrifugal force. This distribution resulted in a compositional gradient of particles, with more particles towards the external zone than in the internal zone of the casting. The hardness analysis also reflects this tendency: higher superficial Rockwell hardness and a higher Vickers microhardness values towards the external zone.

Alloying elements Mg and Cu favored good wettability between the reinforcement particles and the aluminum matrix melt. This reduced the pores formation in the composites to a very little quantity, i.e. between the ranges of 0.01% to 2%. The presence of magnesium favored the partial transformation of AlB_{12} particles into AlB_2 in the Al-2 wt. %B-6 wt. %Mg composites. SEM/EDS analysis helped study the interaction of magnesium and copper levels on the reinforcement particles.

RESUMEN

En esta investigación, la fundición por centrifugado ha sido usada para investigar la influencia de los parámetros de fundición y composición química en la fabricación de compuestos reforzados con partículas de boruro de aluminio con gradiente funcional de Al-2 wt. %B-6 wt. %Mg y Al-2 wt. %B-6 wt. %Cu. La tanto microestructura resultante de los especímenes fundidos fueron caracterizados cuantitativamente como cualitativamente a través de análisis de imágenes usando image J para estudiar la distribución de los refuerzos. La evaluación de la dureza de los compuesto fue llevada a cabo por medio de dureza superficial Rockwell y microdureza Vickers.

El análisis microestructura reveló el gran efecto de los parámetros de la fundición por centrifugado sobre la redistribución de los refuerzo particulados a lo largo del eje de muestra fundida, paralelo a la fuerza centrífuga. Esta distribución resultó en un gradiente de composición de partículas, con más refuerzos en la zona externa que en la zona interna de la muestra fundida. El análisis de dureza también reflejó esta tendencia: valores más altos de dureza Rockwell y microdureza Vickers en la zona externa de los especímenes.

Los elementos de aleación Mg y Cu favorecieron la buena mojabilidad entre la interfase de los refuerzos y la matriz fundida de aluminio. Esto redujo la formación de poros en los compuestos hasta una cantidad muy pequeña: esto es en el rango de 0.01% a 2%. La presencia de magnesio favoreció la transformación parcial de las partículas de AlB_{12} en AlB_2 en los materiales compuestos de Al- 2%B- 6%Mg. Los análisis de SEM/EDS ayudaron a estudiar la interacción de los niveles de magnesio y cobre con las partículas de refuerzos.

DEDICATION

Dedicated to God almighty, my Beloved parents, Captain Remi Adelakin and Mrs. Virginia Adelakin, family members, Dr. Oscar Marcelo Suárez, Dr. Oswald Uwakweh's family and friends whose constant prayers, sacrifice and inspiration led to this wonderful accomplishment.

ACKNOWLEDGMENTS

I wish to give my sincere appreciation and thanks to my supervisor, Dr. O. Marcelo Suárez who contributed greatly to the success of this thesis and also took time off his busy schedule to go through the work and give useful suggestions. I am grateful to my thesis committee members, Dr. Gustavo Gutiérrez, Dr. Ricky Valentin for their helpful criticism.

Also my appreciation goes to professors Paul Sundaram, Oswald Uwakweh, Carlos Rinaldi, and Jeanette Santos from the College of Engineering of the University of Puerto Rico, Mayaguez. I would like to thank the staff of the Chemical Analysis section of Hewlett-Packard, and Dr. Esteban Fachini (University of Puerto Rico – Río Piedras) for their assistance in the course of the analysis of my samples.

My gratitude goes to Mr. Hermes Calderón, graduate student of Civil Engineering, Héctor Rodríguez, Lyllibeth Acosta, Alexis Torres, Riquelme Mendoza, and José Vázquez, Mechanical Engineering undergraduate students, and Ronald Carrasquillo and Jennifer Acosta, Chemical Engineering undergraduate students, for their unconditional support at various stages of this thesis. I am also grateful to Mr. Humberto Melgarejo, a PhD student at the University of Wisconsin Madison, for his assistance in my research.

Puerto Rico EPSCoR and the National Science Foundation (NSF) under Grant No. 0351449 provided the funding and the resources for the development of this research. Finally, I thank God Almighty for His Guidance, protection, inspiration and encouragement rendered to me throughout my stay in this University.

TABLE OF CONTENTS

ABSTRACT	II
RESUMEN	III
DEDICATION	IV
ACKNOWLEDGMENTS	V
TABLE OF CONTENTS	VI
LIST OF FIGURES	IX
LIST OF TABLE	XIII
INTRODUCTION	1
1.1 LITERATURE REVIEW	2
1.2 OBJECTIVES.....	5
1.2.1 <i>Specific objectives</i>	5
1.3 STRUCTURE OF THIS THESIS.....	5
2 THEORETICAL BACKGROUND	7
2.1 FUNCTIONALLY GRADED MATERIALS	7
2.2 TYPES OF COMPOSITE MATERIALS	8
2.2.1 <i>Thermophysical Properties of Composites</i>	9
2.3 METAL MATRIX COMPOSITES	10
2.3.1 <i>Advantages and Disadvantages of Metal Matrix Composites</i>	11
2.4 ALUMINUM MATRIX COMPOSITES (AMCs)	12
2.4.1 <i>Aluminum Borides (AlB_2 and AlB_{12})</i>	13
2.4.2 <i>Aluminum-Magnesium System</i>	14
2.4.3 <i>Aluminum-Copper System</i>	15
2.5 CENTRIFUGAL CASTING PROCESS	16
2.5.1 <i>Basic equations used during centrifugal casting of AMCs</i>	17
2.5.2 <i>Analytical solution</i>	19

2.5.3	<i>Volume fraction and stereological analysis</i>	21
3	EXPERIMENTAL PROCEDURE	22
3.1	CENTRIFUGAL CASTING	23
3.2	PROCESSING OF FUNCTIONALLY GRADED AL-B-MG COMPOSITES BY CENTRIFUGAL CASTING	25
3.2.1	<i>Metallographic Sample (Al-B-Mg composites) Preparation</i>	26
3.3	PROCESSING OF FUNCTIONALLY GRADED AL-CU-B COMPOSITES BY CENTRIFUGAL CASTING.	27
4	STUDY OF AL-B PHASES IN THE AL-B-MG COMPOSITE	28
4.1	CHARACTERIZATION OF THE AL-B-MG COMPOSITES	28
4.1.1	<i>Analysis of Microstructure</i>	28
4.1.2	<i>Volume percent of Reinforcement Particles and Pores</i>	29
4.1.3	<i>Porosity in Centrifugally Cast Al-B-Mg Composites</i>	36
4.1.4	<i>Superficial Rockwell Hardness and Vickers Microhardness Tests</i>	37
4.1.5	<i>Particle size in the Al-B-Mg composites</i>	42
4.1.6	<i>Effect of Magnesium on the Particle Morphology during Centrifugal Casting</i>	43
5	STUDY OF AL-B PHASES IN AL-CU-B COMPOSITE	50
5.1	CHARACTERIZATION OF THE AL-B-CU COMPOSITES.....	50
5.1.1	<i>Analysis of the Microstructure</i>	50
5.1.2	<i>Volume percent of Reinforcement Particles and Pores</i>	51
5.1.3	<i>Porosity in Centrifugally Cast Al-B-Cu Composites</i>	57
5.1.4	<i>Superficial Rockwell Hardness and Vickers Microhardness</i>	58
5.1.5	<i>Particle size in the Al-B-Cu composites</i>	64
6	COMPARISON BETWEEN FUNCTIONALLY GRADED AL-B-MG AND AL-B-CU COMPOSITES	65
6.1	COMPLEMENTARY TESTS.....	65
6.1.1	<i>Energy Dispersive Spectroscopy (EDS)/SEM Analysis on Al- 2 wt. %B- 6 wt. %Mg specimen</i>	65
6.1.2	<i>Energy Dispersive Spectroscopy (EDS)/SEM Analysis on Al- 2 wt. %B- 6 wt. %Cu Specimen</i>	70

6.2	VISCOSITY EFFECTS IN THE CAST SPECIMENS.....	74
6.3	HARDNESS VALUES.....	79
7	CONCLUSIONS AND SUGGESTIONS FOR FUTURE WORKS.....	82
7.1	CONCLUSIONS.....	82
7.2	SUGGESTIONS FOR FUTURE WORK.....	84
8	REFERENCES.....	85

LIST OF FIGURES

Figure 2-1. Aluminum boron equilibrium phase diagram [33]	13
Figure 2-2 Partial Al-Mg binary alloy phase diagram [35]	15
Figure 2-3 Partial aluminum-copper phase diagram [38]	16
Figure 2-4 Schematic diagram of mold and melt in calculating heat transfer	19
Figure 3-1 Schematic diagram of experimental procedure	22
Figure 3.2 Schematic of the Cylindrical Mold	23
Figure 3.3 Schematic of the centrifugal caster with its housing	24
Figure 3.4 Mapped longitudinal specimen along the centrifugal force direction.	26
Figure 4.1 Photomicrograph of Al-2 wt. %B- 6 wt. %Mg composite microstructure showing presence of both aluminum borides.	29
Figure 4.2 Particles distribution in functionally-graded Al-B-Mg composite with variation of casting time at 15 mm.	31
Figure 4.3 Particles distribution in functionally graded Al-B-Mg composite with variation of casting time at 60 mm.	31
Figure 4.4 Effect of casting time on AlB_{12} and AlB_2 particles segregation along the longitudinal distance of cast specimens (Al-B-Mg).	32
Figure 4.5 Particles distribution in functionally-graded Al-B-Mg composite with variation in rotational speed at 15 mm.	33
Figure 4.6 Particles distribution in functionally-graded Al-B-Mg composite with variation in rotational speed at 60 mm.	33
Figure 4.7 Effect of rotational speed on AlB_{12} and AlB_2 particles segregation along the longitudinal distance of the cylindrical centrifugally cast Al-B-Mg specimens.	34
Figure 4.8 Particles distribution in functionally-graded Al-B-Mg composite with variation in pouring temperature at 15 mm.	35
Figure 4.9 Particles distribution in functionally-graded Al-B-Mg composite with	35
Figure 4.10 Effect of pouring temperature on AlB_{12} and AlB_2 particles distribution along the longitudinal axis of a centrifugally cast Al-B-Mg composite.	36
Figure 4.11 Porosity level along longitudinal distance of centrifugally cast Al-B-Mg composites.	37

Figure 4.12 Effect of casting time on superficial Rockwell hardness along the longitudinal axis of the centrifugally cast Al-B-Mg composites.	38
Figure 4.13 Effect of rotational speed on superficial Rockwell hardness along the longitudinal axis of the centrifugally cast Al-B-Mg composites.	39
Figure 4.14 Effect of pouring temperature on superficial Rockwell hardness along the longitudinal axis of the centrifugally cast Al-B-Mg composites.	39
Figure 4.15 Effect of casting time on Vickers microhardness along the longitudinal axis of the centrifugally cast Al-B-Mg composites.	41
Figure 4.16 Effect of rotational speed on Vickers microhardness along the longitudinal axis of the centrifugally cast Al-B-Mg composites.	41
Figure 4.17 Effect of pouring temperature on Vickers microhardness along the longitudinal axis of the centrifugally cast Al-B-Mg composites.	42
Figure 4.18 Phase morphology of the aluminum boride particles in Al-B-Mg composite melt during centrifugal casting.	44
Figure 4.19 Effect of casting time on the formation of aluminum boride phases along the casting.	46
Figure 4.20 Effect of rotational speed on the formation of aluminum boride phases along cylindrical casting.	48
Figure 4.21 Effect of pouring temperature on the formation of aluminum boride phase along cylindrical casting.	49
Figure 5.1 Photomicrograph of Al-B-Cu composite typical microstructure (Al-2 wt. %B- 6 wt. %Cu) showing presence of AlB_{12} and Al_2Cu phases.	50
Figure 5.2 Particles distribution in functionally-graded Al-B-Cu composite with variation of casting time at 15 mm.	52
Figure 5.3 Particles distribution in functionally-graded Al-B-Cu composite with variation of casting time at 60 mm.	52
Figure 5.4 Effect of casting time on AlB_{12} particles segregation along the longitudinal distance of cast specimens (Al-B-Cu).	53
Figure 5.5 Particles distribution in functionally-graded Al-B-Cu composite with variation of rotational speed at 15 mm.	54
Figure 5.6 Particles distribution in functionally-graded Al-B-Cu composite with variation of rotational speed at 60 mm.	54

Figure 5.7 Effect of rotational speed on AlB_{12} particles segregation along the longitudinal distance of centrifugally cast Al-B-Cu specimens.	55
Figure 5.8 Particles distribution and the effect of pouring temperature at 15 mm of a centrifugally cast Al-B-Cu composite.	56
Figure 5.9 Particles distribution and the effect of pouring temperature at 60 mm of a centrifugally cast Al-B-Cu composite.	56
Figure 5.10 Effect of pouring temperature on boride particles distribution along the longitudinal axis of a centrifugally cast Al-B-Cu composite.	57
Figure 5.11 Measured volume percent of pores along the longitudinal axis of a centrifugally cast Al-B-Cu composites.	58
Figure 5.12 Effect of casting time on superficial Rockwell hardness along the longitudinal axis of the centrifugally cast Al-B-Cu composites.	60
Figure 5.13 Effect of rotational speed on superficial Rockwell hardness along the longitudinal axis of the centrifugally cast Al-B-Cu composites.	60
Figure 5.14 Effect of pouring temperature on superficial Rockwell hardness along the longitudinal axis of the centrifugally cast Al-B-Cu composites.	61
Figure 5.15 Effect of casting time on Vickers microhardness along the longitudinal axis of the cast Al-B-Cu composites.	62
Figure 5.16 Effect of rotational speed on Vickers microhardness along the longitudinal axis of centrifugally cast Al-B-Cu composites.	63
Figure 5.17 Effect of pouring temperature on Vickers microhardness along the longitudinal axis of centrifugally cast Al-B-Cu composites.	63
Figure 6.1 SEM image showing the morphology of the AlB_{12} and AlB_2 particles in the functionally graded Al-B-Mg composite.	66
Figure 6-2 X-ray mapping of the Al-B-Mg composites (EDS).	67
Figure 6.3 EDS compositional analysis: (a) Backscattering electron image used to differentiate boride particles: AlB_{12} (labeled 1), AlB_2 (labeled 2), and the matrix of the Al-B-Mg composite (labeled 3); (b) EDS analysis on the AlB_{12} in spot 1; (c) EDS analysis on AlB_2 spot 2; and (d) EDS analysis on the Al-B-Mg matrix of the composite spot 3.	69
Figure 6.4 SEM image showing the morphology of the AlB_{12} particles and Al_2Cu phases on the functionally graded Al-B-Cu composite.	70
Figure 6.5 EDS mapping of the surface of the Al-B-Cu composites.	71

Figure 6.6 EDS compositional analysis: (a) Backscattering electron image displaying AlB_{12} particles (labeled 1), AlB_2 particles (labeled 2), and the matrix (labeled 3) of the Al-B-Cu composite; (b) EDS analysis on the AlB_{12} in spot 1; and (c) EDS analysis on AlB_2 spot. 72

Figure 6.7 Micrographs of Al-B master alloy with various level of heat treatment: (a) As received at room temperature; (b) Annealed at $400^{\circ}C$; (c) Annealed at $850^{\circ}C$. 73

LIST OF TABLE

Table 2-1 Thermophysical properties of materials, metals and secondary phases.....	10
Table 2-2 Physical properties of boron [34]	14
Table 2-3 Al-Cu phases with their crystal structure and lattice parameters [37]	16
Table 3.1 Functionally graded Al-B-Mg composites fabrication conditions: (A) Effect of casting time, (B) Effect of rotational speed, (C) Effect of pouring temperature	25
Table 3.2 Functionally graded Al-B-Cu composites fabricated conditions: (A) Influence of casting time, (B) Influence of rotational speed, (C) Influence of pouring temperature	27
Table 6.1 Apparent viscosities of composites as a function of casting time along the casting of a functionally graded Al-B-Mg composite.	76
Table 6.2 Apparent viscosities of composites as a function of rotational speed along the casting of a functionally graded Al-B-Mg composite.	76
Table 6.3 Apparent viscosities of composite as a function of pouring temperature along the casting of a functionally graded Al-B-Mg composite.....	77
Table 6.4 Apparent viscosities of composites as a function of casting time along the casting of a functionally graded Al-B-Cu composites.....	77
Table 6.5 Apparent viscosities of composite as a function of rotational speed along the casting of a functionally graded Al-B-Cu composite.	78
Table 6.6 Apparent viscosities of composites as a function of pouring temperature along the casting of a functionally graded Al-B-Cu composite.....	78
Table 6.7 3-Dimensional plots of experimental data	80

INTRODUCTION

Aluminum-based matrix composites are materials with improved mechanical and tribological properties when compared to their metallic counterparts. Functionally graded aluminum matrix composites reinforced with aluminum boride particles tend to exhibit gradual but continuous transition in engineering properties at the microscopic or continuum scale. The compositional gradient formed is achieved by rearranging the reinforcing particles by external means, for instance centrifugal casting.

Centrifugal casting has been proposed as one of the most economical and effective methods of fabrication of FG-AMCs [1]. This casting method provides the required pressure that produces good mold filling combined with good microstructural control which usually results in excellent mechanical properties in the as cast samples [2]. When used in the manufacturing of Al matrix composites, this method causes hard particles segregation via differential centrifugal forces when there exists a difference in density between the particles and the melt.

In this investigation, we established a procedure for controlling the compositional gradient of aluminum matrix composites with more precision. As mentioned before, this compositional gradient displayed improvement over monolithic metal in both mechanical properties and tribological properties. The influence of casting time, rotational speed and pouring temperature of the semimolten aluminum matrix composites on the redistribution of the dispersoids made of either AlB_2 or AlB_{12} particles was ascertained. These aluminum boride particles are widely used as grain refiners in aluminum alloys [3]. The density of the aluminum borides are higher, 3190 kg/m^3 for AlB_2 [4], and 2600 kg/m^3 for AlB_{12} [5] than liquid Al (estimated at 2400 kg/m^3) [6] for the casting temperatures, i.e. 700°C [7]. At higher temperatures the density of molten aluminum decreases even more; for instance, the density of molten aluminum at 900°C is 2315 kg/m^3 [8]. This variation in density of the melt brings about the redistribution of

Adelakin Kingsley Tunde, Masters Thesis, UPRM 2009

the dispersoids in the matrix, with the heavier particles moving faster towards the periphery along the longitudinal section of the cast [9].

1.1 Literature review

There are several investigations and peer-reviewed publications devoted to tribological and mechanical properties of functionally-graded materials, and aluminum matrix composite (FGM-AMC's) produced via centrifugal casting method. Most of them demonstrated the influence that the distributed reinforcement particles had on the fabrication of (FGM-AMC's) as a function of hard wear resistance on surfaces of composites. Fabrication of aluminum matrix composites was characterized by a very close relation between experimental and numerical modeling (simulations). In this research, a brief literature survey will be presented as related to this thesis.

In recent years, extensive work has been dedicated to functionally graded materials, and aluminum matrix based composites fabricated by centrifugal casting and reinforced with particles [1, 2, 7 - 10]. This procedure basically involves the microstructural restructuring of the composites material and the tailoring of the compositional gradient, which in returns gives unique properties superior to a monolithic material or alloys. By modeling particle segregation during centrifugal casting of Al- matrix composites, Lajoie and Suery examined particle segregation during centrifugal casting of Al- Matrix composite as a function of a number of variables, such as; casting time, pouring temperature, rotational speed of mold, initial mold temperature, particle radius, solidification delay and density difference. They divided their work into modeling and experimentation. They cited works of Banerji et al, Krishman et al and Nath where the use of ZrO_2 , graphite and mica had been used to achieve some segregation pattern during centrifugal casting. In their investigation, the authors found that the most strongly influenced parameter during segregation was not centrifugal acceleration (or rotational speed of the mold). As it will be detailed later this finding would help explain the results from the present thesis that when rotational

Adelakin Kingsley Tunde, Masters Thesis, UPRM 2009

speed between a close ranges (< 100 rpm) is considered, the speed effect will be lesser [8].

Solidification process of FGM-AMCs can be best explained using numerical technique during centrifugal casting. Kang and Rohatgi [11] systematically carried out a transient analysis of solidification during centrifugal casting for composite materials with particle segregation. The authors discuss primarily a model of particle segregation as a method to study solidification process in casting of composites material (containing Al_2O_3 , SiC_p and graphite particles) with respect to the thickness of the mold used, but did not specifically address the dispersion of the reinforcement in terms of variation of the casting parameters. For the purpose of making recommendations or establishing future baseline study of phase-change process during centrifugal casting process of composite materials, their description is useful. The authors described three core factors that strongly influenced segregation of particles during centrifugal casting, i.e. rotational speed of the mold, the solidification time and the density difference between their base alloy and the reinforcement. Kang and Rohatgi were able to validate their numerical model with the experimental work of Lajoie and Suery, and reported that there was a good agreement between both investigations. The authors parametric study suggest the idea of using a graphite mold with the thickness used in the present thesis, instead of an assembly of molds such as the ones used in their research. This resulted in simpler design of the mold.

Addition of alloying elements into aluminum matrix composites during fabrication has been used to improve infiltration behavior rather than to increase the matrix strength. These alloying elements lower the surface tension of liquid aluminum. This improves the use of particles such as SiC , graphite, mica and Al_2O_3 in aluminum matrix composites. However, this is a non-issue in the use of aluminum boride particles as there seems to be a good wettability between aluminum borides and the aluminum matrix [3]. In this thesis, alloying elements were used to strengthen the aluminum matrix though they might have some effect on fostering the wettability between the matrix and the particles. This is one reason why magnesium was used in this research, as

Adelakin Kingsley Tunde, Masters Thesis, UPRM 2009

suggested by Melgarejo et al [7], who studied the wear resistance of a functionally-graded aluminum matrix composite. They reported the hardness values of their composite to increase along the same direction as the segregation of the reinforcement particles.

Melgarejo et al gave an in-depth look at the effects of the amount of aluminum borides in the centrifugal casting of Al-B-Mg composites on the redistribution of those particles. The present research is built around those author's recommendation, suggesting a further study on the use of magnesium during fabrication of Al-B-Mg composites. What differentiated the present research from that work are the composition of the master alloy used and the detailed investigation of the centrifugal casting parameters.

In general, it could be deduced from the sampled literature that the use of SiC, Graphite, Al_2O_3 and Mica is common amongst different investigators and that, the dispersion trend of the reinforcement particles in their work are in good agreement. The present research work tend to not only show how the variation of the centrifugal casting parameters influence the redistribution of the reinforcement particle in an aluminum based functionally graded material, but also to show the advantages in terms of mechanical properties that could be achieved with the use of Al-7.2 wt% B master alloy where the addition with magnesium furnished the co-existence of AlB_2 and AlB_{12} . The viability of the use of this Al-B master alloy with copper as alloying element in aluminum-based matrix composite was also demonstrated.

In the present thesis we will elaborate on the use of AlB_2 and AlB_{12} [3, 12] in the overall data agreement with Lajoie and Suery experimental results, when variation of the casting parameters are taken into account. We were also able to detect the effect of the mold temperature, which in this thesis is based on the steadiest segregation pattern observed in those authors' work.

1.2 Objectives

The present research focuses on the influence of casting time, rotational speed of the mold and pouring temperature of the melt on the distribution of the reinforcements (aluminum boride particles) during centrifugal casting of FGMs made of Al-B-Mg and Al-B-Cu composites. The fabricated FGMs will also be characterized to analyze the compositional gradients and mechanical properties.

1.2.1 Specific objectives

- To fabricate FGM-AMCs reinforced with AlB_2 or AlB_{12} reinforcement particles.
- Characterize the composite microstructure including an analysis of the volume percent distribution of the reinforcements.
- To perform qualitative analysis based on the use of secondary electron spectroscopy (SEM)/energy dispersive spectroscopy (EDS) on the manufactured specimens.
- Obtain microstructural and mechanical properties such as, particle size, Vickers microhardness test values and 15T Rockwell superficial hardness test values on the fabricated FGM-AMCs, i.e. Al-B-Mg and Al-B-Cu.

1.3 Structure of this Thesis

In Chapter 2 the basic theoretical background as related to this thesis is presented. Chapter 3 describes the experimental procedure considered in the fabrication and metallurgical samples preparation of the functionally graded aluminum based matrix composites.

Chapter 4 deals with the characterization of the Al-B-Mg composites by determining the volume percent distribution of reinforcement particles, Rockwell superficial hardness and Vickers microhardness test. It also addresses the effect of

Adelakin Kingsley Tunde, Masters Thesis, UPRM 2009

magnesium on the particle morphology during centrifugal casting. Chapter 5 considers the characterization of the fabricated Al-B-Cu in terms of volume percent of particles distribution, Rockwell superficial hardness and Vickers microhardness analysis.

Chapter 6 contains discussions on the comparison between the functionally graded Al-B-Mg and Al-B-Cu composites in terms of hardness, wettability between the aluminum matrix and the composites, viscosity variation along cast and EDS analysis. Chapter 7 provides conclusions and some important suggestions for future work.

2 THEORETICAL BACKGROUND

2.1 *Functionally Graded Materials*

A functionally graded material (FGM) is a material whose composition or functions vary continuously or step-wisely from one direction to the other. In particle-reinforced composites these gradual changes can be a result of increasing volume fraction of the reinforcements across the material. The particle volume fraction of those FGMs can be varied over a macroscaled geometrical dimension such as casting length. These materials are constituted by two components characterized by compositional gradient from one component to the other, with a microstructure that produces continuously or discretely changing thermal and mechanical properties at the macroscopic or continuum scale. The gradient can be continuous on a microscopic level, for metallic matrix reinforced with ceramic particles [10]. FGMs are multifunctional in terms of their properties, as they provide hard, corrosion-resistance and temperature-resistant surfaces on the one hand or tougher surfaces. In particle-reinforced FGMs engineers accomplish this by employing reinforcements with different properties, sizes, and shapes, as well as by interchanging the roles of the reinforcement and the matrix phases in a continuous manner [13].

The concept of FGMs originated in Japan in 1984 during the space plane project, in the form of a proposed thermal barrier material capable of withstanding a surface temperature of 2000 K and a temperature gradient of 1000 K across a given section or length of material [14-16]. FGMs have been named as an ideal candidate for applications involving severe thermal gradients, varying from thermal structures in advance aircraft and aerospace engines to computer circuit boards. These materials were introduced to take advantage of ideal behavior of its constituents, e.g. heat and corrosion resistance of ceramics together with mechanical strength and toughness of metals to suit material design [17]. The original idea of FGMs has been later expanded

Adelakin Kingsley Tunde, Masters Thesis, UPRM 2009

for a variety of applications (cutting tools, coatings, packages, semiconductors, optical and biomaterials). In 1972, Bever et al [18] carried out a theoretical prediction of the usefulness of functional composite with a graded structure. During the last years, FGMs have been developed from single specimens to industry oriented applications. Furthermore, several national R&D programs (Japan, China, and Germany) have started in this field very recently [19]. The overview of the production routes, properties and applications of FGMs are described in several monographs [18, 20, and 21].

2.2 Types of Composite Materials

In general, composites are categorized according to the nature of the material that makes up their matrix: polymer (plastic) matrix (PMC), ceramic matrix (CMC) and metal matrix (MMC) composites. They could also be classified in terms of the reinforcement embedded in the matrix [22]:

- (1) Dispersion strengthened composites: They contain fine hard particles, uniformly distributed, ranging in size from 0.01 μm to 0.5 μm with a volume fraction from 1 to 15%. When embedded in the matrix, those particles strengthened the matrix. A typical example is silicon carbide reinforced aluminum composites used in high-performance bicycle frames.
- (2) Fiber reinforced composites: They are composites that contain all types of fibers, filaments and whiskers, both continuous and non-continuous with wide variation of concentration of the reinforcements. They possess excellent abrasive resistance due to surface smoothness. Carbon-fiber composites used in high-performance aircraft and sports equipment are a good example of these composites.
- (3) Particle reinforced composites: They have larger particles than that of the dispersion-strengthened composites. Volume fraction of these particles could also be higher than 25%. The matrix of the composites could be strengthened by the particles bearing significant parts of the load on the matrix and by restricting

Adelakin Kingsley Tunde, Masters Thesis, UPRM 2009

the flow of the matrix material. Carbide cutting tools are good example of this material.

2.2.1 Thermophysical Properties of Composites

Design engineers are concerned with three main aspects apart from cost and delivery:

- (1) The mechanical and physical properties as supplied by the manufacturer,
- (2) Reliability related to properties and performance from beginning to the end of each delivery and from one delivery to the next,
- (3) And safety in terms of material maneuvering and handling.

Based on the above points utmost attention must be paid to proper selection of matrix materials and reinforcements, which allow the tailoring of the desired properties of a specific design.

The rule of mixture (ROM) (equation 0-1) can be used to estimate any composite property that does not depend on the spatial relationship of the component. This rule states that the property of a composite material is the sum of products of the property of an individual constituent and its volume fraction in the composite. For a composite made of reinforcement and matrix, it is assumed that many of its properties will be the sum of an average product of its constituents. This equation could be written as a contribution from each phase that forms the composites,

$$P_C = P_m V_m + P_p V_p \quad \text{Equation 2-1 [23]}$$

where P_C is the property of the composite, while P_m and P_p is the corresponding property of the matrix and the particulates respectively. V_p is the volume fraction of particulate and V_m stands for volume fraction of the matrix material.

Properties such as thermal conductivity, density and specific heat of composites liquid could be described using equation (0-2) to (0-4) as shown below,

$$K_{LC} = [1 - V_f(t)]K_L + V_f(t)K_L \quad \text{Equation 2-2}$$

Adelakin Kingsley Tunde, Masters Thesis, UPRM 2009

$$\rho_{LC} = [1 - V_f(t)]\rho_L + V_f(t)\rho_P \quad \text{Equation 2-3}$$

$$C_L = [1 - V_f(t)]C_L + V_f(t)C_P \quad \text{Equation 2-4}$$

where $V_m = [1 - V_f]$ and V_f is volume fraction of particles.

Another physical property can be readily affected by the volume fraction and distribution of the particles along the composite casting: the viscosity of the molten composite upon processing. Other factors affecting viscosity are: the size of the particles, the mold rotational speed and the difference in density between the reinforcement and the molten metal or alloy during fabrication process. Table 2.1 shows the thermophysical properties of materials, metals and secondary phases, as surveyed from literature.

Table 2.1 Thermophysical properties of materials, metals and secondary phases.

MATERIAL	SOLID DENSITY (KG/M ³)	LIQUID DENSITY (KG/M ³)	THERMAL CONDUCTIVITY K (W/M.K)	COEFF. THERMAL EXPANSION (X10 ⁻⁶ /°C)	MELTING POINT (°C)
Al	2700	2390	159	23	660
Mg	1740	1566	156	27	650
Cu	8960	7900	401	32	1083
AlB ₂	3190	-	-	-	1655
AlB ₁₂	2600			-	2214
Al ₂ Cu	4340	-	-	17.2	540
Graphite	1900	-	38	8.2	3650

2.3 Metal Matrix Composites

In the past years, metal matrix composites technology has been regarded as a welcome innovation in industry for ease in the study and maneuvering of the architecture (morphology and geometry distribution) of the reinforcement particles embedded in the matrix. Nevertheless, MMC could be classified in terms of their matrix being ferrous (iron based) or non-ferrous materials. The noted employed matrix

Adelakin Kingsley Tunde, Masters Thesis, UPRM 2009

materials include magnesium, beryllium, titanium, iron, nickel, cobalt, silver and aluminum but aluminum seem to be the most attractive one [24]. The reinforcing particle phase that furnishes the composite with good tribological properties had already been discussed earlier. Hence a good bond between the reinforcement grain and the matrix is required for proper load transfer and to provide a homogeneous structure for good load bearing and uniform deformation.

2.3.1 Advantages and Disadvantages of Metal Matrix Composites

The wide diversity of MMCs in engineering applications is as a result of the numerous superior qualities and properties they possess. The advantages and disadvantages of using MMCs over monolithic or polymer matrix composites are as follows [25].

Over monolithic metal:

- (1) Better properties at elevated temperatures, such as higher mechanical strength and lower creep rate.
- (2) Smaller thermal expansion coefficients.
- (3) Better wear resistance.
- (4) Higher toughness and impact properties.
- (5) Higher stiffness to density ratio.

Over polymer matrix composites;

- (1) No out-gassing.
- (2) Ease fabrication of whisker and particulate-reinforced MMCs with conventional metalworking tools.
- (3) Resistance to fire.
- (4) Higher transverse stiffness and strength.
- (5) No moisture absorption.

The disadvantages of using MMCs over monolithic metals and polymer matrix composites are related to their limited service experience, higher cost of material systems, complex manufacturing technique for fiber-reinforced systems and not well

Adelakin Kingsley Tunde, Masters Thesis, UPRM 2009

developed technology. However, these apparent disadvantages leave room for further developments and processing methods.

2.4 Aluminum Matrix Composites (AMCs)

Because of its low density aluminum is undoubtedly the most attractive matrix material employed in structural components and parts for the transportation and aerospace industries. An in-depth literature research revealed the difficulties observed when aluminum matrix is used with the commonly reinforcement particles [26, 27, 28]: Al_2O_3 , graphite, SiC, [29] etc. The first one is the lack of good wettability between the matrix and these particles [30]. During the liquid phase processing, the reinforcement particles are incorporated into a molten metallic matrix using different processing methods. In all of these, a strong bond between the metal matrix and the reinforcement is necessary to affect wetting. In such case, the introduction of an alloying element such as magnesium [31] or copper could enhance wetting by reducing the surface tension of the liquid melt. However, the use of AlB_2 as reinforcing particles has recently been proven to be an alternative to particles/matrix wettability in aluminum matrix composites. As previously mentioned, master alloys of the Al-B system containing AlB_2 [3] or AlB_{12} are being used as grain refiners in aluminum alloys.

Interfacial reaction brought about by chemical interaction is also another issue in the use of aluminum as a matrix material. For instance, the aluminum melt is in contact with particles like SiC, deleterious reaction products (e.g. Al_4C_3) can form [30, 32] These reaction products weaken the particle-matrix interface and can affect the proper load transfer between matrix and reinforcing particles during service. With the use of Al-B alloys containing aluminum borides such interfacial reactions could be avoided while reducing the cost of production.

2.4.1 Aluminum Borides (AlB_2 and AlB_{12})

According to the literature the most reported stable solid phases in an aluminum-boron alloy are βB , αAlB_{12} , βAlB_{12} , AlB_{10} , AlB_2 and Al. Duschanek and Rogl [12] concluded that the βAlB_{12} and AlB_{10} phases are carbon stabilized and are ternary compounds of $\text{Al}_2\text{B}_{48}\text{C}_2$ and $\text{AlB}_{24}\text{C}_4$ respectively. Formation of the different boride phases is basically due to the boron content in the sample, compound or alloys at specified temperatures illustrated on the Al-B phase diagram of Figure 2.1. A peritectic reaction, $\text{Al}_{(l)} + \text{AlB}_{12} \leftrightarrow \text{AlB}_2$ occurs at $\sim 975^\circ\text{C}$ and the liquidus lines shows the practical insolubility of boron in the matrix of aluminum. A eutectic reaction $L \leftrightarrow (\text{Al}) + \text{AlB}_2$ is observed at 659.7°C . Table 2.2 displays data of the physical properties of boron.

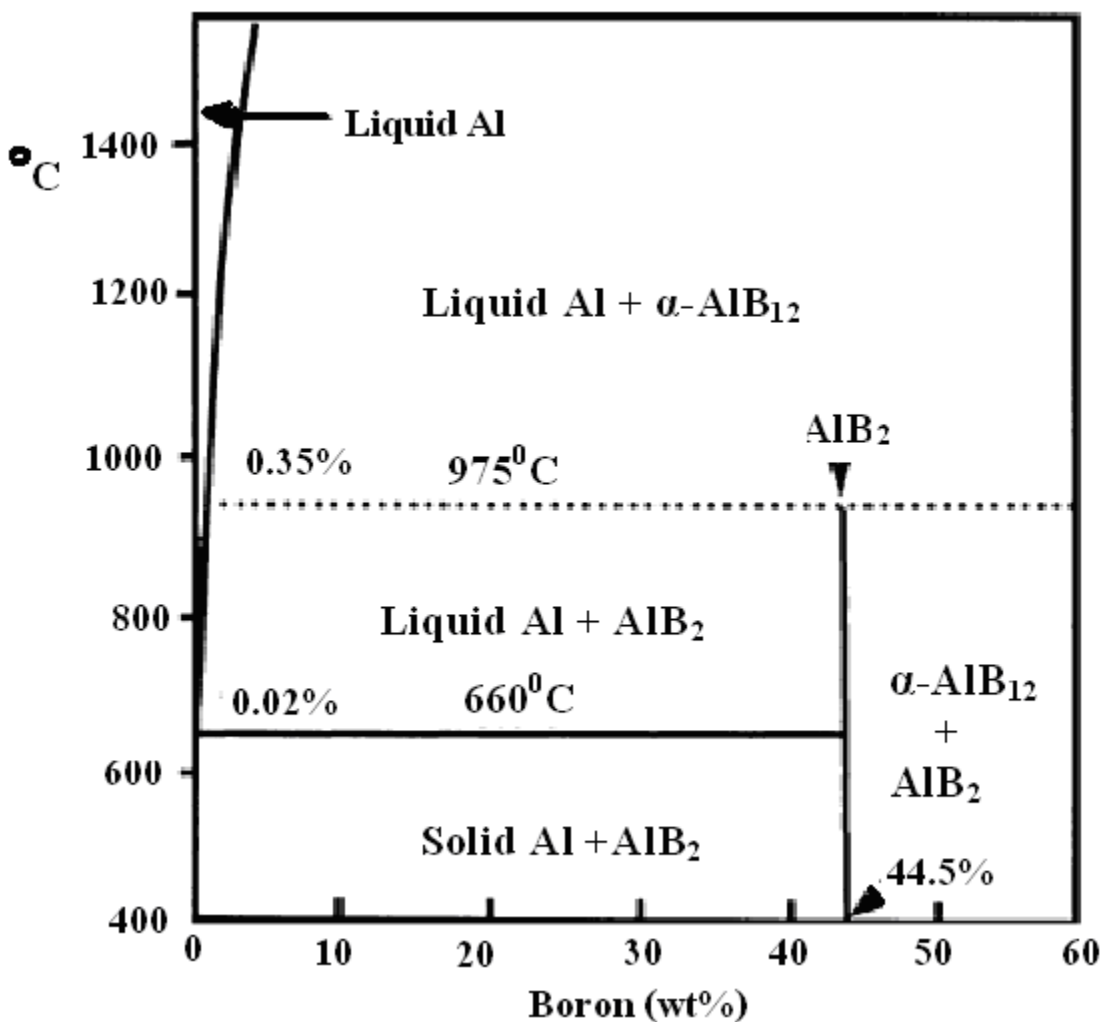


Figure 2-1. Aluminum boron equilibrium phase diagram [33]

Table 2.2 Physical properties of boron [34]

VICKERS MICROHARDNESS VALUE	4900 MNM ⁻²
Bulk Modulus	320 GPa
Density of solid	2460 Kgm ⁻³
Thermal Conductivity	27 Wm ⁻¹ K ⁻¹
Melting point	2349 K (2076°C)
Boiling point	4200 K (3927°C)

2.4.2 Aluminum-Magnesium System

When magnesium is dissolved in aluminum a considerable increase in strength of the alloy has been observed: For every 1 wt% Mg in solid solution aluminum density decreases linearly by approximately 0.5 % [35]. The maximum solid solubility of Mg in solid aluminum on the phase diagram in figure 2.2 is 14.9 wt% at the eutectic temperature of 450°C. However, this solubility decreases at room temperature to an approximate value of 1.7 wt%, but the rate of precipitation of β is very low. This equilibrium precipitate has an approximate stoichiometry of Al_3Mg_2 observed at 451°C and 37.3 wt% Mg. At low temperature this complex FCC structure can be transformed martensitically to another structure that may be a distortion of the β structure. In the Mg-rich side the maximum solid solubility of Al in Mg is 11.8 at. % at a eutectic temperature of 437°C.

Alloys containing greater than 7 percent magnesium are heat treatable, although thermal treatments are often used to stabilize properties that could otherwise change in some compositions over long periods of time. The precipitation resulted to an increment in strengthening by work hardening in alloys [36].

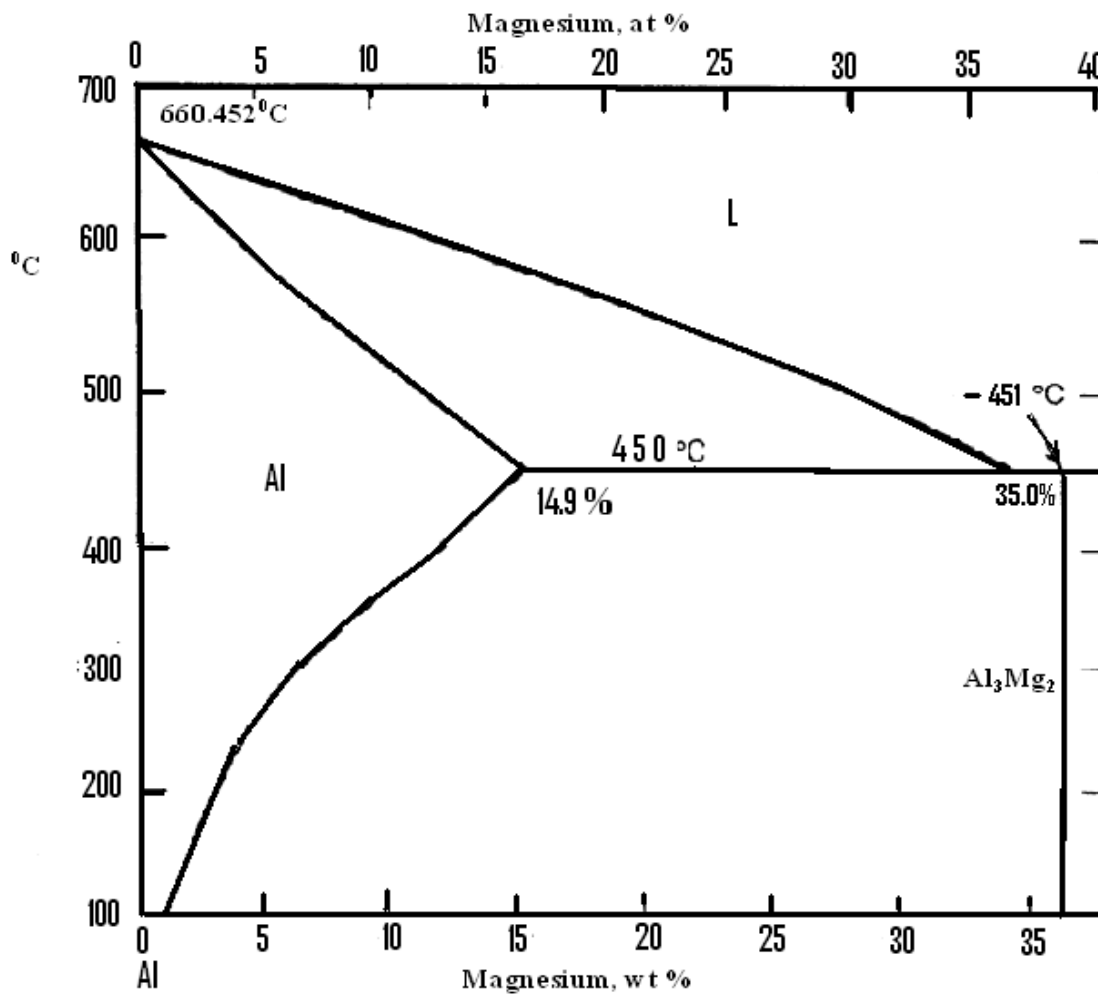


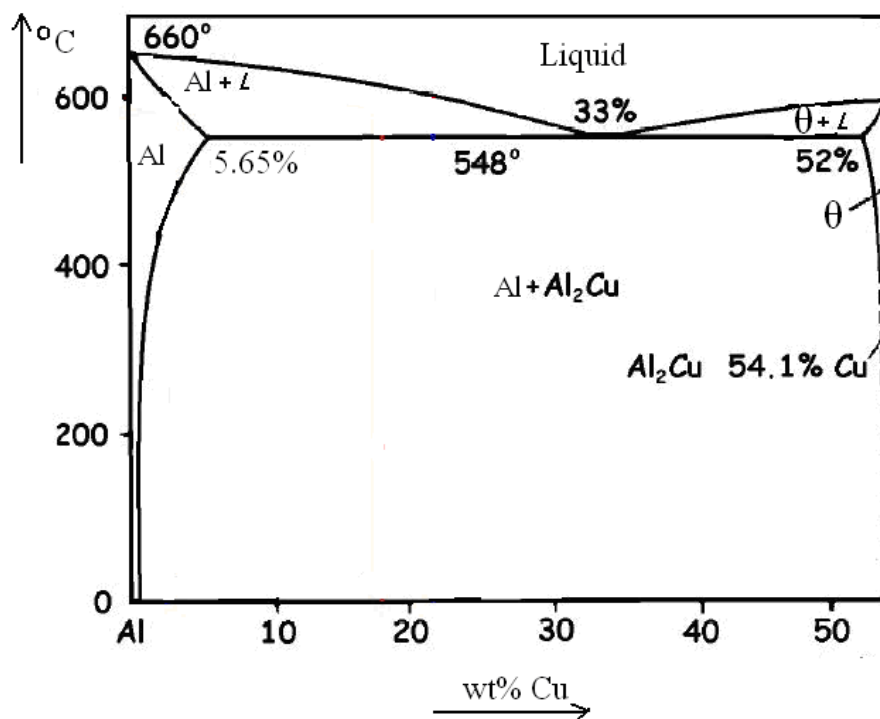
Figure 2-2 Partial Al-Mg binary alloy phase diagram [35]

2.4.3 Aluminum-Copper System

Addition of copper to aluminum results in an important strength increase in the alloy. This results in higher hardness, but the strength, and ductility depend on the distribution of Cu in the aluminum matrix during heat treatment [35]. Rapid cooling of a supersaturated solid solution of aluminum alloy containing 4.5 wt % copper from a high temperature could increase the strength of the alloy due to the formation of metastable precipitates: GP zones, θ'' , θ' and θ are formed. Table 2.3 shows the metastable Al-Cu phases with their crystal structures and lattice parameters. It can be seen from the phase diagram (figure 2.3) that at a temperature of 548°C eutectic reaction occurs.

Table 2.3 Al-Cu phases with their crystal structure and lattice parameters [37]

PHASE	CRYSTAL STRUCTURE	LATTICE PARAMETERS NM	
		A	C
θ''	Tetragonal	0.404	0.768
θ'	Tetragonal	0.404	0.580
θ	Tetragonal	0.6066	0.4874

**Figure 2-3 Partial aluminum-copper phase diagram [38]**

2.5 Centrifugal Casting Process

An economical and attractive processing route of cast Al alloys is centrifugal casting [39]. This type of casting process differs from other foundry processes in that it requires special knowledge, practices and skills not found in other types of fabrication operations. The concept of employing centrifugal casting to produce castings has been

Adelakin Kingsley Tunde, Masters Thesis, UPRM 2009

long known, although A. G. Eckhard's original patent of 1809 reviewed an understanding of basic principles of operation [40]. These operation variables (or parameters) are: speed of rotation of the mold, pouring molten metal, proper solidification rate, and extraction of the casting from the mold.

The technique involves applying centrifugal force to a uniformly mixed molten metal containing reinforcement particles, causing segregation of the denser particles with a graded profile. If the density of the molten metal is greater than the density of the reinforcement particles, the particles move towards the inner zone close to the axis of rotation. Conversely, if the density of the particles is greater than that of the molten metal, the particles move towards the outer periphery of the casting.

The production of FGMs dispersed with ceramic or intermetallic compounds by the centrifugal casting technique can be classified into two categories based on the relation between the melting temperature of the ceramic or intermetallic dispersed phase and the processing temperature. The first category is called centrifugal solid-particle technique while the other is called centrifugal in-situ technique [41]. In centrifugal solid-particle technique, the processing temperature is lower than the melting temperature of the dispersed ceramic or intermetallic phase. The intermetallic compound or ceramic remains solid in the liquid melt. In the in-situ technique the processing temperature is much higher than that of the melting temperature of the intermetallic compound. This technique employs the use of centrifugal force coupled with crystallization phenomena during solidification to form graded composition [42]

2.5.1 Basic equations used during centrifugal casting of AMCs

Generally, the motion of a solid particle in a viscous liquid under centrifugal force is explained theoretically by Stokes' law [43]. The shape of the reinforcement particles is assumed to be spherical. As mentioned before, Brinkman [44] provided a relationship between viscosity of the melt and the volume fraction of the reinforcement particles as

$$\eta_{app} = \eta_c \left[1 + \frac{5}{2} V_f + 7.6 V_f^2 \right]$$

Equation 2-5

However, this equation does not consider the effects of particle interactions and collision, which should depend on the particle size distribution as well as the volume fraction. Various models agreed that the forces acting on the reinforcement particles in the melt are centrifugal force due to mold rotation and viscous force due to drag effect. The distance moved by the particles and their velocity were obtained from the solution of the net force acting on the particles.

The distance traveled by the particles as a function of time is expressed in Equation 0-6,

$$r(t) = r_o(t) \exp\left[2\omega^2(\rho_p - \rho_L)R_p^2 \frac{t}{9\eta_c}\right] \quad \text{Equation 2-6 [12]}$$

The velocity of the particles can be calculated by Equation 0-7,

$$V_p = 2R_p^2(\rho_p - \rho_L)\frac{\gamma}{9\eta_c} \quad \text{Equation 2-7 [2]}$$

Where η_{app} , is apparent viscosity, η_c is viscosity of the composite melt, V_f is volume fraction of the reinforcement particles, $r(t)$, is radial distance covered by the particles at time t , $r_o(t)$ is radial distance or position at initial time t_0 , ω is rotational speed of the mold, R_p is the radius of the particles, “ t ” is the time at any point in the cast while ρ_p and ρ_L indicate the density of the particle and the density of the molten metal respectively.

The segregation of the particles towards the inner or outer zone could be predicted due to difference in density between the particles and the liquid matrix ($\rho_p - \rho_L$) involved. If $\Delta\rho = (\rho_p - \rho_L) > 0$ the particles migrate towards the outer zone of the cast with a compositional gradient which could be controlled by adjusting the rotational speed of the mold “ ω ”. However, if the value $\Delta\rho = (\rho_p - \rho_L) < 0$, then the particle migrates towards the inner zone of the cast [1]. The heat transfer aspect is modeled with respect to the material of the mold set up or materials. In the literature not much emphasis was spent in this aspect mainly because of the difficulties involved in studying the heat transfer when the mold is rotating during centrifugal casting.

2.5.2 Analytical solution

The heat problem involved when operating under centrifugal force can be best demonstrated by a transient heat transfer process. Figure 2-4 show a schematic diagram of the mold filled with the melt and the reinforcement particles. Cooling of the mold is normally multidimensional in nature because the temperature within the body is a function of time and at least one space dimension. However, approximate analysis can be ascertained from the Biot number point of view.

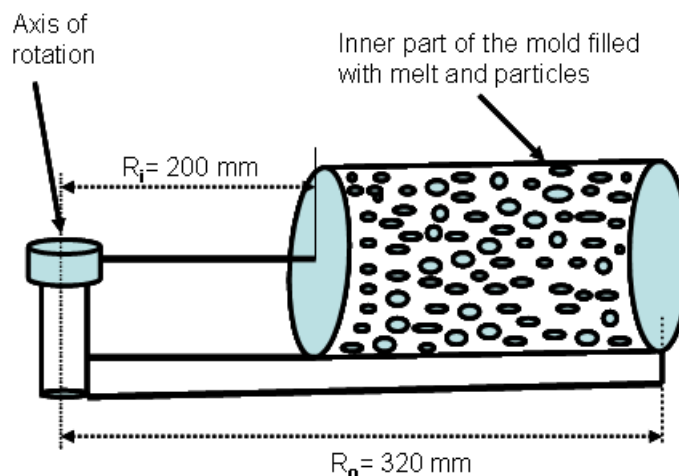


Figure 2-4 Schematic diagram of mold and melt in calculating heat transfer

Calculation of Biot number (Equation 0-8) from the parameters from figure 2.4 revealed that this is less than 0.1 ($Bi=0.0126$). L_c = characteristic length (body volume/area of body), h = heat transfer coefficient ($\text{W}/\text{m}^2\text{K}$) and K = thermal conductivity ($\text{Wm}/\text{m}^2\text{K}$).

$$Bi = \frac{hL_c}{K} \quad \text{Equation 2-8 [45]}$$

For small Bi the thermal resistance of the interface dominates that of the casting and this maintain an approximated constant temperature. This could be called Newtonian cooling; therefore energy balance gives the equation 0-5.

$$q = \bar{h}A_s(T - T_\infty) = -C_s\rho V \frac{dT}{dt} \quad \text{Equation 2-9}$$

Adelakin Kingsley Tunde, Masters Thesis, UPRM 2009

Upon integrating equation (0-9) from $t = 0$, at which $T = T_i$, to any time t , at which $T = T(t)$, we have the equation 0-10.

$$\frac{T(t) - T_\infty}{T_i - T_\infty} = \exp\left(\frac{-\bar{h}}{\rho V C_s} At\right) \quad \text{Equation 2-10}$$

The temperature of casting will be a function of time according to equation 0-11.

$$T(t) = (T_i - T_\infty) \exp\left(\frac{-\bar{h}}{\rho V C_s} At\right) + T_\infty \quad \text{Equation 2-11}$$

Equation (0-11) can be written in terms of the time taken for the mold to cool to a temperature T (equation 0-12).

$$t_{sc} = \frac{\rho L_c C_v}{\bar{h}} \ln\left[\frac{T_w - T}{T_w - T_i}\right] \quad \text{Equation 2-12 [46]}$$

where ρ is density of the mold, T_w is temperature at the mold wall, T_i is the pouring temperature, T is temperature to be calculated and \bar{h} is the heat transfer at the interface between the wall of the mold and the casting.

According to the literature [46] the total time taken for the casting of a pure metal melt can be computed according to equation 0-13.

$$t = \frac{L}{h} \left(C_v \ln\left[\frac{T_w - T_m}{T_w - T_p}\right] - \frac{\Delta H_F}{(T_w - T_m)} \right) \quad \text{Equation 2-13 [46]}$$

However, this equation could be modified to model the composite solidification during casting (equation 0-14).

$$t_c = \frac{L_c \rho_c}{\bar{h}} \left(C_{vc} \ln\left[\frac{T_w - T_m}{T_w - T_p}\right] - \frac{\Delta H_F}{(T_w - T_m)} \right) \quad \text{Equation 2-14}$$

where t_c is the total time taken for the composite casting to solidify after the melt has been poured; T_p is the pouring temperature; T_m is the melting temperature of casting; ρ_c is density of composite; C_{vc} is the specific heat capacity of the composite; and ΔH_F is the latent heat of fusion of the melt. This seems to be consistent since the thermophysical properties of the composite could be approximated from the rule of

Adelakin Kingsley Tunde, Masters Thesis, UPRM 2009

mixture. For equation (0-14) to be valid, the heat transfer coefficient between the wall of the mold and the melt must be used determine the Biot number in order to be within the limit of acceptance. It is assumed that the cooling is uniform throughout the casting, and that the melt cools with good thermal contact with the mold. The mass of particles is given by equation 0-15.

$$m = \rho_p V_p \quad \text{Equation 2-15}$$

The use of various equations presented for both the total solidification time of casting and the time for cooling the mold to certain temperature, the centrifugal casting parameters would aid the processing of a composite material with a refined microstructure such as will be discussed later on in this thesis.

2.5.3 Volume fraction and stereological analysis

Stereology provides geometrical tools that make possible the relation of a structure that exist in three-dimensions and the images of that structure that are basically two-dimensional. Metallography books agree that area fractions measured by microscopy techniques are equal to the volume fraction, a fact that is specially relevant “for a system of particles in a matrix” [47];

$$A_f = V_f \quad \text{Equation 2-16}$$

where A_f is area fraction and V_f volume fraction. It could be said that area fraction is a measured value while volume fraction could be calculated from the relationship given in equation 0-16.

3 EXPERIMENTAL PROCEDURE

The centrifugal casting technique was used to produce Al-B-Mg and Al-B-Cu functionally graded composites. The master alloys used in the fabrication of these composites were: Al-B (7.2 weight % B), Al-Mg (10 weight % Mg), Al-Cu (33.3 weight % Cu) and 99% pure aluminum. A commercial Al-B alloy containing AlB_2 and AlB_{12} reinforcement particles was used. Figure 3.1 shows the experimental sequence for the fabrication and characterization of FGM-AMCs via centrifugal casting.

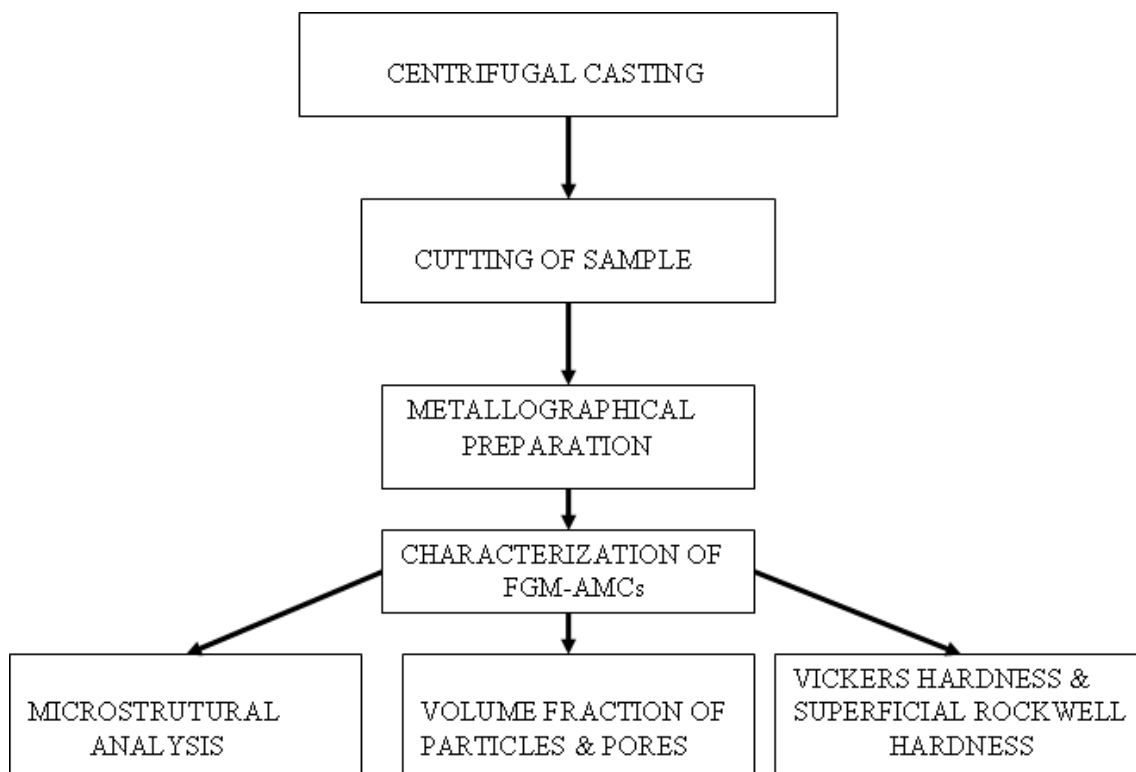


Figure 3-1 Schematic diagram of experimental procedure

A cylindrical graphite mold was used because of its high thermal conductivity, high machinability, and simple geometry. The mold was designed to suit the shape of the composites specimens with the dimensions shown in figure 3.2

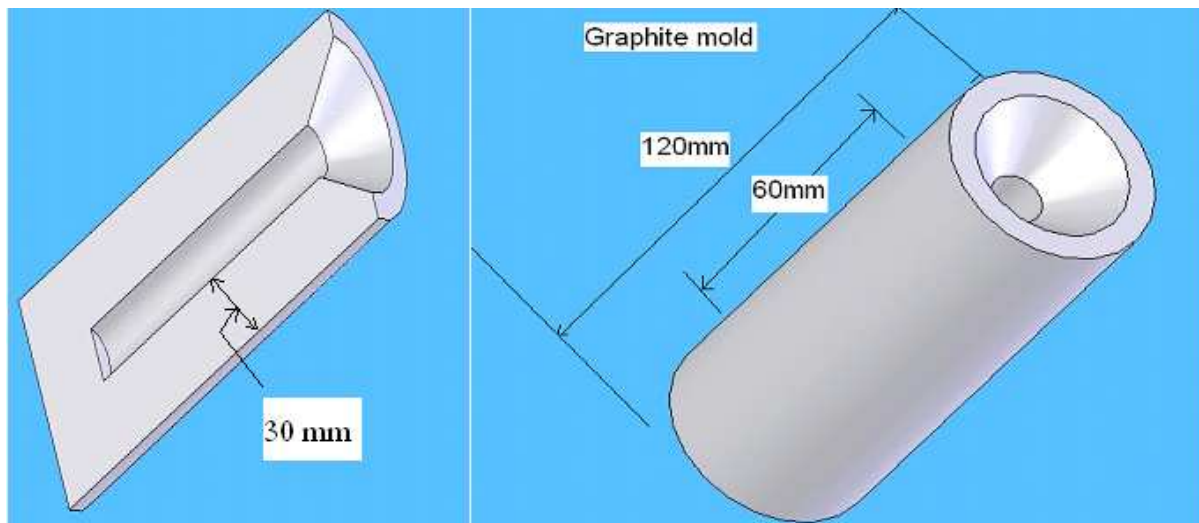


Figure 3.2 Schematic of the Cylindrical Mold

A resistance furnace was used to preheat the mold to the desired temperature for the experiment. The graphite crucible containing the required composition was placed inside the melting furnace to permit the remelting and homogeneous mixture of the melt at 850^oC.

3.1 Centrifugal Casting

The centrifugal caster used has a variable speed mechanism which allows adjusting the rotational speed from 300 rpm to 550 rpm. It also has a screen timer where the casting time or set time for the casting could be varied. The position of the scoop and the mold are shown in figure 3.3 where the direction of the centrifugal force is also indicated. The arm is used to balance the lever carrying the mold and the scoop during the centrifugal casting process. The scoop has a mass of 340g and it was used to transfer a charge of 40g into the cylindrical graphite mold. The distance of the cylinder close end to the axis of rotation is 200 mm and the distance of the cylinder outer end from the rotational axis is 320 mm (figure 2.4). A low speed precision saw was used to cut the specimens at regular intervals, i.e. 15mm.

Adelakin Kingsley Tunde, Masters Thesis, UPRM 2009

The microstructures of the cut samples were characterized both quantitatively and qualitatively. The Image J software was used to evaluate the effects of the casting parameters on the redistribution of the reinforcement particles in terms of volume fraction. Vickers microhardness and superficial hardness tests were then used to complement the study of the volume fraction of the distributed particles along the cast specimens. A Phillips XL30S FEG scanning electron microscopy (SEM) coupled with x-ray energy dispersive spectroscopy (EDS) were also employed to further study the microstructure and chemical composition of the composites.

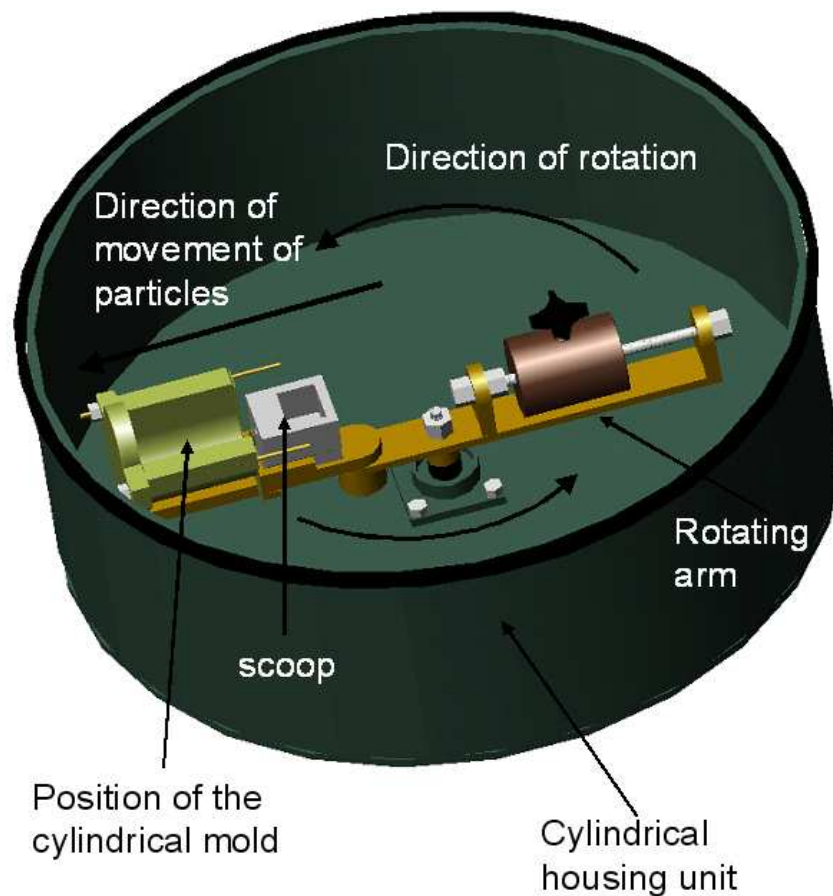


Figure 3.3 Schematic of the centrifugal caster with its housing

3.2 Processing of Functionally Graded Al-B-Mg Composites by Centrifugal Casting

The charge material made of master alloys was melted in the graphite crucible at 850⁰C and kept at this temperature for 25 minutes to ensure proper alloying; melt stirring permitted good homogenization of the molten material. The melt was then poured into the scoop through which the melt flowed into the cylindrical mold placed horizontally on the arm of the centrifugal caster (figure 3.3). The scoop and the mold had been previously preheated to 500⁰C for 50 minutes to facilitate the cast metal flow into the mold and to prevent frozen “skin” which would have constricted the flow of the melt into the mold [48]. The material was then centrifuged according to the parameters indicated in Table 3.1.

Table 3.1 Functionally graded Al-B-Mg composites fabrication conditions: (A) Effect of casting time, (B) Effect of rotational speed, (C) Effect of pouring temperature

Parameter	Specimens	Conditions
A	Specimen 1a	1 minute, 300 rpm, 820 ⁰ C
	Specimen 2a	2 minutes, 300 rpm, 820 ⁰ C
	Specimen 3a	3 minutes, 300 rpm, 820 ⁰ C
B	Specimen 3a	3 minute, 300 rpm, 820 ⁰ C
	Specimen 4a	3 minutes, 350 rpm, 820 ⁰ C
	Specimen 5a	3 minutes, 400 rpm, 820 ⁰ C
C	Specimen 6a	3 minute, 400 rpm, 690 ⁰ C
	Specimen 7a	3 minutes, 400 rpm, 755 ⁰ C
	Specimen 5a	3 minutes, 400 rpm, 820 ⁰ C

3.2.1 Metallographic Sample (Al-B-Mg composites) Preparation

The cylindrical specimens had 60 mm in length and 12 mm in diameter (figure 3.4). They were then cut with a low speed saw perpendicular to the cylindrical axis into four sections, each one having a length of 15 mm (figure 3.4).

The cut specimens were ground with 320, 400, 600, 800 and 1200 grit SiC paper and polished with 3 μm diamond suspension and with a 0.05 μm SiO₂ emulsion. Few drops of highly diluted HF solution were used in the final polishing of the surface to remove stains and residues left by the diamond suspension.

The polished samples were then characterized qualitatively and quantitatively. Hardness values were obtained using a superficial Rockwell hardness and Vickers microhardness testing machines to correlate the results obtained from the metallographic analysis.

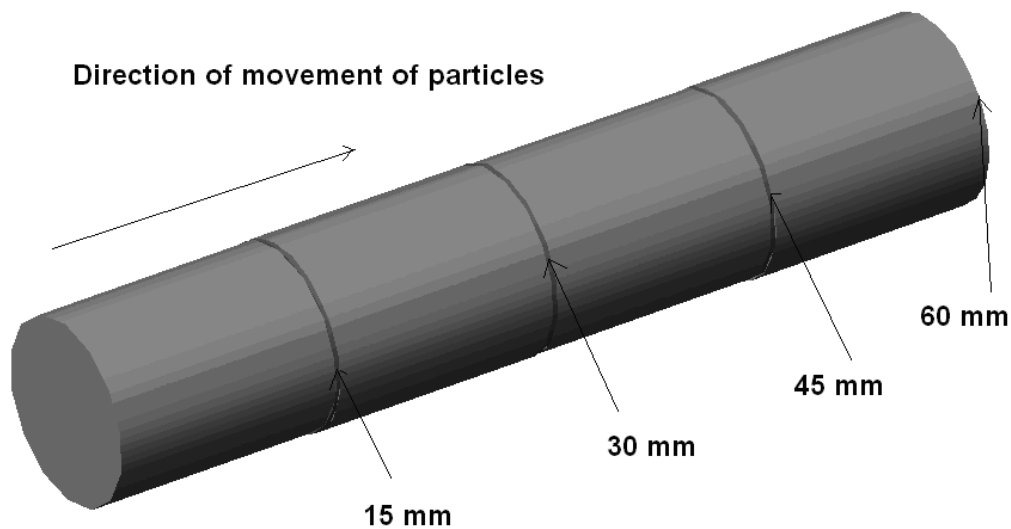


Figure 3.4 Mapped longitudinal specimen along the centrifugal force direction.

3.3 Processing of Functionally Graded Al-Cu-B Composites by Centrifugal Casting

The Al-B-Cu composite containing 6 wt. % Cu and 2 wt. % B was obtained by mixing commercial aluminum master alloys to the desired composition. The Al-B commercial alloy contains AlB_{12} reinforcement particles whose wettability with the aluminum melt is excellent. The materials were melted in a graphite crucible at $850^{\circ}C$ and was kept at this temperature for 25 minutes for proper alloying while the melt was stirred to permit good homogenization. The casting process was then similar to the Al-Mg-B composites. The centrifugal casting parameters are provided in Table 3.2.

Table 3.2 Functionally graded Al-B-Cu composites fabricated conditions: (A) Influence of casting time, (B) Influence of rotational speed, (C) Influence of poring temperature

Parameter	Specimens	Conditions
A	Specimen 1b	1 minute, 300 rpm, $820^{\circ}C$
	Specimen 2b	2 minutes, 300 rpm, $820^{\circ}C$
	Specimen 3b	3 minutes, 300 rpm, $820^{\circ}C$
B	Specimen 3b	3 minute, 300 rpm, $820^{\circ}C$
	Specimen 4b	3 minutes, 350 rpm, $820^{\circ}C$
	Specimen 5b	3 minutes, 400 rpm, $820^{\circ}C$
C	Specimen 6b	3 minute, 400 rpm, $690^{\circ}C$
	Specimen 7b	3 minutes, 400 rpm, $755^{\circ}C$
	Specimen 5b	3 minutes, 400 rpm, $820^{\circ}C$

4 STUDY OF Al-B PHASES IN THE Al-B-Mg COMPOSITE

4.1 *Characterization of the Al-B-Mg composites*

This chapter deals with an in-depth characterization of the aluminum-based FGMs (Al-B-Mg composites) reinforced with AlB_2 and AlB_{12} particles.

4.1.1 Analysis of Microstructure

In the optical micrograph (figure 4.1) of the functionally graded Al-B-Mg composites dark brown phases observed were believed to be AlB_{12} particles while light orange brown phases with more faceted edges are known to be AlB_2 particles [7]. A first analysis of the photomicrographs revealed uniform distribution of these aluminum borides in the Al matrix. It was believed that additional formation of AlB_2 particles is due to the decomposition of AlB_{12} during the composite fabrication. One would have expected this to occur at temperatures above the operation ones used in this research since the reaction temperatures reported by the literature is above $900^{\circ}C$ for higher boron concentrations. The following question was therefore posed: Is magnesium favoring the decomposition of AlB_{12} into AlB_2 ? This question will be answered later in this thesis.

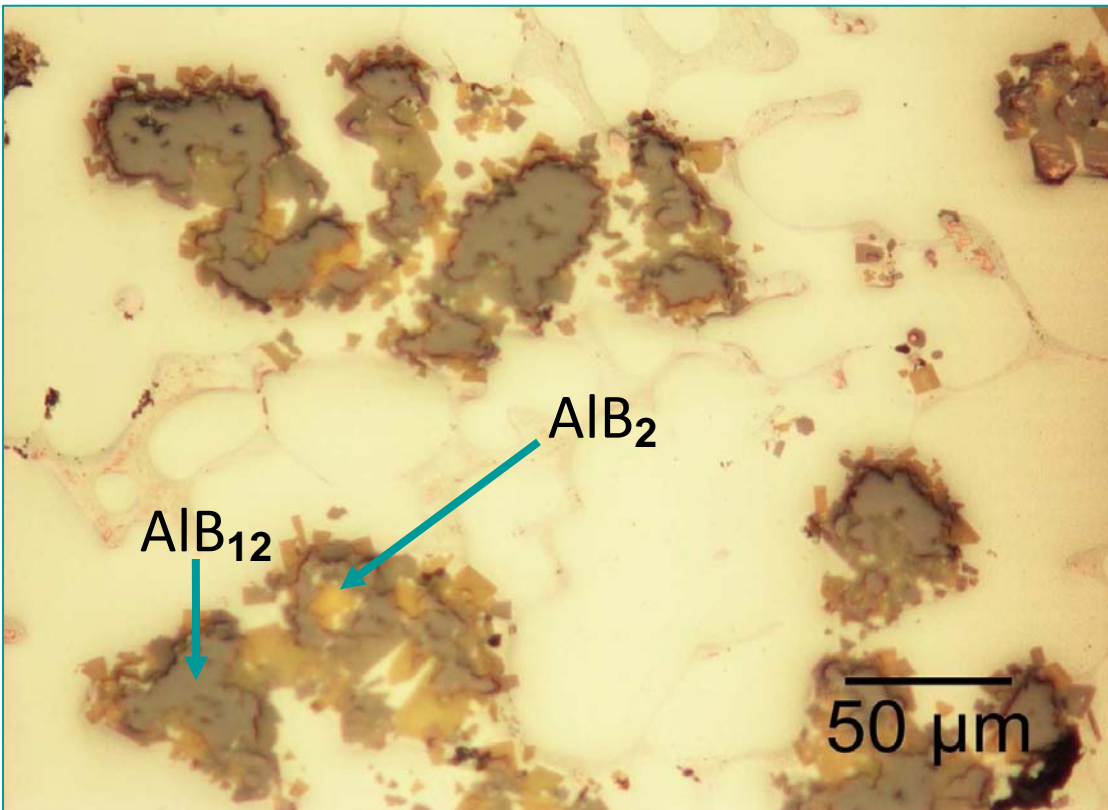


Figure 4.1 Photomicrograph of Al-2 wt. %B- 6 wt. %Mg composite microstructure showing presence of both aluminum borides.

4.1.2 Volume percent of Reinforcement Particles and Pores

The photomicrographs (figures 4.2, 4.3, 4.5, 4.6, 4.8 and 4.9) displayed the manifest effect of the casting parameters (casting time, pouring temperature, and rotational speed) on the redistribution of the reinforcement particles. For the sake of brevity only the micrographs obtained at 15 mm (internal zone) and 60 mm (external zone), Figures 4.3, 4.6, 4.9 and figures 4.2, 4.5, 4.8 are shown respectively. In all cast specimens it was observed that the number of particles increased along the centrifugal

Adelakin Kingsley Tunde, Masters Thesis, UPRM 2009

force direction; the largest particles concentrations occurred, as expected, at the external zones. Nevertheless, there are significant differences in their distribution pattern among different specimens.

When the casting time increased from 1 to 3 minutes, and the rotational speed and pouring temperature are kept constant at 300 rpm and 820°C respectively, noticeably low concentrations of reinforcement particles were observed at 15mm in specimen 2a. This means that the particle segregation rate was heightened by a longer casting time. Although the temperature affects the viscosity of the melt (i.e. the melt fluidity) and the rate of movement of the particles, the preheating (500°C) of the mold and its thickness apparently prevailed as they slowed the heat dissipation rate. Therefore, there exists a larger amount of aluminum boride particles towards the outer periphery of the cast specimens, leaving an inner zone almost depleted of particles.

The comparison between composite specimens with casting time increasing from 1 to 2 minutes (figure 4.4) shows that the lowest amount of particles was found in specimen 2a at 15mm. This shows that longer casting times favored the segregation of the particles towards the outer region of the cast. However, when the casting time increased from 2 to 3 minutes at 15 mm ends more particles segregation was observed in specimen 3a. One would have expected the opposite result, i.e. specimen 3a having lesser amount of particles than specimen 2a. At a distance of 60 mm the amount of aluminum borides increases as their casting time increases from 1 minute to 2 minutes. Detailed observation made on volume percent plots against longitudinal distance (figure 4.4) between specimens, showed that as casting time increases, the concentration of reinforcement particles along casting also increases. It is important to note that the mold helped keep the temperature of the melt to attain low viscosity, which facilitated the movement of the particles.

The solidification time depends on a number of variables, such as heat-transfer coefficient at the composite-mold interface and the thermophysical properties of the solidifying material. In the literature on centrifugal casting, most of the reported experiments were conducted at shorter times and higher rotational speeds [3, 5].

Nonetheless, for the casting times considered in this research particle segregation is still evident. The results obtained are in good agreement with prior works [1, 2, 6-10]; this could be an incentive to study the solidification time during centrifugal casting of functionally graded materials.

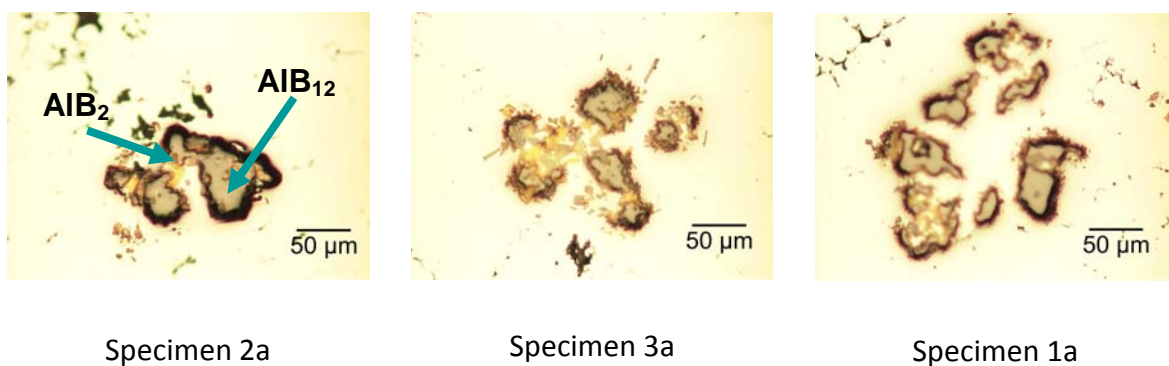


Figure 4.2 Particles distribution in functionally-graded Al-B-Mg composite with variation of casting time at 15 mm.

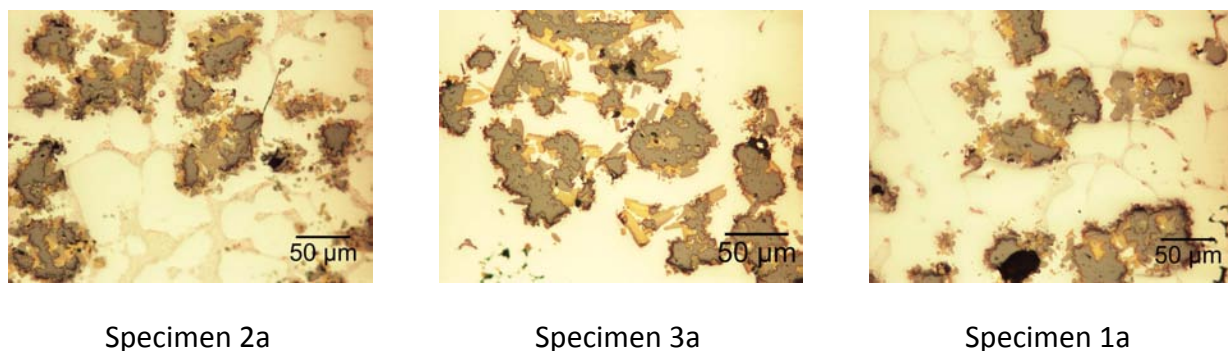


Figure 4.3 Particles distribution in functionally graded Al-B-Mg composite with variation of casting time at 60 mm.

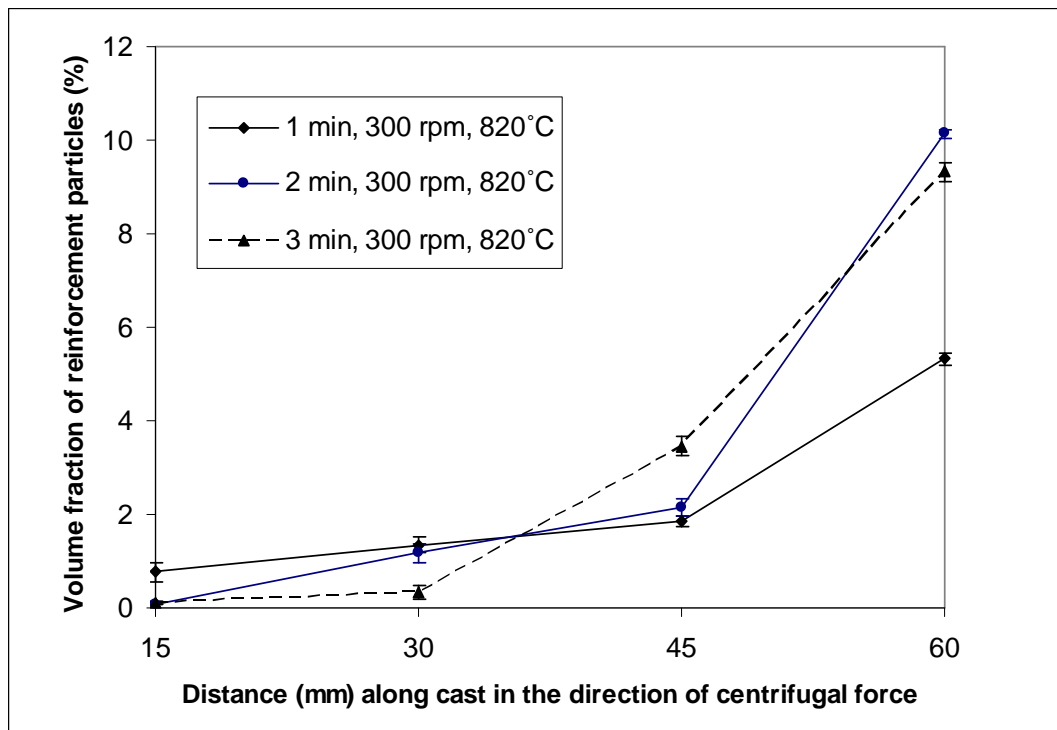


Figure 4.4 Effect of casting time on AlB_{12} and AlB_2 particles segregation along the longitudinal distance of cast specimens (Al-B-Mg).

The effect of the rotational speed could be inferred from figures 4.5 – 4.7. The volume percent of reinforcing particles, i.e. AlB_{12} and AlB_2 , in specimens 3a, 4a and 5a tended to decrease at 15 mm in the following sequence: specimens 3a, 4a and 5a respectively, as rotational speed increased from 300 rpm to 400 rpm. At 60 mm the volume percent of the reinforcement increased as the rotational speed increased when specimens 3a, 4a and 5a are compared. In short, as rotational speed increased the particles steeply increased along the casting towards the outer zones in all specimens. The steepness could be used to differentiate the effect of rotational speed between specimens (figure 4.5 - 4.7). Specimens with higher rotational speed had lesser concentrations of particles at the inner zones (15 mm) and higher particles concentration at the outer zones (60 mm).

Adelakin Kingsley Tunde, Masters Thesis, UPRM 2009

As stated before, the density of the melt affects the viscosity of the melt. An increase in density of the melt results in a higher viscosity of the melt. In such situations, the movement of the particles would be reduced and the solidification front might catch up with moving particles as they travel towards the outer periphery of casting. The centrifugal force plays a very important role in addition to facilitating good mold filling: It compels the particles to move with appreciable speed. This could be the reason why various regions of the cylindrical castings have always been particle rich region and particle depleted zones. At this high speed, most of the particles would have migrated to the outer region of the casting in a shorter time. However, with the rotational speed used in this research, we were able to observe particles segregation along castings [49].

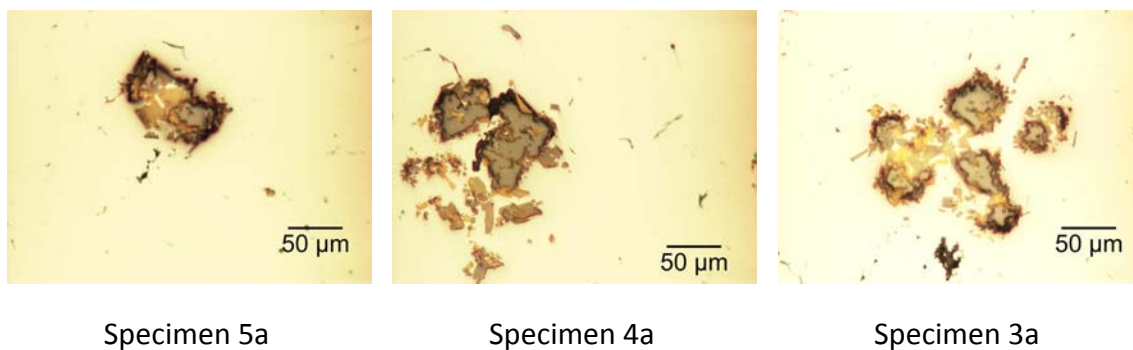


Figure 4.5 Particles distribution in functionally-graded Al-B-Mg composite with variation in rotational speed at 15 mm.

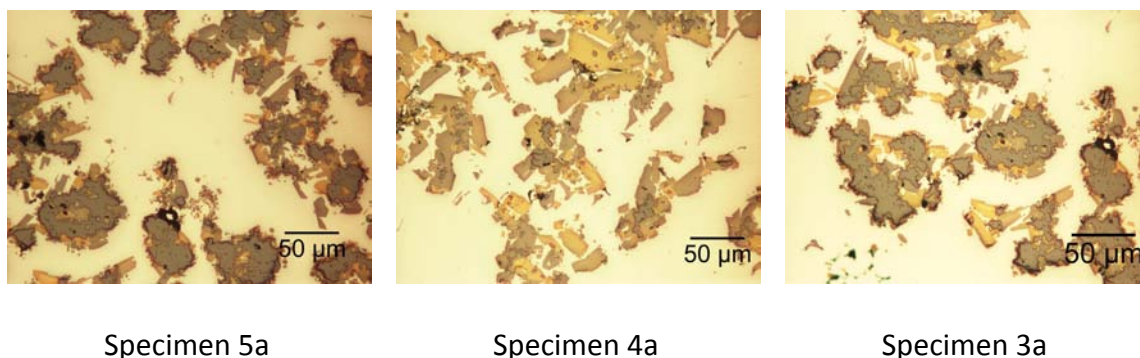


Figure 4.6 Particles distribution in functionally-graded Al-B-Mg composite with variation in rotational speed at 60 mm.

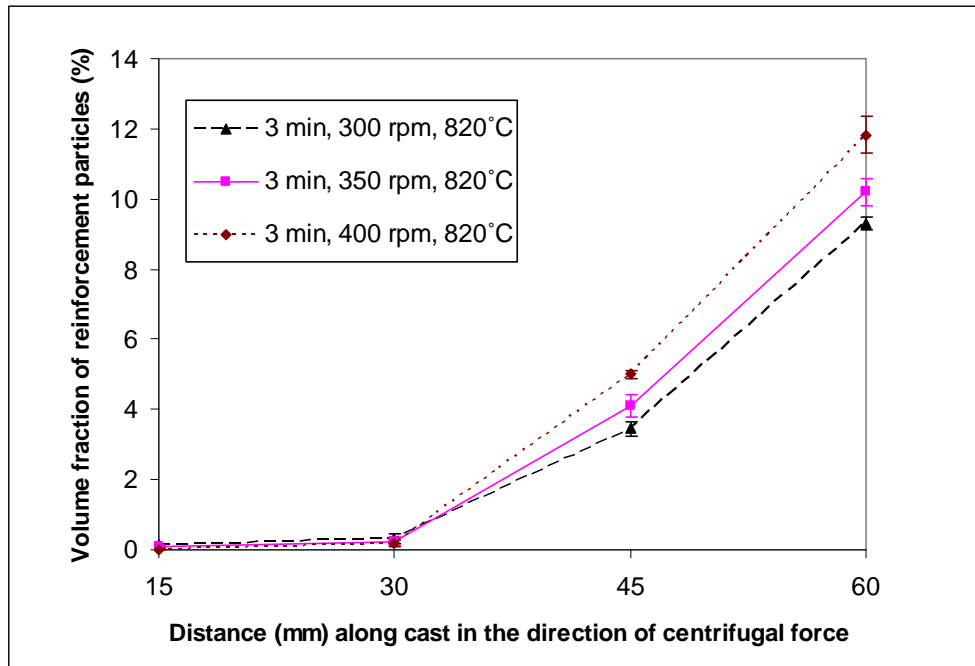


Figure 4.7 Effect of rotational speed on AlB_{12} and AlB_2 particles segregation along the longitudinal distance of the cylindrical centrifugally cast Al-B-Mg specimens.

Pouring temperature is also a critical factor affecting the viscosity of the melt. The interaction among temperature, density and viscosity is of ultimate interest in casting processes [50]. This relation is further studied in Chapter 6. The effect of such temperature on the resulting microstructures is shown in figures. 4.8 – 4.9.

An unambiguous example of temperature effect on the movement of the particles at various distances is presented in figures 4.8 - 4.10. At 15 mm, the amount of particles increased as the pouring temperature decreased from 820°C to 690°C. Conversely, at 60 mm, as the temperature had dropped below the solidification range, a reverse trend is apparent. The specimen 6a (690°C) solidifies before specimen 7a (755°C) and specimen 5a (820°C). Therefore, the particles movement in specimen 6a becomes slower as the viscosity becomes much larger as a result of the solidifying melt.

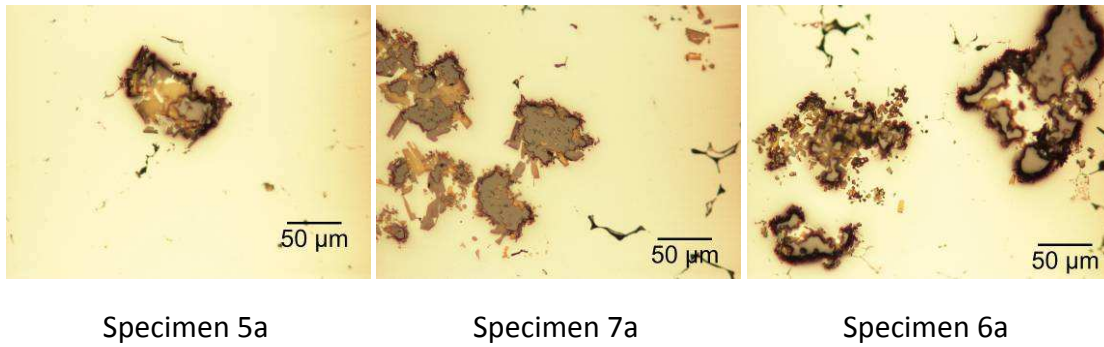


Figure 4.8 Particles distribution in functionally-graded Al-B-Mg composite with variation in pouring temperature at 15 mm.

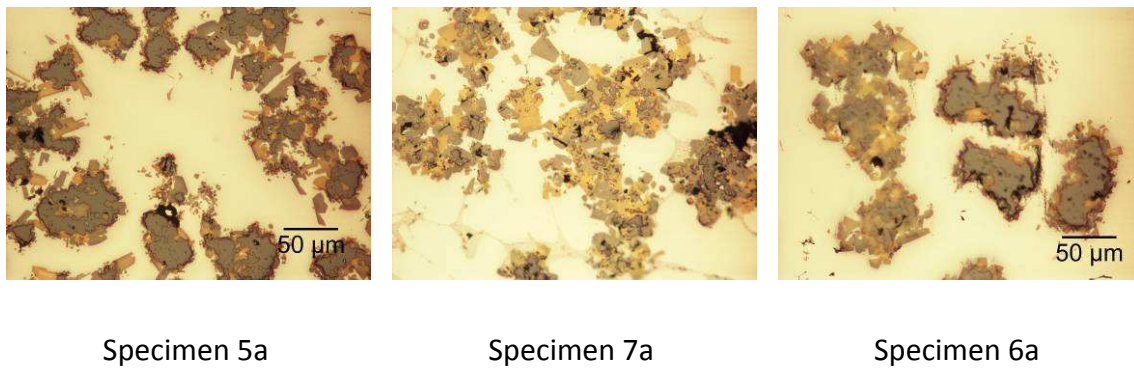


Figure 4.9 Particles distribution in functionally-graded Al-B-Mg composite with variation in pouring temperature at 60 mm.

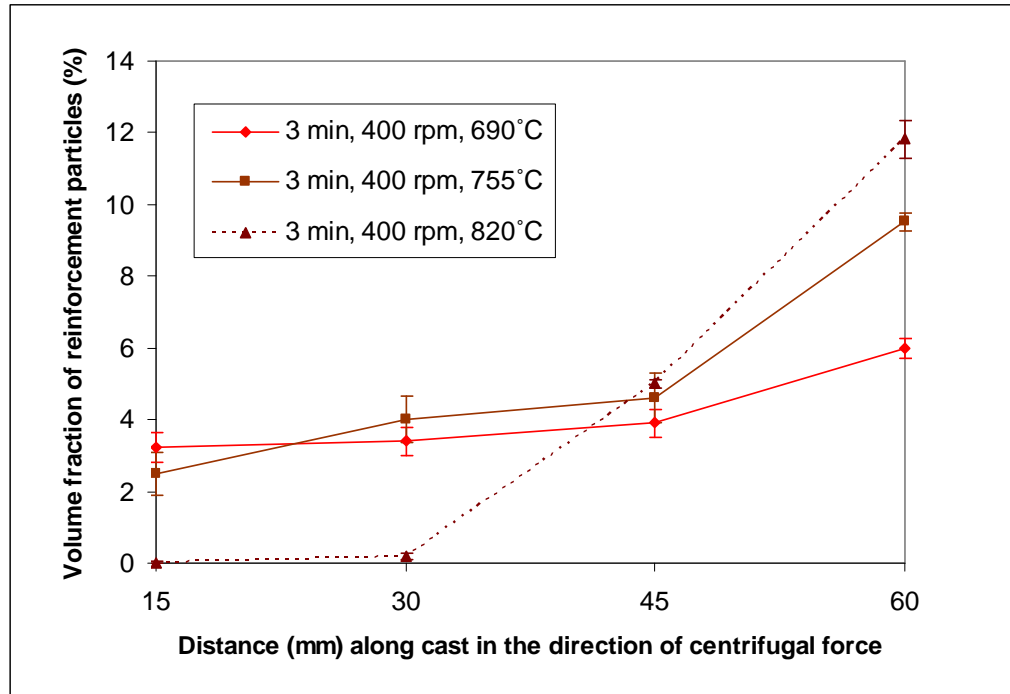


Figure 4.10 Effect of pouring temperature on AlB_{12} and AlB_2 particles distribution along the longitudinal axis of a centrifugally cast Al-B-Mg composite.

4.1.3 Porosity in Centrifugally Cast Al-B-Mg Composites

Figure 4.11 displays the porosity level observed in the castings. The volume percent of pores, as measured in the micrographs of the composites via Image J, ranged from 0.01% to 1.09%. These porosity levels are small and its presence is understandable since the semisolid composites were not degassed before pouring and the fabrication was done in open atmosphere. We did observed influence of casting parameters but the effect of the reinforcement particles was more apparent. In addition, the rotational speeds employed were relatively low and did not cause turbulence that would have helped form high porosity in the casting by trapping air. In general, it was observed that centrifugal casting conditions favored low porosity level in the casting. Our result seems to be in good agreement with previous research [2 and 7].

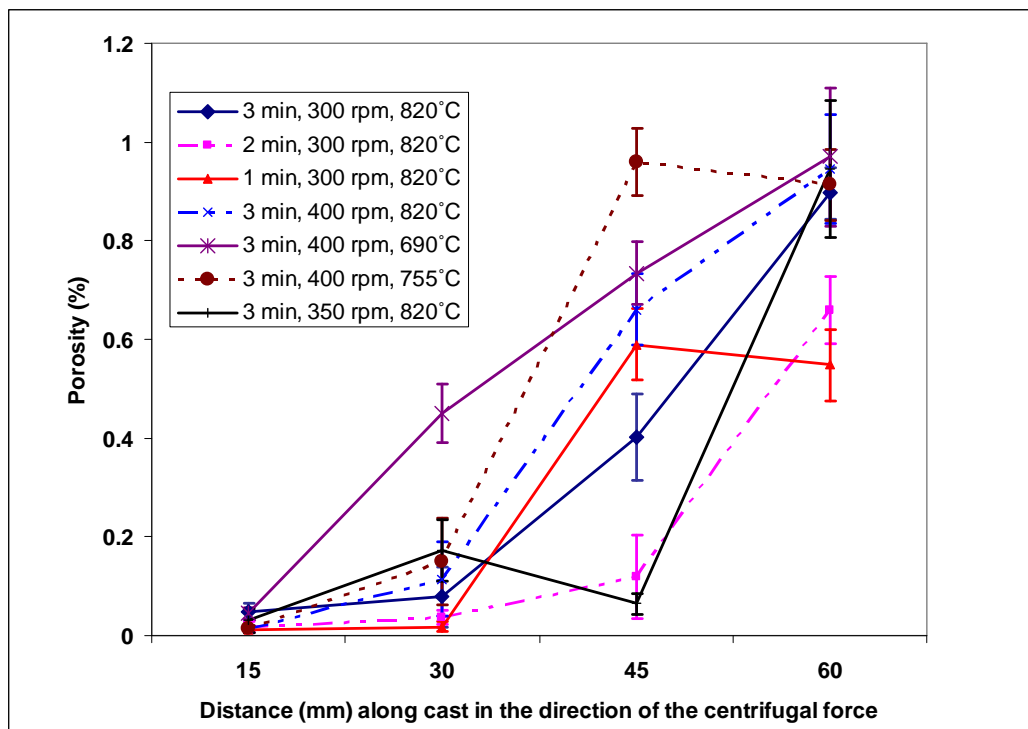


Figure 4.11 Porosity level along longitudinal distance of centrifugally cast Al-B-Mg composites.

4.1.4 Superficial Rockwell Hardness and Vickers Microhardness Tests

The superficial Rockwell hardness test was done following the ASTM E 18 standard. The superficial hardness scale employed on the Al-2wt% B- 6%Mg composite was 15T: This is 15 kgf of final load applied with a 1/16" ball indenter. Fifteen indentations were done on surfaces along the cast to measure data dispersion and to increase accuracy in the hardness values.

Results of the superficial Rockwell hardness tests conducted on the Al-B-Mg specimens are displayed in figures 4.12, 4.13, and 4.14 considering the variation of the casting parameters: casting time, rotational speed and pouring temperature of melt.

Adelakin Kingsley Tunde, Masters Thesis, UPRM 2009

These results further corroborate the fact that the composite is not only compositionally graded but also functionally graded, as the hardness values on each composite specimen follows the same pattern as that of the volume amount of reinforcement along the direction of the centrifugal force. In other words, these results are a direct consequence of the segregated aluminum boride particles along the cast.

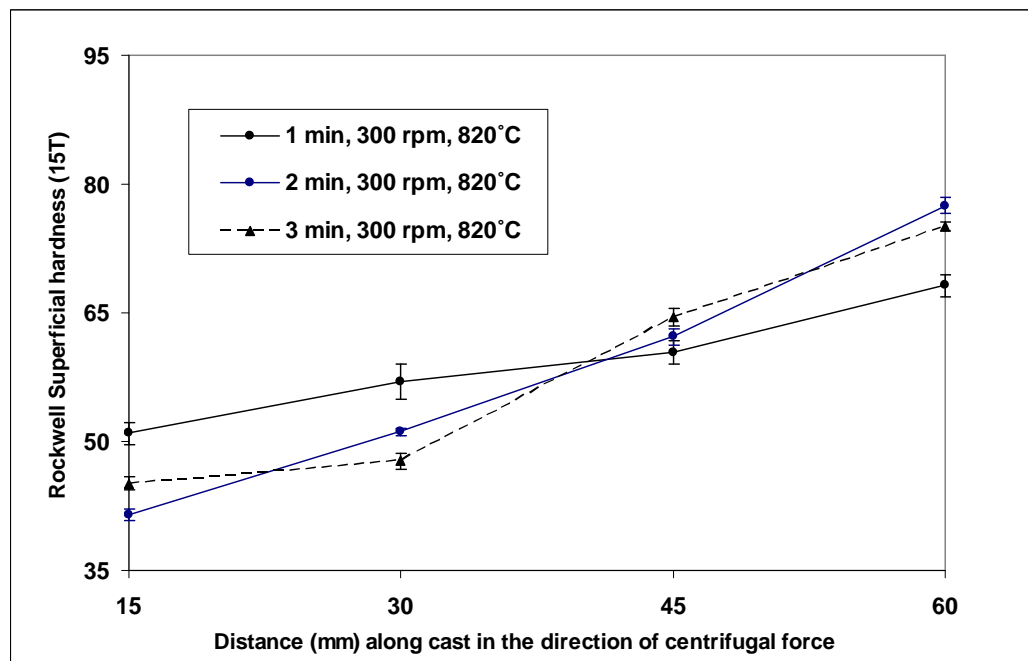


Figure 4.12 Effect of casting time on superficial Rockwell hardness along the longitudinal axis of the centrifugally cast Al-B-Mg composites.

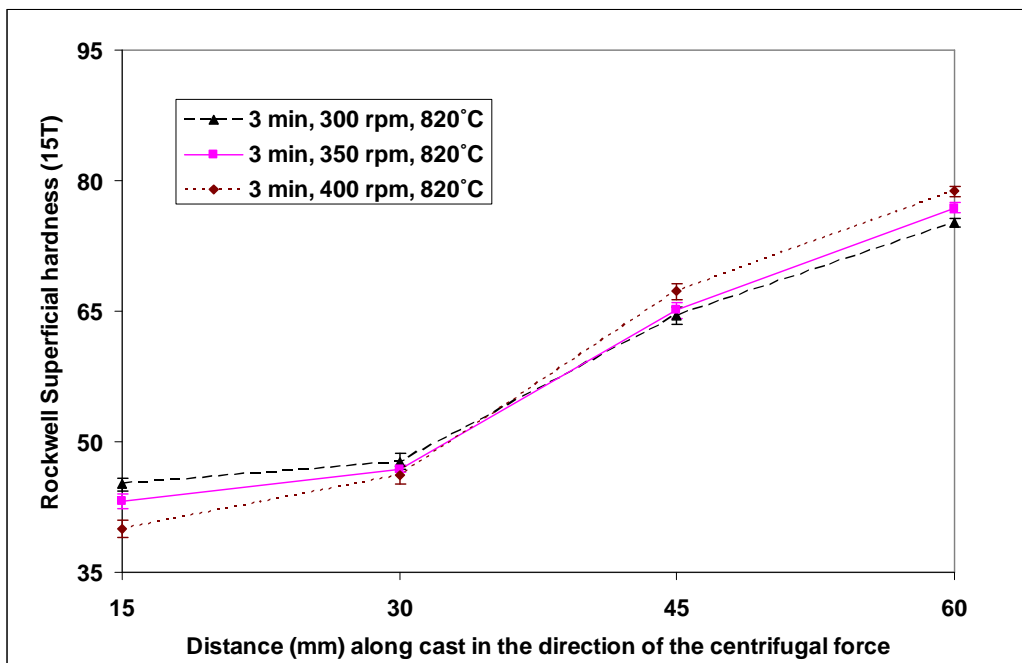


Figure 4.13 Effect of rotational speed on superficial Rockwell hardness along the longitudinal axis of the centrifugally cast Al-B-Mg composites.

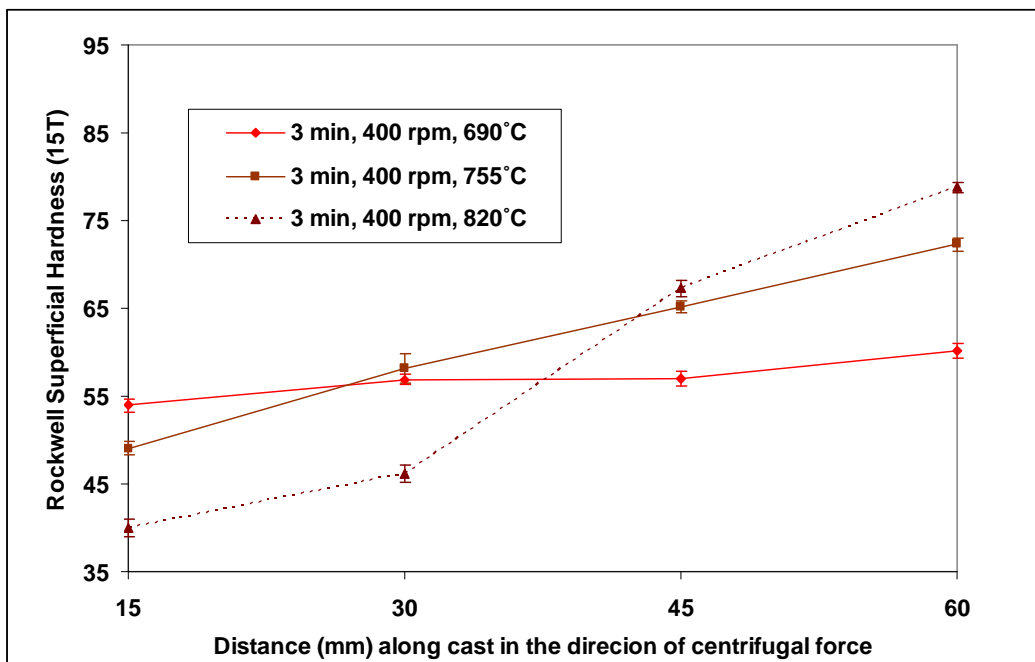


Figure 4.14 Effect of pouring temperature on superficial Rockwell hardness along the longitudinal axis of the centrifugally cast Al-B-Mg composites.

ASTM E 384 standard was followed to determine microhardness value of the Al-B-Mg composite. These microhardness measurements were made exclusively on the matrix of the Al-B-Mg composite specimens at room temperature (25°C). A Buehler-Micromet II microhardness indenter was employed with 25 gf of test load applied for 15 seconds for each indentation. A total of 15 evenly spaced indentations were made on the matrix surfaces of each samples. From these data, an average Vickers microhardness value (Hv_{25}) was determined.

Results of microhardness measurements are summarized in figures 4.15 – 4.17, reflecting the effect of the casting parameters. It should be noted that these results also exhibit a similar pattern as those of the volume amount of particles and the superficial Rockwell hardness values reported previously. This is discussed in detail in Chapter 6.

In an earlier investigation [7] on a similar composite Vickers microhardness values did not noticeably increased as superficial Rockwell hardness values along a similar cylindrical casting. Conversely, in this thesis the value of the Vickers microhardness reflect a similar trend as the superficial hardness values along the cast. This could have been influenced by the higher Mg concentration in the present composites. It is apparent then that the magnesium level strengthened the Al matrix resulting in higher hardness values.

Superficial Rockwell hardness followed the same trend as Vickers microhardness along the cast specimens. However, the mechanism for the raise in Vickers microhardness values along the castings is not yet clearly understood. Nevertheless, the trend observed is that, as the number of reinforcement particles increased along the castings, Vickers microhardness also increased.

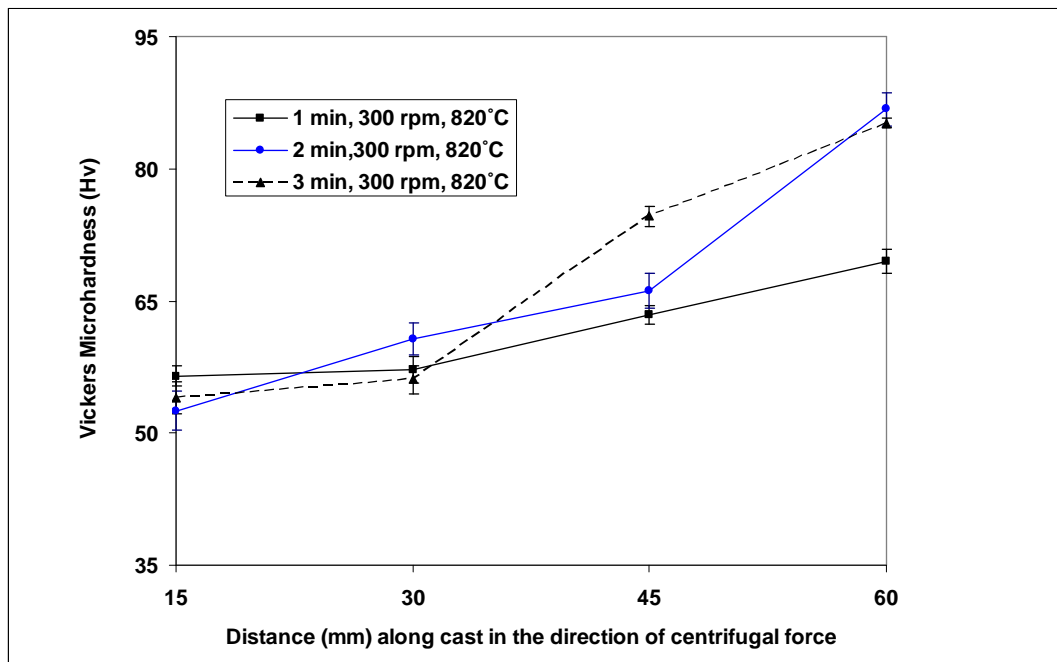


Figure 4.15 Effect of casting time on Vickers microhardness along the longitudinal axis of the centrifugally cast Al-B-Mg composites.

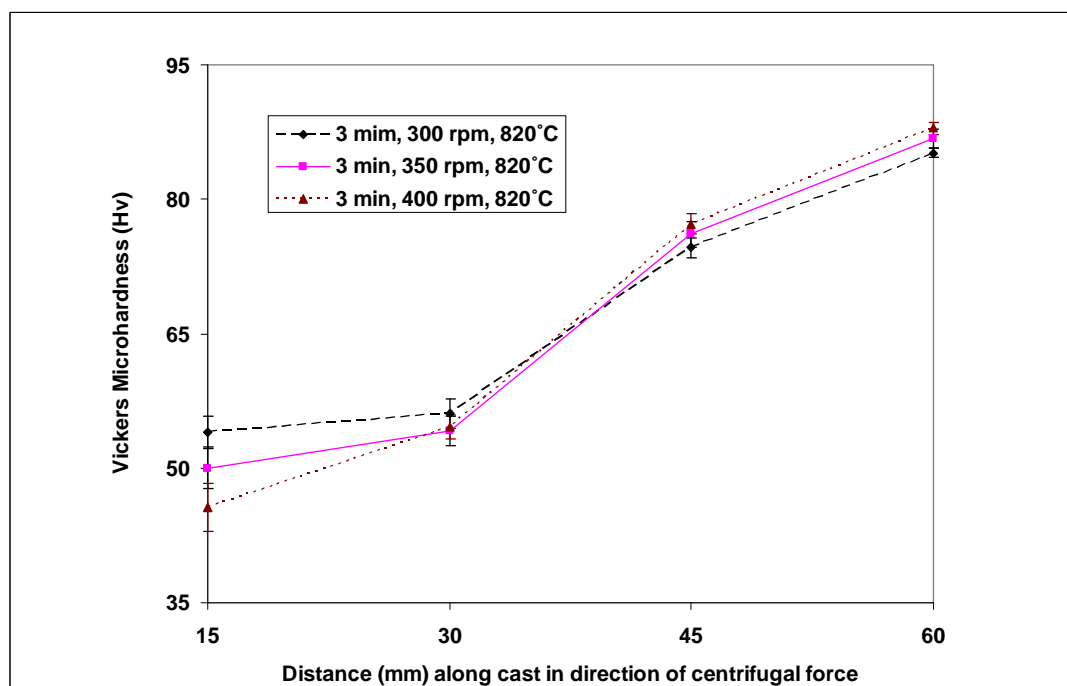


Figure 4.16 Effect of rotational speed on Vickers microhardness along the longitudinal axis of the centrifugally cast Al-B-Mg composites.

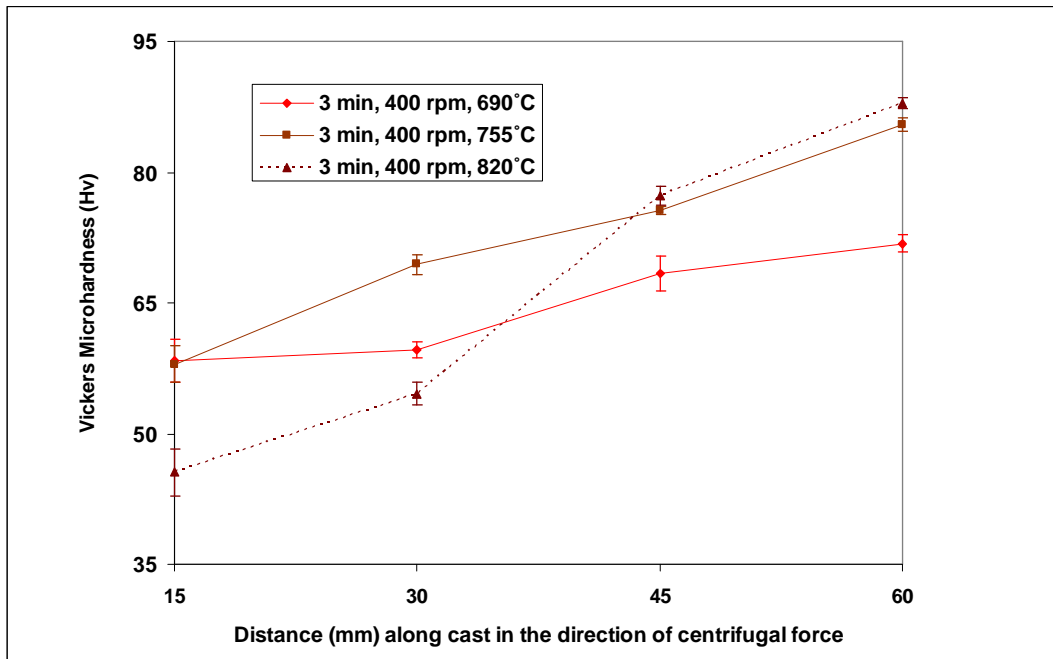


Figure 4.17 Effect of pouring temperature on Vickers microhardness along the longitudinal axis of the centrifugally cast Al-B-Mg composites.

4.1.5 Particle size in the Al-B-Mg composites

Quantitative analysis with Image J permitted measuring the average size of the particles. However, the results will not be discussed in this thesis because the morphology of the aluminum boride particles and the clustering of the particles made it difficult to obtain a clear size distribution. However, particle size ranging from 1 μm to 18 μm with an average size of 5 μm was determined. The smaller particles are likely the result of a phase transformation of the aluminum dodecaboride particles. This topic is discussed later.

4.1.6 Effect of Magnesium on the Particle Morphology during Centrifugal Casting

It is believed that magnesium had a significant influence in this functionally graded Al-B-Mg composites. This alloying element not only favors excellent wettability between particles and the liquid matrix [31], but also aid in the decomposition of the AlB_{12} particles. Since the density of the transformed phase is more than that of the melt, the AlB_2 particles (3.19 g/cm^3) move towards the periphery of the cast specimens [7]. The segregation of AlB_{12} particles is also favored in great extent as Mg decreases the density of Al linearly by approximately 0.5% for every 1 wt% Mg in the Al melt [35]. At the same time Mg decreases the liquid viscosity favoring the particles movement. The affinity of magnesium to aluminum boride reinforcement particles is discussed in detail in Chapter 6 of this thesis.

The transformation kinetics of the AlB_{12} into AlB_2 involves two stages, which may occur simultaneously. The first one involves forming of the faceted AlB_2 by decomposing the larger dodecaborides while the second one entails the diffusion of magnesium into the aluminum diborides formed. This is further explained by the schematic in figure 4.18. Stage "A" shows the AlB_{12} in contact with the liquid containing Mg atoms just before the transformation; the particle still retains its original irregular morphology. At stage, "B" the irregularly shaped AlB_{12} starts decomposing with the formation of very small AlB_2 particles. Further contact of the dodecaboride with the the aluminum melt results in more development of the faceted diboride particles. Moreso, at stage "D" the AlB_{12} is much tranformed into small AlB_2 particles that then break away from the edges of the dodecaboride but remains surrounding the AlB_{12} . The role played by the centrifugal casting parameters can provide more explanation on the phase transformation kinetics involved as the particles move from the inner zones of casting

Adelakin Kingsley Tunde, Masters Thesis, UPRM 2009

towards the outer periphery. It is believed also that the diffusion of magnesium into the diborides is the last stage that occurs during the transformation process. As mentioned previously, this is to be further studied by microchemical analysis. Since the transformation stages happened in short time or, perhaps, simultaneously one might not be able to differentiate the phase change from the diffusion stage. The micrographs (figures 4.2 and 4.3) also corroborated the transformation of the AlB_{12} large particles into more faceted but smaller AlB_2 particles.

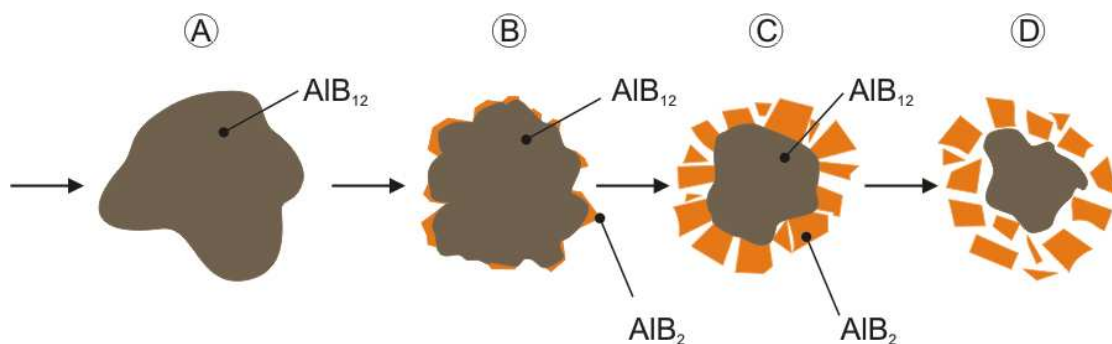


Figure 4.18 Phase morphology of the aluminum boride particles in Al-B-Mg composite melt during centrifugal casting.

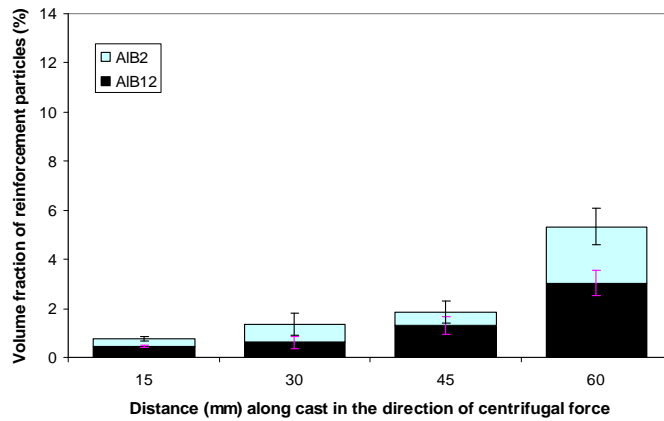
Figures 4.19 - 4.21 show the results obtained from the volume fraction analysis of aluminum boride phase transformation occurring during the Al-B-Mg composite processing. The effect of magnesium interacts with the effect of the centrifugal casting parameters (casting time, rotational speed and pouring temperatures). The analysis of the volume percent of the reinforcing particles was completed using Image J. Figure 4.18 along with figures 4.19 – 4.21 will be used to explain such interaction. In effect stages A, B, C, and D in figure 4.18 might very well be occurring at the distances of 15 mm, 30 mm, 45 mm, and 60 mm of the functionally graded cylindrical specimens. As the AlB_{12} particle migrates from 15 mm to 30 mm, the chances of getting in contact with a fresh melt increases the destabilization of the AlB_{12} and some AlB_2 particles are formed.

Adelakin Kingsley Tunde, Masters Thesis, UPRM 2009

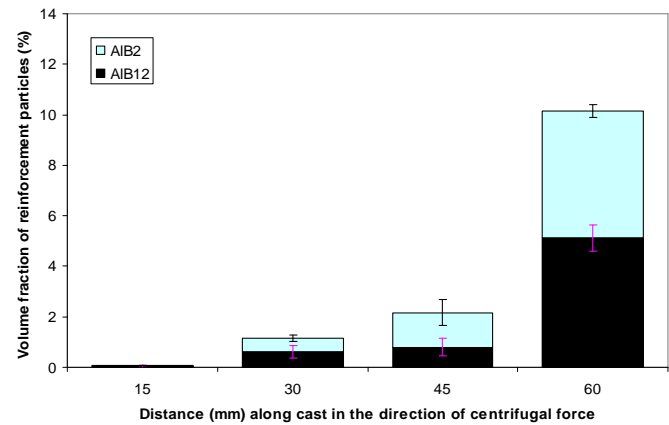
Further movement to the 60 mm point, i.e. stages C to D, increases the formation rate of the AlB_2 on those regions of the casting.

The effect of magnesium as a function of casting time in the transformation of AlB_{12} phases into AlB_2 is shown in figure 4.19. These results demonstrate the segregation pattern along the casting with the phase transformation of the aluminum boride phases. In figure 4.18, initially the melt was saturated with magnesium at the operation temperature. This particle then moves in intimate contact with the melt. As the particle becomes in contact with fresh melt more smaller diborides form. The magnesium effect increases as the particles further maintain contact with fresh melt as they move towards the outer periphery (60 mm) of casting.

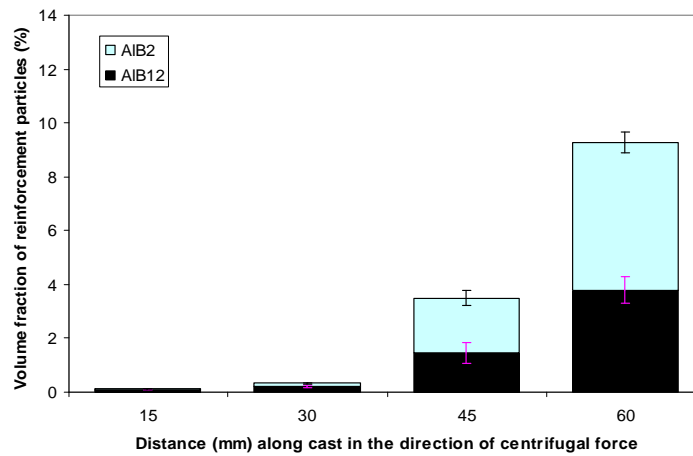
The results displayed in figure 4.19 show that as the transformation takes place, the particles continue to move towards the outer periphery of the casting assisted by a lower melt viscosity. A comparison among specimens 1a, 2a, and 3a shows that long casting time at the same rotational speed and pouring temperature favor more AlB_2 at 60 mm of specimen 3a. This is understandable because the longer the time particles are in contact with the melt, the longer the time available for AlB_2 to form. The appearance of this phase at 60 mm or its depletion at 15 mm is enhanced by the rate of contact of the particles with the melt and further aided by the centrifugal casting parameters.



Specimen 1a



Specimen 2a

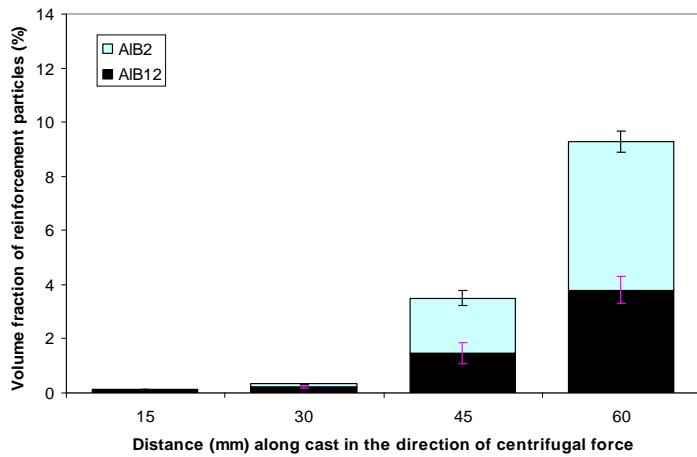


Specimen 3a

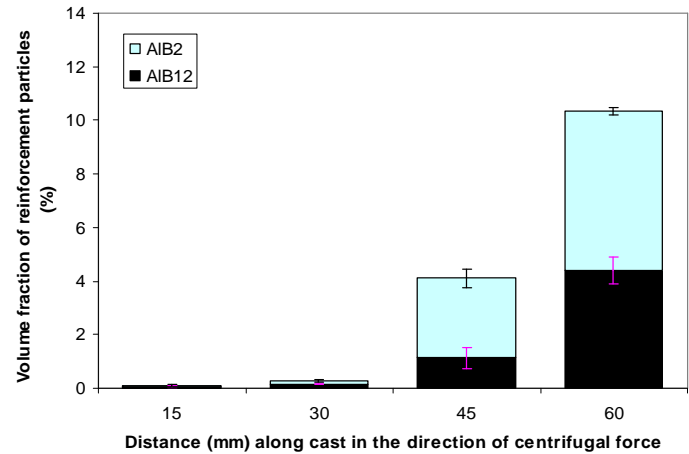
Figure 4.19 Effect of casting time on the formation of aluminum boride phases along the casting.

The effect of rotational speed in the formation of AlB_2 can be observed in figure 4.20 and reflects what was previously explained in figure 4.18. Comparison among specimens 3a, 4a and 5a shows that the increase in rotational speed caused an increase in the formation of AlB_2 phases at 60 mm. Apparently, the rotational speed prompted the formation of aluminum diboride particles by increasing the centrifugal forces acting on the dodecaboride dispersoids, which become in contact faster with fresh liquid Al (with Mg in solution). As the AlB_2 particles formed, they are also impelled by the centrifugal forces towards the periphery of the casting. Specimen 5a (400 rpm) has the highest amount of AlB_2 phase formed, followed by that of 4a (350 rpm) and 3a (300 rpm).

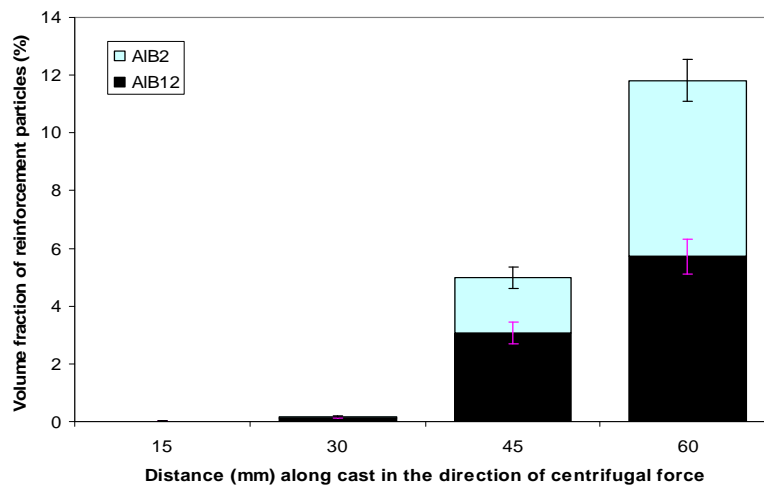
Figure 4.21 shows the effect of pouring temperature on the formation of the AlB_2 along the cylindrical cast specimens. At the various pouring temperatures, the aluminum dodecaboride phase decomposed but the rate of decomposition is evidently affected by temperature. The specimen fabricated at the highest pouring temperature had more time before it reached the solidification temperature range; as a result, the particles could move faster to make contact with fresh liquid Al-Mg. As more contact was made, more aluminum boride phase formed at 60 mm. It is observed that the transformed particles concentration gradient is steepest at the 60 mm for specimen 5a, then specimen 7a and 6a. These results were further corroborated by the micrographs and energy dispersion spectroscopy analysis.



Specimen 3a

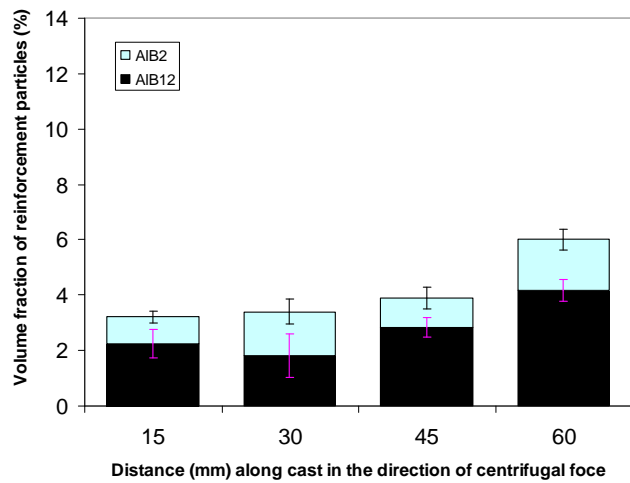


Specimen 4a

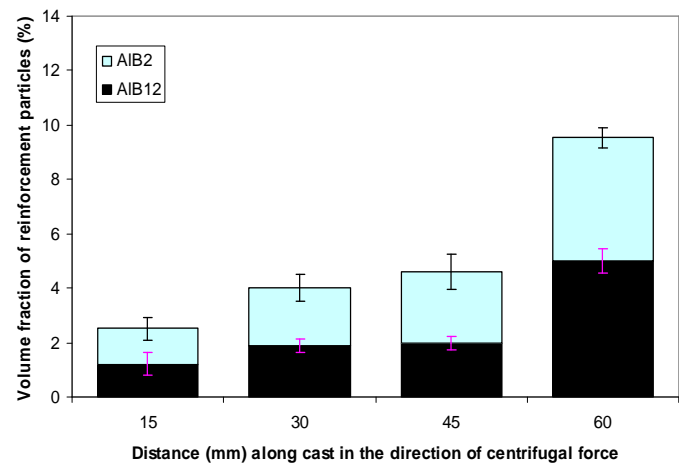


Specimen 5a

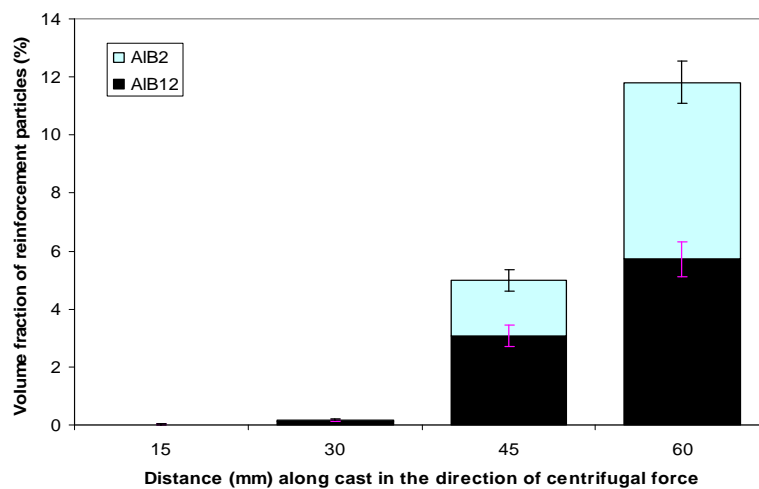
Figure 4.20 Effect of rotational speed on the formation of aluminum boride phases along cylindrical casting.



Specimen 6a



Specimen 7a



Specimen 5a

Figure 4.21 Effect of pouring temperature on the formation of aluminum boride phase along cylindrical casting.

5 STUDY OF Al-B PHASES IN Al-Cu-B COMPOSITE

5.1 Characterization of the Al-B-Cu composites

This chapter deals with the characterization of an Al-B-Cu composites produced via centrifugal casting method. The influence of the centrifugal casting parameters is discussed.

5.1.1 Analysis of the Microstructure

The photomicrographs in figures 5.1 – 5.3 of the functionally graded Al-B-Cu composites revealed two dispersed phases embedded in the Al matrix: a dark brown one (later found to be AlB_{12} particles) and a goldish grey one, later identified as Al_2Cu [33]. It was observed that most of the AlB_{12} phase (figure 6.7a, in section 6.1) originally present in the Al-7.2 wt. %B master alloy did not transform upon processing.

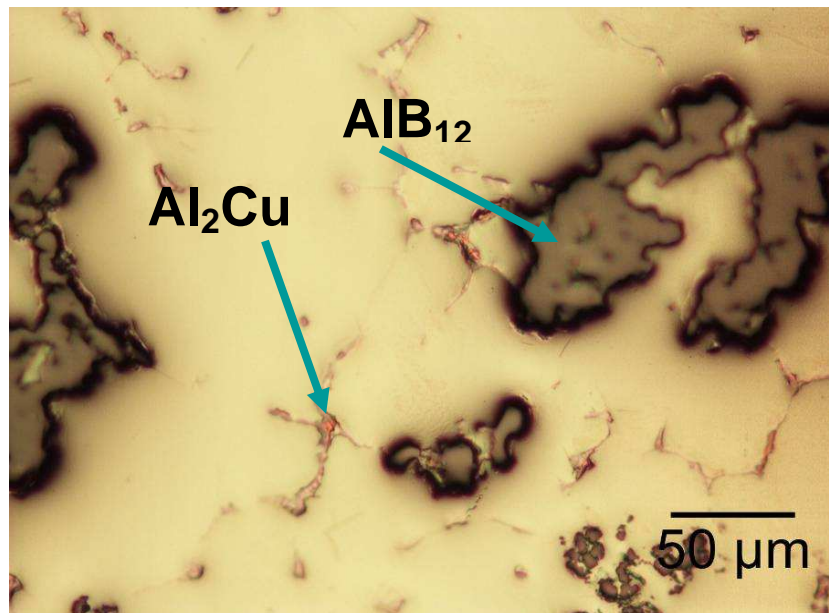


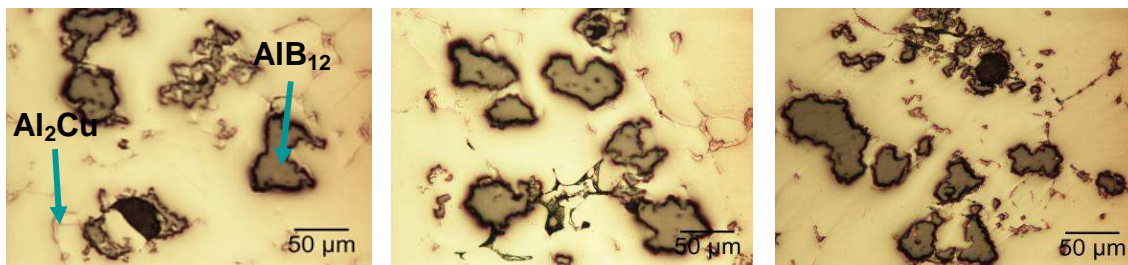
Figure 5.1 Photomicrograph of Al-B-Cu composite typical microstructure (Al-2 wt. %B-6 wt. %Cu) showing presence of AlB_{12} and Al_2Cu phases.

5.1.2 Volume percent of Reinforcement Particles and Pores

Quantitative image analysis of the reinforcement redistribution throughout the castings of Al-B-Cu composites permitted studying the role of the centrifugal casting parameters. The microstructural gradient was mapped throughout the four cross sections (figure 3.4, in section 3.1.1). For the sake of conciseness, only the ones obtained at the both end sections of the casting, i.e. 15 mm (internal zones) and 60 mm (external zones), are presented in figures 5.2, 5.3, 5.5, 5.6, 5.8 and 5.9. The microstructural observations of sections of these centrifugal castings show that the AlB_{12} particles are in effect segregated towards the outer zones of the castings.

In a previous investigation, it was established that one of the major factors that controlled the composition gradient of aluminum matrix composites is the viscosity of the semi-solid mixture [51]. The movement of the AlB_{12} particles was significantly affected as a result of the composition of the alloying element (namely copper) present in the melt. It is believed that copper contributed to an increase in viscosity. Nevertheless, microsegregation of the intermetallic phase (Al_2Cu) probably due to coring (caused by a limited Cu diffusion in the freshly solidified Al) is beyond the scope of this thesis.

The result obtained from the plots of volume percent of AlB_{12} particles along the longitudinal axis of cast Al-B-Cu composites (figure 5.4) shows the effect of casting time. When this is varied from 1 to 3 minutes, and the rotational speed and pouring temperature are kept constant at 300 rpm and 820C respectively, the increase in concentration of particles at 15 mm are in shown in specimen 3b to specimen 1b in figures 5.2 – 5.4. At 60 mm, the concentration of particles increased as their casting time increases, as shown in specimens 1b to 3b in figure 5.4. The longer casting time results in an increase in particles concentration at the external zones of the casting. The viscosity is only affected when the melt temperature drops with time.

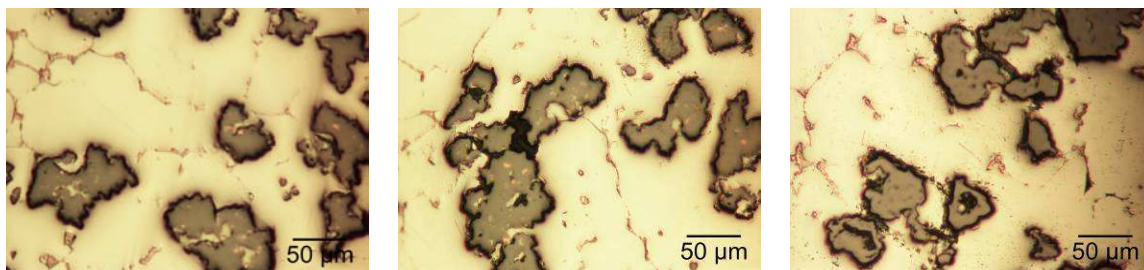


Specimen 3b

Specimen 2b

Specimen 1b

Figure 5.2 Particles distribution in functionally-graded Al-B-Cu composite with variation of casting time at 15 mm.



Specimen 3b

Specimen 2b

Specimen 1b

Figure 5.3 Particles distribution in functionally-graded Al-B-Cu composite with variation of casting time at 60 mm.

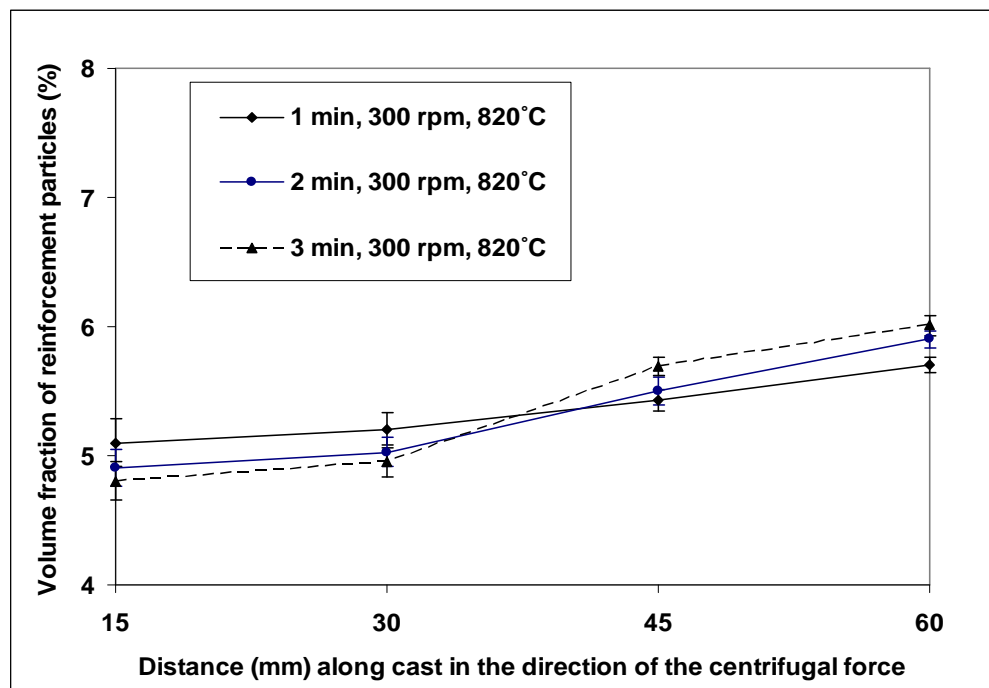


Figure 5.4 Effect of casting time on AlB_{12} particles segregation along the longitudinal distance of cast specimens (Al-B-Cu).

Figures 5.5 through 5.7 show the effect of rotational speed of the mold on the redistribution of the reinforcement particles along the main axis of the castings. An increase in the concentration of particles from the inner zones to the outer ones along the casting was also noticed. A comparison between specimens in terms of concentration of reinforcement particles along the castings (figure 5.7) shows the effect of the rotational speed. At 15 mm (figure 5.7), volume percent of the reinforcement particles (AlB_{12}) in specimens, i.e. from specimens 3b to 5b decreases as the rotational speed increases from 300 rpm to 400 rpm. However, at 60 mm the concentration of the reinforcement particles increases as the rotational speed increases. This is well illustrated in specimen 5b, which shows a significant increase at 60 mm compared to the other two specimens.

The rotational speed appears to be a strong factor during centrifugal casting by directly influencing the motion of the particles. This means that, with more speed at

Adelakin Kingsley Tunde, Masters Thesis, UPRM 2009

constant casting time and pouring temperature, we could obtain more particles migrating towards the outer zones of the casting.

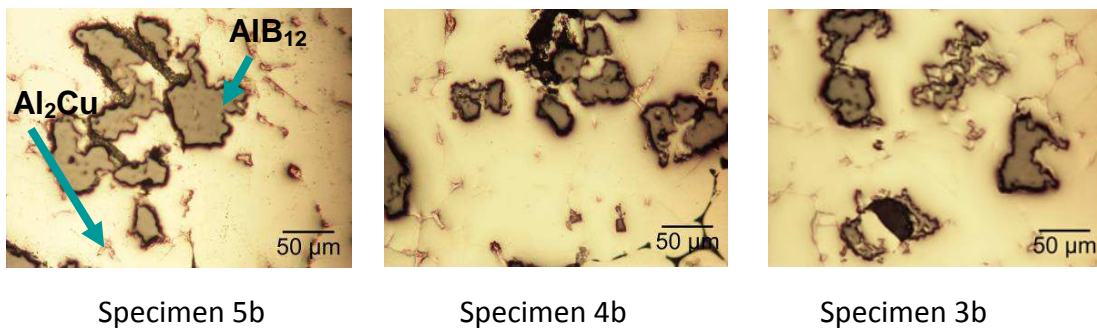


Figure 5.5 Particles distribution in functionally-graded Al-B-Cu composite with variation of rotational speed at 15 mm.

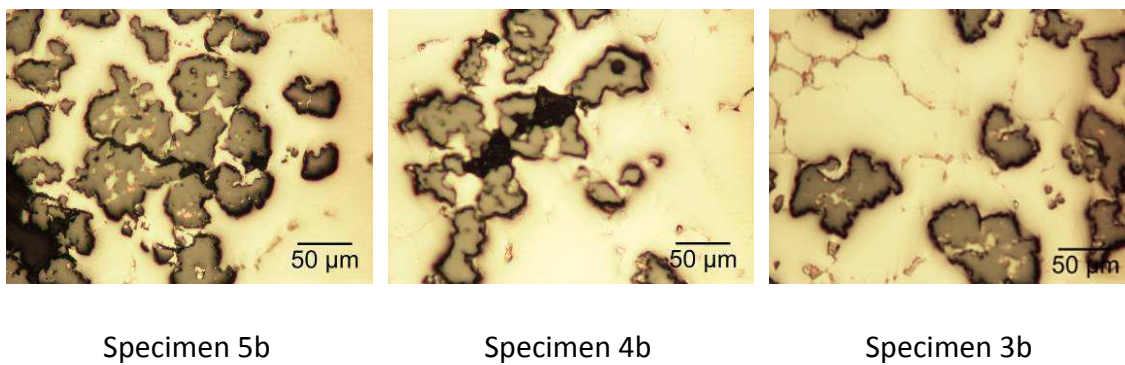


Figure 5.6 Particles distribution in functionally-graded Al-B-Cu composite with variation of rotational speed at 60 mm.

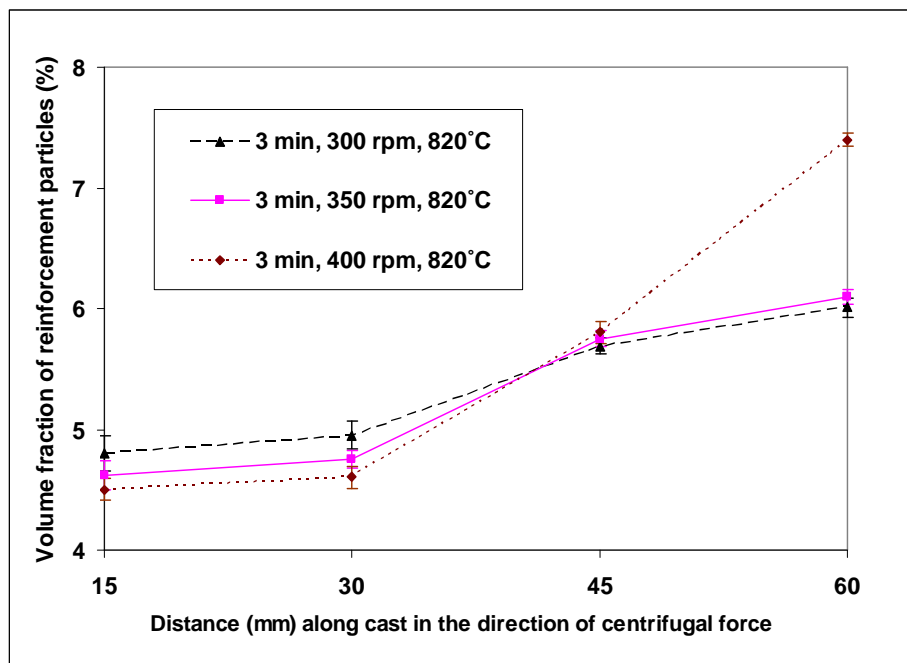


Figure 5.7 Effect of rotational speed on AlB_{12} particles segregation along the longitudinal distance of centrifugally cast Al-B-Cu specimens.

Figures 5.8 and 5.9 demonstrate the effect of pouring temperature on the microstructure of Al-2 wt. %B- 6 wt. %Cu composite. Figure 5.10 shows how the volume fraction of reinforcements varied along the main axis of the centrifugally cast specimens when the pouring temperature of the melt changes. The results again showed an increase in the amount of particles AlB_{12} particles towards the outer region of the casting. The effect of the pouring temperature on the segregation is manifest and has been attributed to the viscosity of the melt. In effect, at higher pouring temperatures ($820^{\circ}C$), the melt is less viscous when compared to melts at temperatures $755^{\circ}C$ and $690^{\circ}C$. At 15mm (figure 5.10), the amount of particles increased as the pouring temperature decreased from $820^{\circ}C$ to $690^{\circ}C$. In other words, the lack of sufficient viscosity hampers the particle segregation caused by the centrifugal forces. This change in viscosity along the cast specimen will be further discussed in Chapter 6, where the

Adelakin Kingsley Tunde, Masters Thesis, UPRM 2009

volume fraction of the reinforcement and the aluminum melt are used to estimate apparent viscosities.

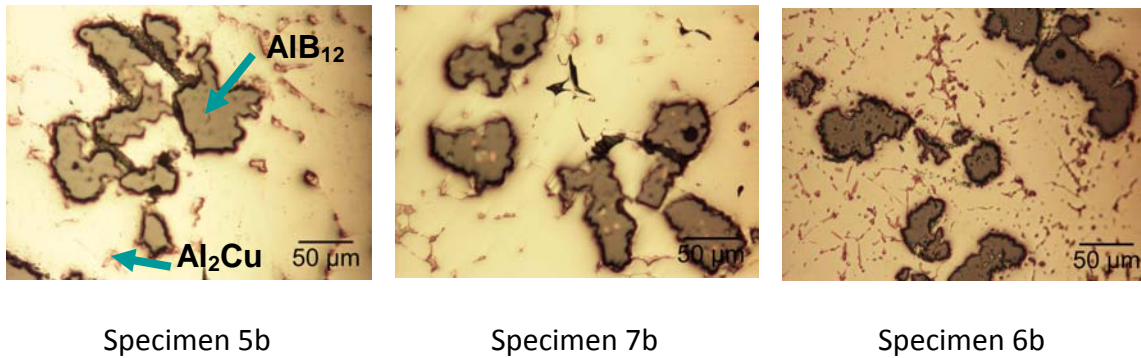


Figure 5.8 Particles distribution and the effect of pouring temperature at 15 mm of a centrifugally cast Al-B-Cu composite.

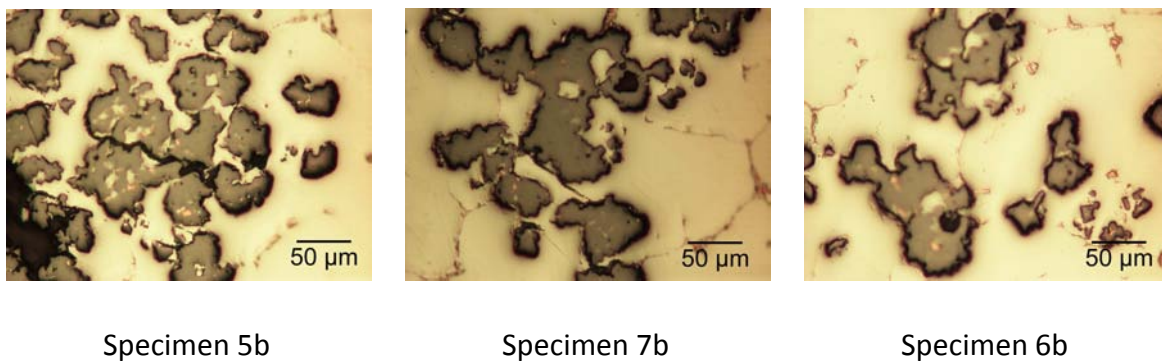


Figure 5.9 Particles distribution and the effect of pouring temperature at 60 mm of a centrifugally cast Al-B-Cu composite.

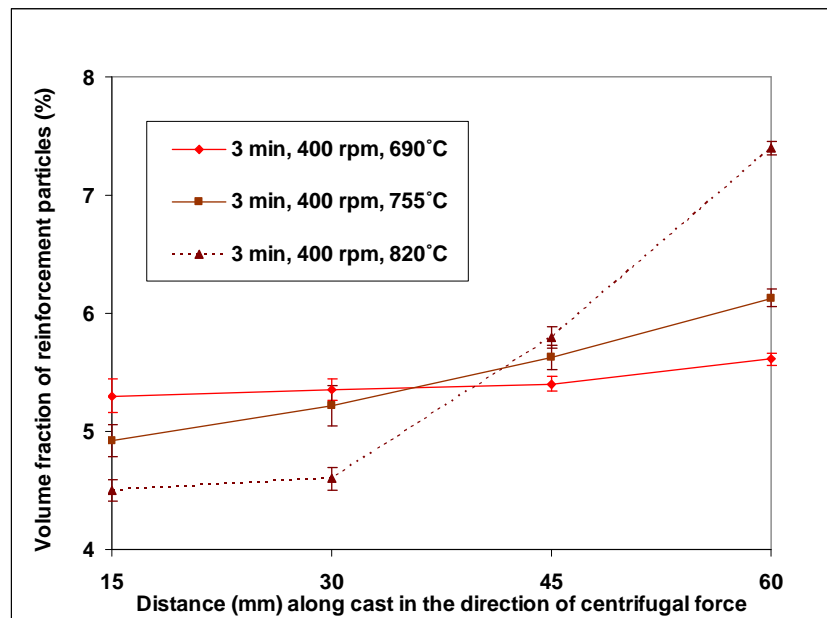


Figure 5.10 Effect of pouring temperature on boride particles distribution along the longitudinal axis of a centrifugally cast Al-B-Cu composite.

5.1.3 Porosity in Centrifugally Cast Al-B-Cu Composites

The porosity levels obtained from the experimental functionally grade Al-B-Cu composites via image J ranged 0.04% to 2.0%. Figure 5.11 presents the porosity variation caused by centrifugal casting parameters along the longitudinal distance of the cast Al-B-Cu composites. In the fabrication of the Al-B-Cu composites, both reinforcement particles and gas bubbles moved under the influence of centrifugal force.

The porosity level increased along the cast as the concentration of the reinforcement increases. It was also observed that the pore volume percent increased as the rotational speed of the mold was raised from 300 rpm to 400 rpm. Based on the microstructure it is believed that the reinforcement particles encircled the gas bubbles (a feature inherited from the Al-B master alloys), trapped them and force them to move along as the particles travel under the action of the centrifugal force. As a consequence,

Adelakin Kingsley Tunde, Masters Thesis, UPRM 2009

porosity increased with the concentration of particles along the casting. Variation of casting time, rotational speed and pouring temperature has been shown to affect the porosity level in the castings. It is likely that an increase in the melt viscosity is affecting the resulting porosity: At lower casting temperatures (690°C and 755°C), the porosity levels at the outer periphery seems to be high.

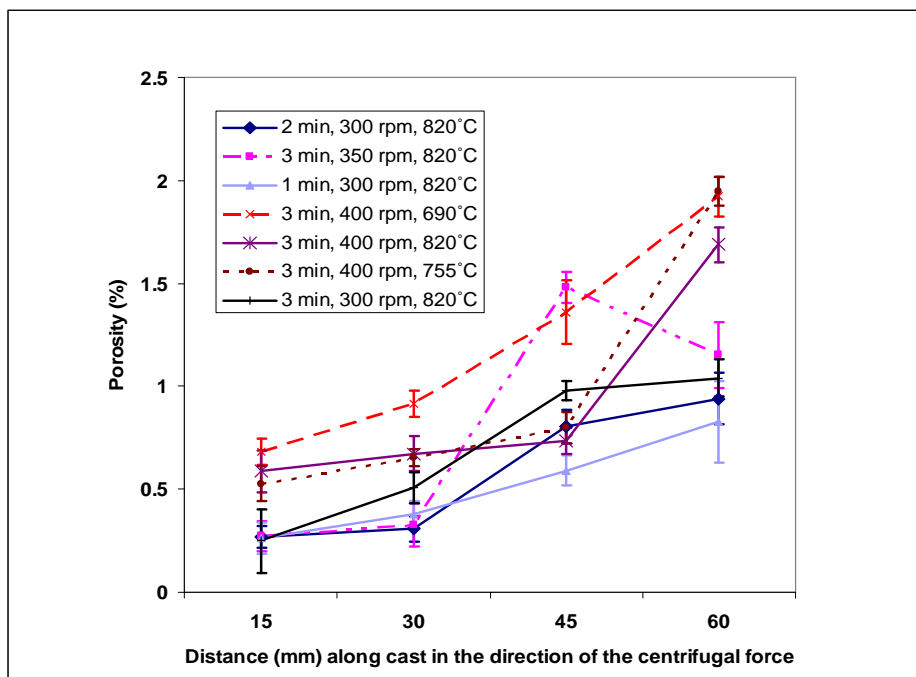


Figure 5.11 Measured volume percent of pores along the longitudinal axis of a centrifugally cast Al-B-Cu composites.

5.1.4 Superficial Rockwell Hardness and Vickers Microhardness

Figures 5.12 – 5.14 show the influence of the various centrifugal casting parameters on the measured hardness along the main axis of the centrifugally cast specimens. It is apparent that superficial hardness increases with the distance from the internal zone in the Al-2 wt. %B- 6 wt. %Cu composite. This trend is consistent with the trend observed in the plots of volume percent of reinforcement particles along the

Adelakin Kingsley Tunde, Masters Thesis, UPRM 2009

castings (figures 5.4, 5.7, 5.10). As in the Al-B-Mg composites, increasing all the centrifugal casting parameters resulted in the steady increase of hardness values along the Al-B-Cu composites. Nonetheless, at 60 mm measured hardness was not as high as that observed in the Al-B-Mg composites at the same distance. This could be as a result of particle segregation patterns observed in the plots of volume percent along the main axis of the centrifugally cast Al-B-Cu composites. In these plots, it was apparent that the high viscosity imposed by the alloying element (copper) could not permit a more pronounced redistribution of the reinforcement particles and, as a consequence, higher hardness values.

A detailed comparison among the produced specimens; i.e. 1b, 2b and 3b considering casting time is discussed. In figure 5.12, at 15 mm, specimen 1b with casting time of 1 minute revealed the maximum hardness values, followed by specimen 2b and specimen 3b. At 60 mm of the castings, specimen 3b shows the maximum and specimen 1b was observed to have the minimum hardness values. As previously mentioned, this profile is in conformity with the particle distribution pattern in the Al-B-Cu composites.

Figure 5.13 shows the effect of rotational speed for specimens 3b, 4b and 5b. The plots show that as the rotational speed increased from 300 rpm through 400 rpm, the hardness values at 15 mm decreased from 3b through 5b. Conversely, at 60 mm specimen 5b exhibited the maximum hardness value while 3b was observed to have the minimum hardness value.

To further establish the effect of the pouring temperature on the centrifugally cast Al-B-Cu composites in terms of hardness, figure 5.14 was examined. In these plots, at 60 mm, hardness was maximum for specimen 5b, followed by specimen 7b and then specimen 6b. This showed that as the pouring temperature increased, the hardness increased while the reverse is obtained at 15 mm of the castings. For all plots, the impact of pouring temperature proved to be more pronounced in this investigation both in terms of particles redistribution and hardness values along the castings than the casting time and rotational speed.

Adelakin Kingsley Tunde, Masters Thesis, UPRM 2009

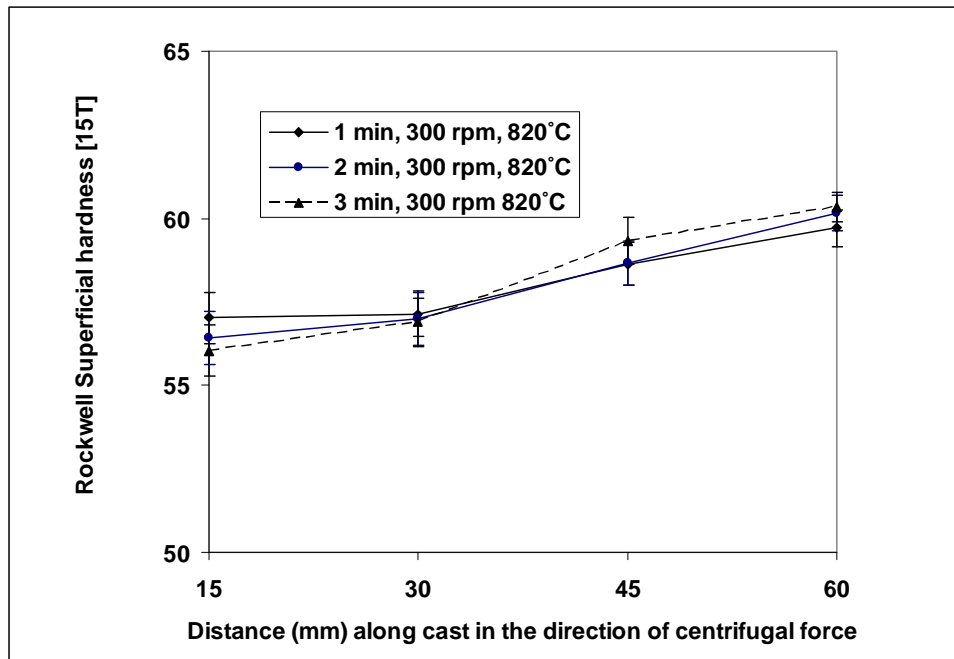


Figure 5.12 Effect of casting time on superficial Rockwell hardness along the longitudinal axis of the centrifugally cast Al-B-Cu composites.

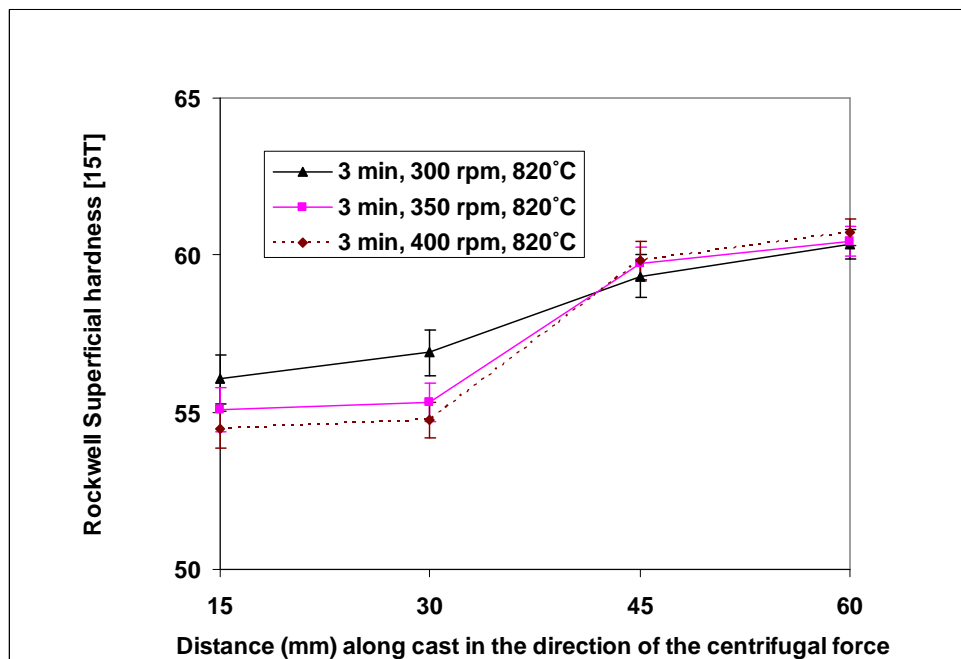


Figure 5.13 Effect of rotational speed on superficial Rockwell hardness along the longitudinal axis of the centrifugally cast Al-B-Cu composites.

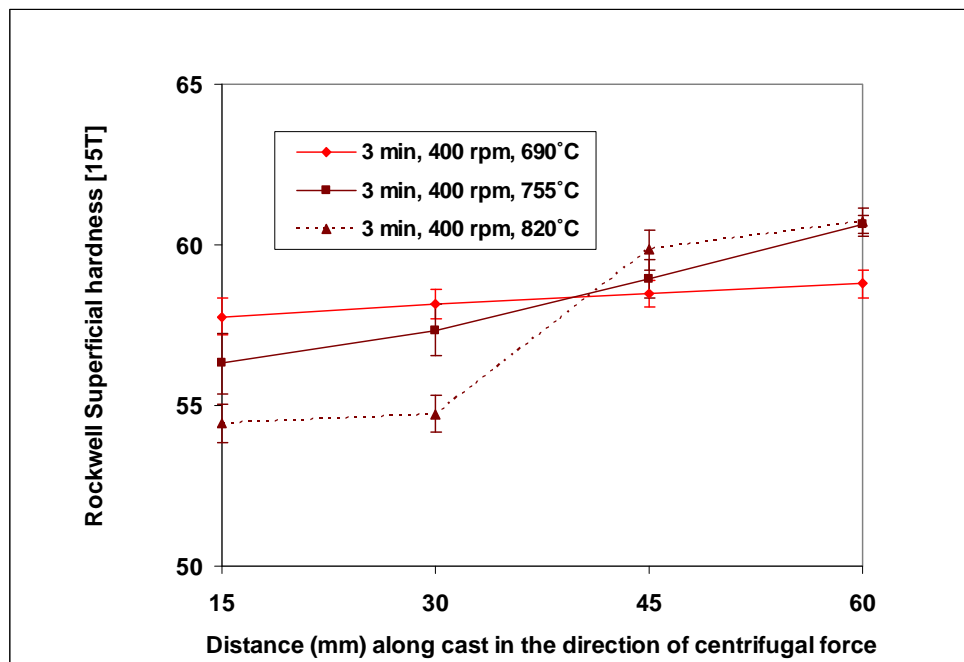


Figure 5.14 Effect of pouring temperature on superficial Rockwell hardness along the longitudinal axis of the centrifugally cast Al-B-Cu composites.

Microindentation was done on the matrix of the Al-B-Cu composites exclusively. Care was taken to avoid indenting the reinforcements. A total of 15 evenly spaced indentations were made on the matrix surface of each samples. An average Vickers microhardness value (HV_{25}) was then obtained.

The results of the Vickers microhardness measurement on the matrix of the Al-B-Cu composites are displayed in figures 5.15 through 5.17. The measured high hardness values could have been promoted by the presence of Al_2Cu phase on the matrix and probably by some influence of the reinforcement particles present in the surrounding matrix. Appreciable higher microhardness numbers were observed as the value of the centrifugal casting parameters increased. Nevertheless, these results bear the same trend along with the superficial Rockwell hardness recorded along the cast. The close

Adelakin Kingsley Tunde, Masters Thesis, UPRM 2009

resemblance in the hardness plots (figures 5.15 – 5.17) on the Al-B-Cu composites could have been as a result of an additional contribution from the Al_2Cu phase present in the composite matrix.

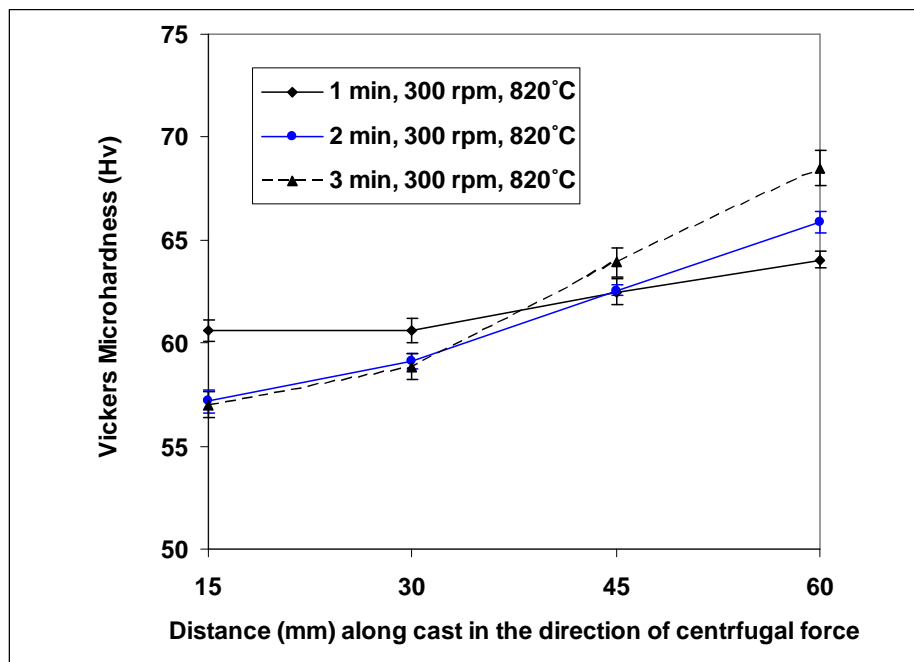


Figure 5.15 Effect of casting time on Vickers microhardness along the longitudinal axis of the cast Al-B-Cu composites.

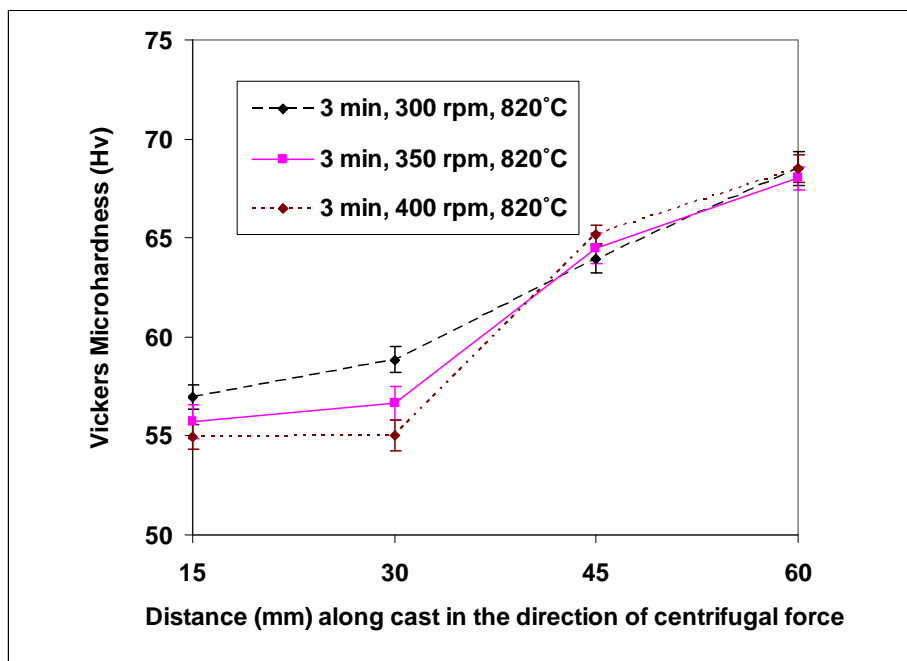


Figure 5.16 Effect of rotational speed on Vickers microhardness along the longitudinal axis of centrifugally cast Al-B-Cu composites.

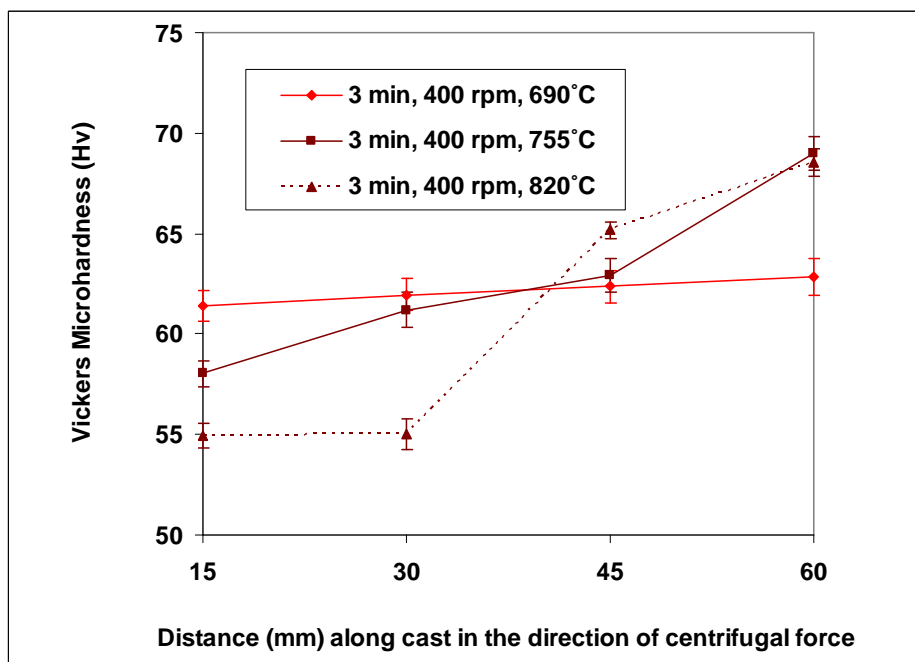


Figure 5.17 Effect of pouring temperature on Vickers microhardness along the longitudinal axis of centrifugally cast Al-B-Cu composites.

5.1.5 Particle size in the Al-B-Cu composites

The result from the analysis of particles size via Image J displayed a range of particles size from 4 μm to 40 μm , with an average of 19 μm . As shown on the micrographs of the Al- 2 wt.%B- 6 wt.%Cu composites, no marked variation in particles size along the longitudinal distance of cast was observed. It is obvious that the rotational speeds considered in the investigation did not cause turbulence which would have resulted in some breaking of the particles due to particles interaction with themselves and also with the wall of the mold. In some cases, the morphology of the decaboride became so irregular that estimation of those particles size was not possible.

6 COMPARISON BETWEEN FUNCTIONALLY GRADED Al-B-Mg AND Al-B-Cu COMPOSITES

6.1 *Complementary Tests*

The issue raised earlier in chapter four, on whether magnesium is favoring the phase transformation of the AlB_{12} particles into AlB_2 is being addressed at this point. However, there are two ways of addressing this question. One is by conducting complementary analysis with the aid of energy dispersive spectroscopy (EDS) on the compositionally graded material produced by the centrifugal casting method and the second one is by performing heat treatment analyses between room temperature and the highest melting temperature achieved during centrifugal casting.

6.1.1 Energy Dispersive Spectroscopy (EDS)/SEM Analysis on Al- 2 wt. %B- 6 wt. %Mg specimen

In the SEM image shown in figure 6.1, the reinforcement particles in the Al-2wt. %B-6wt. %Mg composites show difference in contrast and shapes. The dark, irregular in shape and larger aluminum dodecaboride particles are being surrounded by the more faceted aluminum diboride particles. This is quite different from what was observed in the micrograph of the non-solutionized and solutionized samples of the Al-7.2wt. %B master alloy as shown in this chapter. This shows that a phase transformation occurred, which resulted in a change in shape and sizes of reinforcement particles. A detailed X-ray dispersive spectroscopy analysis was done to attain the composition of (Al, B and Mg) on the composites.

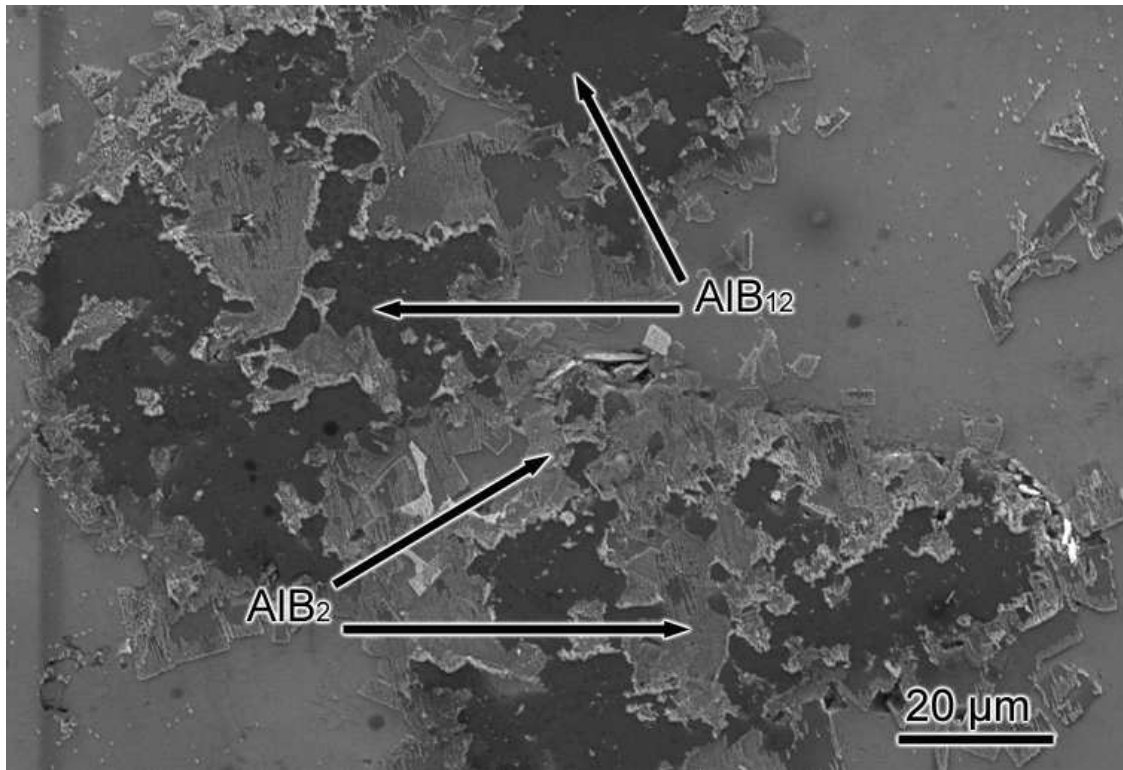


Figure 6.1 SEM image showing the morphology of the AlB₁₂ and AlB₂ particles in the functionally graded Al-B-Mg composite.

Figure 6.2 provides an overall idea of the result of the elemental mapping: distribution of the Al, B and Mg on the composite. Magnesium is evenly distributed in the matrix of the Al-B-Mg composite and also segregates more within the AlB₂ particles (spot 2) than any other part of the composite. This suggests that magnesium has a great affinity for aluminum diboride particles. However, within the AlB₁₂ particles (spot 1) magnesium is absent. As expected, boron signals are stronger in the AlB₁₂ (spot 1) than in the AlB₂ particles corroborating the nature of the diborides. Figures 6.3 a, b c d revealed the result of the EDS analysis on the Al-B-Mg composites, which allowed determining the elemental composition of both the matrix and the reinforcement particles.

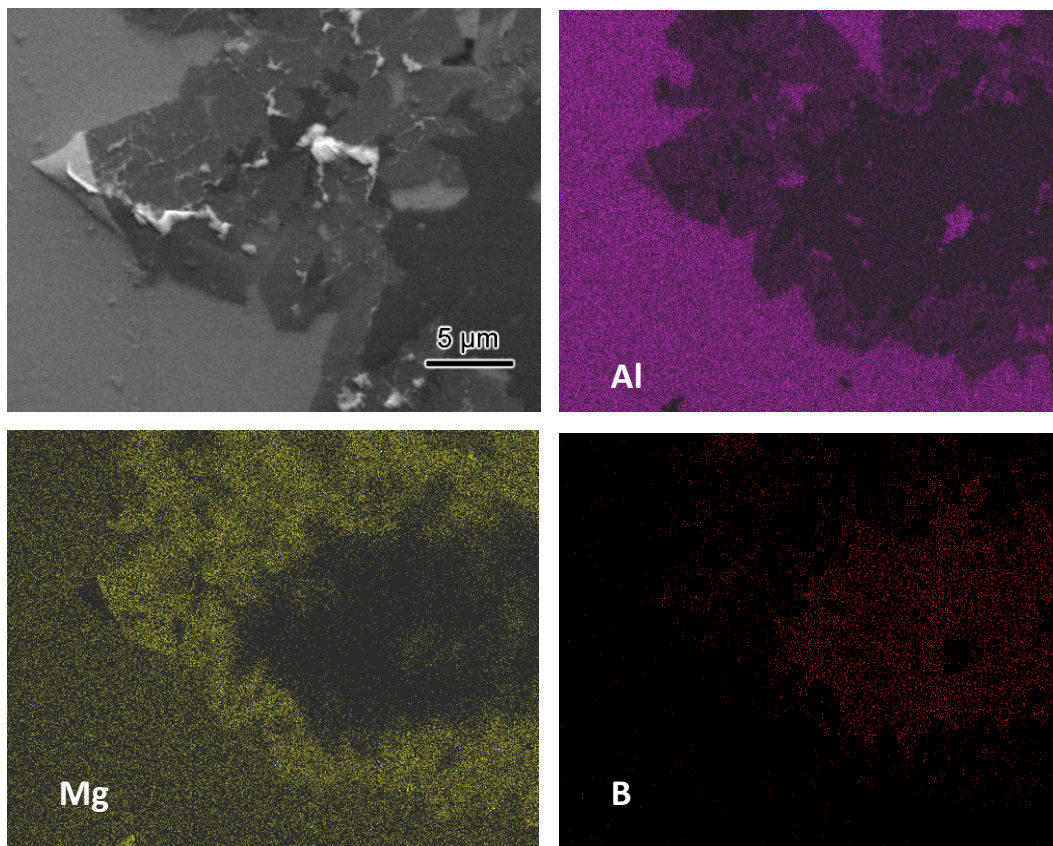
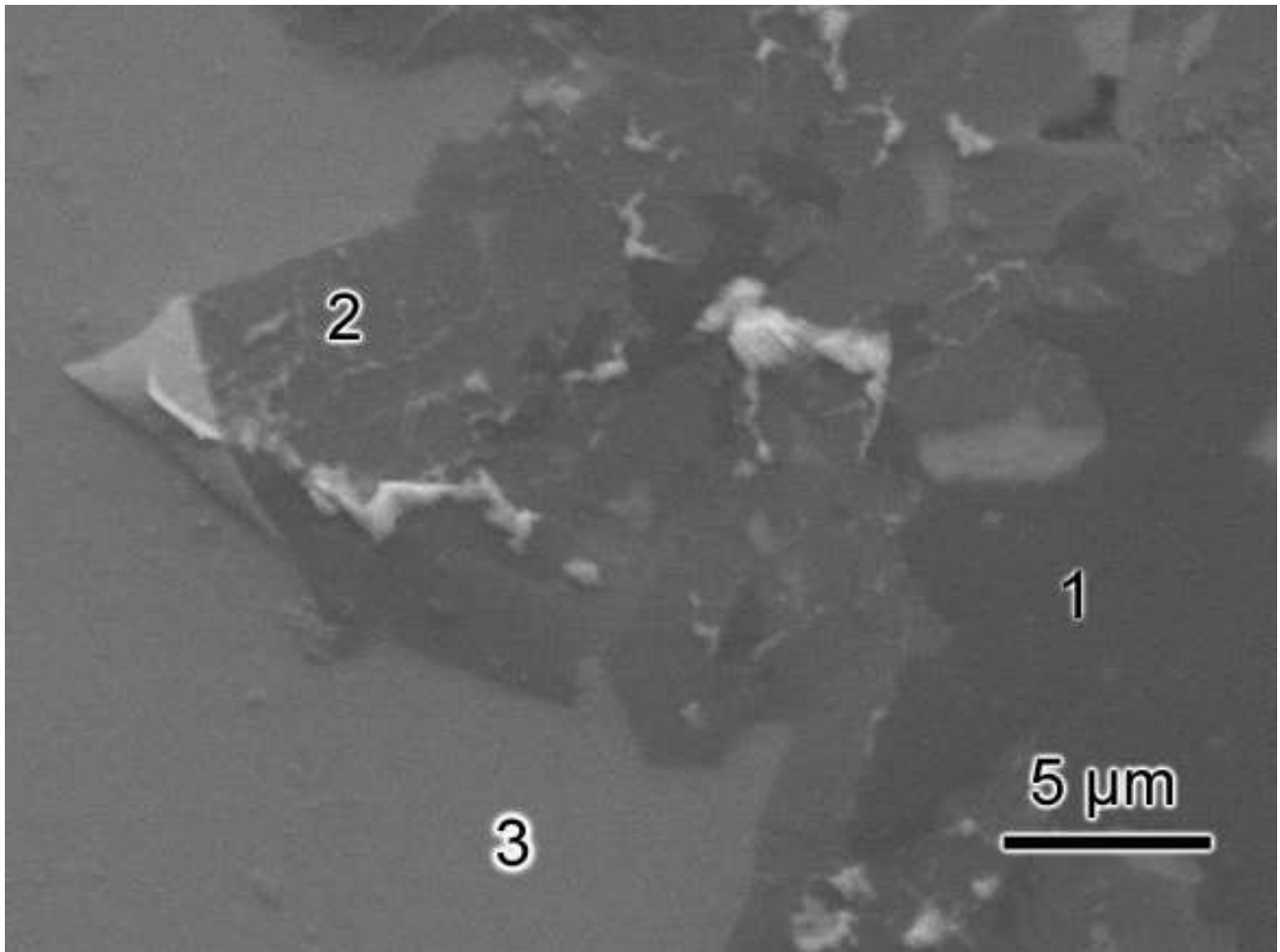


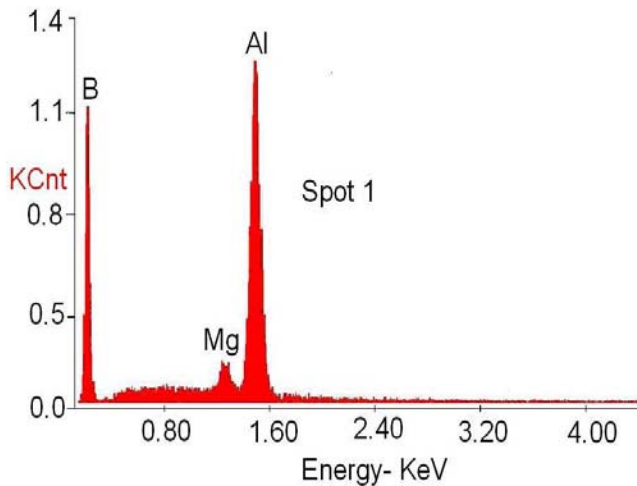
Figure 6-2 X-ray mapping of the Al-B-Mg composites (EDS).

The microstructure and the EDS spectra obtained on an Al-B-Mg composite are shown in figures 6.3 a, b, c. And d. This analysis was done on the AlB_{12} and AlB_2 particles and on the matrix of the composite. On a AlB_{12} particle (labeled 1) in figure 6.3 a, there is very low level of magnesium while, as expected, boron signal is stronger, higher than in the AlB_2 (labeled 2 in figure 6.3) as shown on the spectrum of fig. 6.3c. On the AlB_2 particle, magnesium content is higher than what is observed on the AlB_{12} particle. The analysis on the Al-B-Mg matrix also revealed the presence of magnesium. It should be noted that there is a much higher level of magnesium in the diboride particles than in the matrix. Oxygen observed on the spectrums of both AlB_2 particles and the matrix is normal as the borides oxidized upon processing. Naturally boron is not found on the matrix so the boron signal in the EDS spectrum of the matrix could be as a result of the subsurface boride particles.

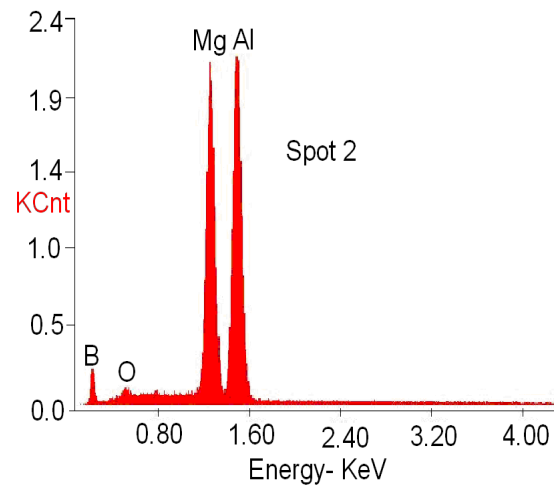


(a)

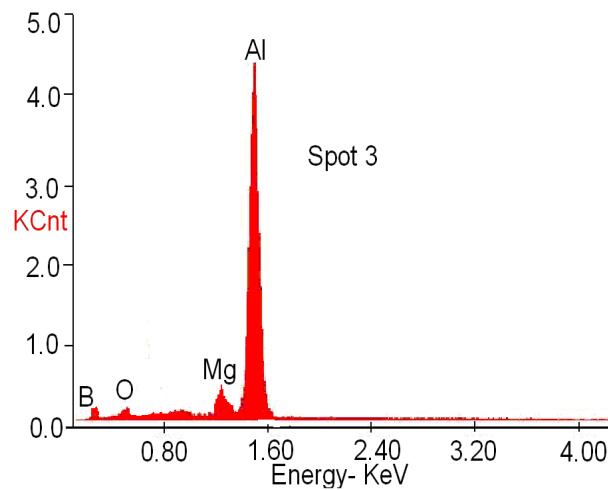
Adelakin Kingsley Tunde, Masters Thesis, UPRM 2009



(b)



(c)



(d)

Figure 6.3 EDS compositional analysis: (a) Backscattering electron image used to differentiate boride particles: AlB_{12} (labeled 1), AlB_2 (labeled 2), and the matrix of the Al-B-Mg composite (labeled 3); (b) EDS analysis on the AlB_{12} in spot 1; (c) EDS analysis on AlB_2 spot 2; and (d) EDS analysis on the Al-B-Mg matrix of the composite spot 3.

6.1.2 Energy Dispersive Spectroscopy (EDS)/SEM Analysis on Al- 2 wt. %B- 6 wt. %Cu Specimen

The SEM image in Figure 6.4 shows the particles present on the Al-2wt. %B-6wt. %Cu composite. The dark larger AlB_{12} particles are again observed along with the brighter Al_2Cu phase. Cu was not found in the reinforcement particles but were observed forming Al_2Cu near the reinforcement particles and along the grain boundaries of the matrix.

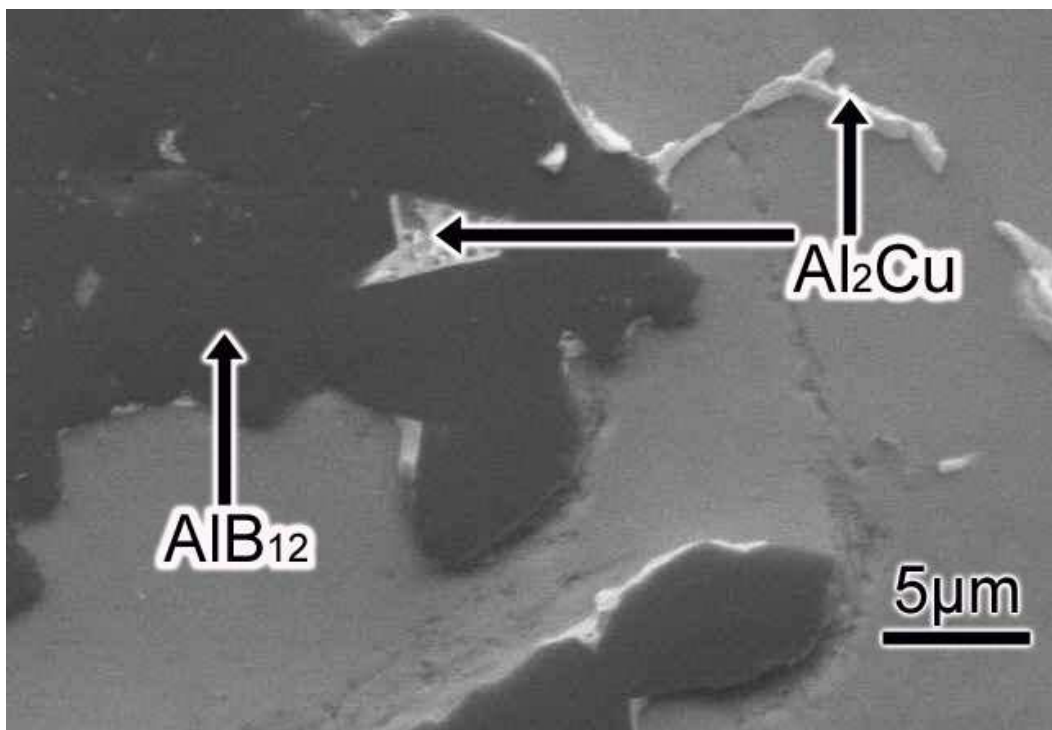


Figure 6.4 SEM image showing the morphology of the AlB_{12} particles and Al_2Cu phases on the functionally graded Al-B-Cu composite.

The EDS mapping of the Al-B-Cu composite in figure 6.5 shows higher concentration of copper on the Al_2Cu phase but not on the AlB_{12} particles. Copper is also present in the composite matrix. Boron is also present on the matrix of the composite but we believe that this could have been signal from subsurface boride particles.

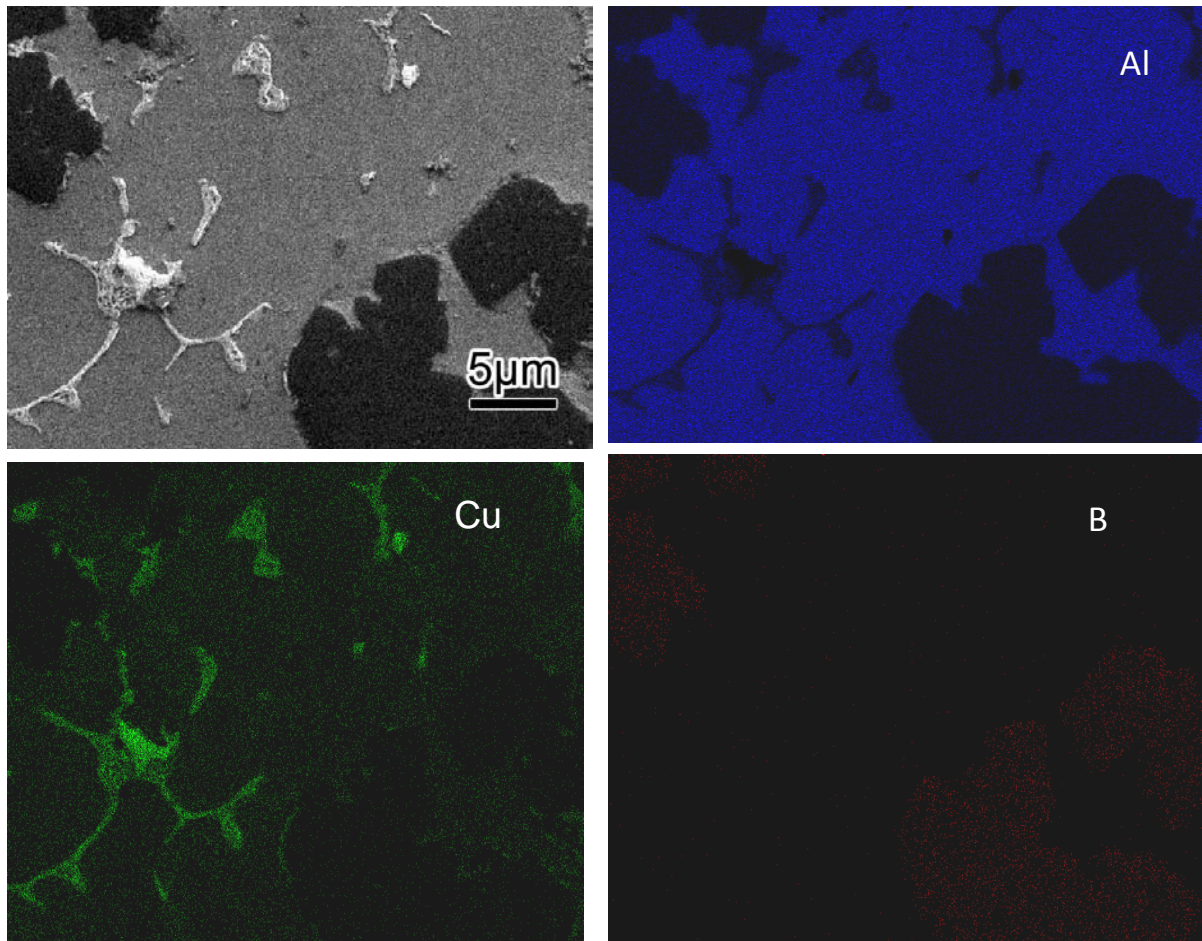
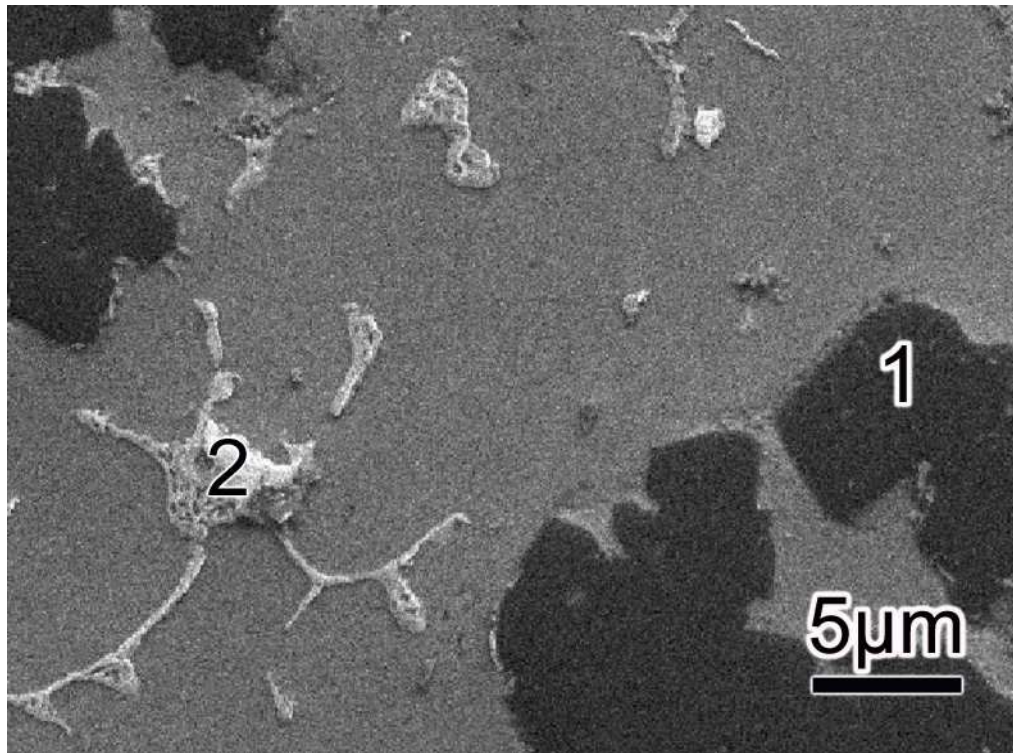
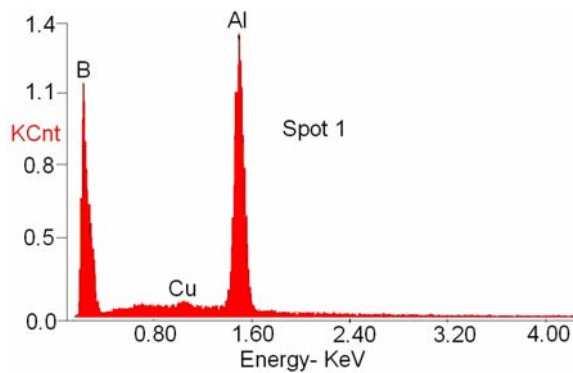


Figure 6.5 EDS mapping of the surface of the Al-B-Cu composites.

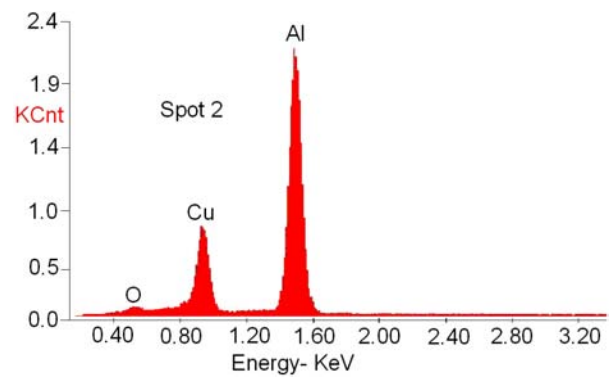
The EDS spectra on specific spots of the Al-B-Cu composite in figure 6.6a are shown in figures 6.6 b and c. As expected in the AlB_{12} particles the boron signal is very strong while there is a small amount of oxygen present. The Cu peak on the Al_2Cu phase corroborates the composition of this phase. There is some oxygen present on this spot. The matrix also shows traces of oxygen, boron and copper.



(a)



(b)



(c)

Figure 6.6 EDS compositional analysis: (a) Backscattering electron image displaying AlB_{12} particles (labeled 1), AlB_2 particles (labeled 2), and the matrix (labeled 3) of the Al-B-Cu composite; (b) EDS analysis on the AlB_{12} in spot 1; and (c) EDS analysis on AlB_2 spot.

Adelakin Kingsley Tunde, Masters Thesis, UPRM 2009

In order to clarify the issue related to the phase transformation of the Al-B phases observed in this thesis, a complementary experiment was deemed essential. Details of this experiment are discussed as follows.

The microstructure of the Al-7.2wt.%B master alloy (used to formulate the composites) is shown in figure 6.7a at room temperature. Micrographs of the Al-B annealed at 400°C and 850°C are also displayed in figures 6.7b and 6.7c respectively. It is evident that the Al-B phases present in this master alloy are predominantly AlB_{12} with very small amounts of AlB_2 . After annealing it is apparent that the AlB_{12} phase was still retained. It remains intact without any transformation due to the heat treatment. The higher temperature did not cause the transformation of the AlB_{12} phase found in the master alloy. This appears to corroborate literature information suggesting that the phase transformation occurs at higher temperatures above 900°C [36] (also shown on Al-B phase diagram).

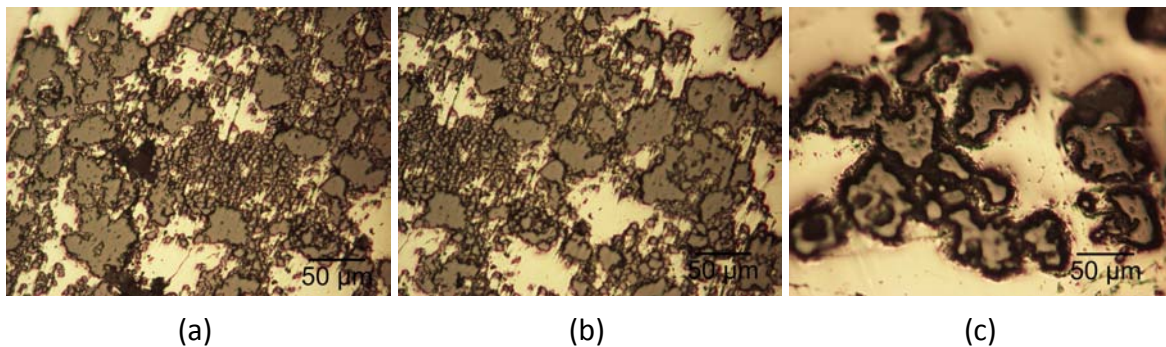


Figure 6.7 Micrographs of Al-B master alloy with various level of heat treatment: (a) As received at room temperature; (b) Annealed at 400°C; (c) Annealed at 850°C.

In summary, the EDS analyses showed the presence of some oxides in the matrix and on the reinforcement particles. They also suggest the formation of a ternary diboride $Al_xMg_{1-x}B_2$ instead of the AlB_2 particles in the Al-B-Mg composites, when magnesium is dissolved in the diboride. The results of the complimentary tests conducted on the Al-B master alloy, Al-B-Mg and Al-B-Cu composites, demonstrated the

Adelakin Kingsley Tunde, Masters Thesis, UPRM 2009

existence of the $Al_xMg_{1-x}B_2$ particles co-existing with the AlB_{12} particles due to the phase transformation cause by magnesium.

In this study, the presence of the Al_3Mg_2 phase (equilibrium phase in the Al-Mg phase diagram) in the Al- 2wt. %B- 6wt. %Mg composite has not been detected with the various characterization techniques employed. One would have expected the presence of Al_3Mg_2 in the composite considering the level of magnesium (6 wt. %) used in the production of the composite. In previous work [7] the presence of such phase was reported; in that research an Al-B composite containing 2 wt. % Mg was studied but the reinforcement particle used was AlB_2 . The formation kinetics of Al_3Mg_2 phase has been reported in literature to be very slow. Nevertheless, the absence of such intermetallic phases might be attributed to partly, the type of reinforcement used in the present study and the reaction kinetics in the composite system. It is likely that in the present composites the interaction of Mg with the AlB_{12} particles to form $Al_xMg_{(1-x)}B_2$ further depleted the matrix of dissolved Mg that would have favored the eventual formation of Al_3Mg_2 .

6.2 Viscosity Effects in the Cast Specimens

The change in melt viscosity affects the velocity with which a particle moves in such melt [44]. For example, if the initial velocity of a particle decreases due to lower temperature (as a result of cooling or temperature variation) or higher density (increase in effective fraction of particles), the fluidity of the melt then becomes affected. The implication is that, a drop in velocity with which the particle move is inevitable. Nevertheless, there is a need to corroborate that the viscosity of the semi-solid composite depends on the volume fraction of the reinforcement particles and the liquid.

In metal matrix composite casting the state of viscosity of the melt or semi-solid composite determines the ease with which the casting is fabricated. For instance addition of copper (denser than aluminum) (table 2.1) results in an increase in the density of the Al-B-Cu melt and, therefore, an increase in the viscosity of the composite

Adelakin Kingsley Tunde, Masters Thesis, UPRM 2009

melt. As a consequence, this resulted in the lack of a more pronounced segregation of the reinforcement particles in certain region of the Al-B-Cu casting.

Moreover, the addition of magnesium (table 2.1) to the Al-B composites tends lower the density of the molten aluminum matrix and, therefore, reduces the dynamic viscosity of that matrix. This could be associated with the direct relationship between viscosity and density [52] of the melt, which is favored by the high solubility of magnesium in liquid aluminum.

Tables 6.1 through 6.6 show the estimated apparent viscosities of the composites at different distances along the castings. The result clearly shows that the higher concentration of reinforcement particles along the castings resulted in higher viscosity values. This is demonstrated using equation 0-5 [5] to estimate the apparent viscosity of the composites:

$$\eta_{app} = \eta_c \left[1 + \frac{5}{2} V_f + 7.6 V_f^2 \right] \quad \text{Equation 6-1}$$

The value of viscosity of pure aluminum melt at 660°C (1.38 mPa-s) [53] was selected for the estimation of the apparent viscosity of the composites. The values of viscosity obtained at the inner zones (15 mm) are much higher for the Al-B-Cu composites than for the Al-B-Mg composites while at the outer periphery (60 mm), the values of viscosity for the Al-B-Cu are lower than those of Al-B-Mg composites. In summary, the viscosity of the composites seems to be the core factor that drives the movement of the particles as a result of density difference between the matrix melt and the reinforcements.

Table 6.1 Apparent viscosities of composites as a function of casting time along the casting of a functionally graded Al-B-Mg composite.

FUNCTIONALLY GRADED Al-B-Mg COMPOSITES	CENTRIFUGAL CASTING PARAMETERS	VISCOSITY (mPa-s) ALONG CAST			
		15 mm	30 mm	45 mm	60 mm
Specimen 1a	1 min, 300 rpm, 820°C	1.4071	1.4285	1.4474	1.5931
Specimen 2a	2 min, 300 rpm, 820°C	1.3829	1.4220	1.4590	1.8373
Specimen 3a	3 min, 300 rpm, 820°C	1.3839	1.3916	1.5115	1.7925

Table 6.2 Apparent viscosities of composites as a function of rotational speed along the casting of a functionally graded Al-B-Mg composite.

FUNCTIONALLY GRADED Al-B-Mg COMPOSITES	CENTRIFUGAL CASTING PARAMETERS	VISCOSITY (mPa-s) ALONG CAST			
		15 mm	30 mm	45 mm	60 mm
Specimen 3a	3 min, 300 rpm, 820°C	1.3839	1.3916	1.5115	1.7925
Specimen 4a	3 min, 350 rpm, 820°C	1.3835	1.3887	1.5400	1.8410
Specimen 5a	3 min, 400 rpm, 820°C	1.3807	1.3862	1.5787	1.9348

Table 6.3 Apparent viscosities of composite as a function of pouring temperature along the casting of a functionally graded Al-B-Mg composite.

FUNCTIONALLY GRADED Al-B-Mg COMPOSITES	CENTRIFUGAL CASTING PARAMETERS	VISCOSITY (mPa-s) ALONG CAST			
		15 mm	30 mm	45 mm	60 mm
Specimen 5a	3 min, 400 rpm, 820°C	1.3807	1.3862	1.5787	1.9348
Specimen 6a	3 min, 400 rpm, 755°C	1.4728	1.5348	1.5609	1.8035
Specimen 7a	3 min, 400 rpm, 690°C	1.5020	1.4989	1.5305	1.6248

Table 6.4 Apparent viscosities of composites as a function of casting time along the casting of a functionally graded Al-B-Cu composites.

FUNCTIONALLY GRADED Al-B-Cu COMPOSITES	CENTRIFUGAL CASTING PARAMETERS	VISCOSITY (mPa-s) ALONG CAST			
		15 mm	30 mm	45 mm	60 mm
Specimen 1b	1 min, 300 rpm, 820°C	1.5832	1.5876	1.5978	1.6107
Specimen 2b	2 min, 300 rpm, 820°C	1.5742	1.5787	1.6015	1.6201
Specimen 3b	3 min, 300 rpm, 820°C	1.5698	1.5765	1.6103	1.6248

Table 6.5 apparent viscosities of composite as a function of rotational speed along the casting of a functionally graded Al-B-Cu composite.

FUNCTIONALLY GRADED Al-B-Cu COMPOSITES	CENTRIFUGAL CASTING PARAMETERS	VISCOSITY (mPa-s) ALONG CAST			
		15 mm	30 mm	45 mm	60 mm
Specimen 3b	3 min, 300 rpm, 820°C	1.5698	1.5765	1.6103	1.6248
Specimen 4b	3 min, 350 rpm, 820°C	1.5613	1.5675	1.6131	1.6295
Specimen 5b	3 min, 400 rpm, 820°C	1.5565	1.5609	1.6154	1.6927

Table 6.6 Apparent viscosities of composites as a function of pouring temperature along the casting of a functionally graded Al-B-Cu composite.

FUNCTIONALLY GRADED Al-B-Cu COMPOSITES	CENTRIFUGAL CASTING PARAMETERS	VISCOSITY (mPa-s) ALONG CAST			
		15 mm	30 mm	45 mm	60 mm
Specimen 5b	3 min, 400 rpm, 820°C	1.5565	1.5609	1.6154	1.6927
Specimen 6b	3 min, 400 rpm, 755°C	1.5751	1.5882	1.6061	1.6309
Specimen 7b	3 min, 400 rpm, 690°C	1.5923	1.5946	1.5969	1.6061

6.3 Hardness values

The trend in hardness observed on both types of composites is as a reflection of the compositional gradient. A detailed comparison of the hardness values between the two composites along the casting, particularly at 15 mm and 60 mm are discussed. At 15 mm the Al-B-Mg composites hardness values are lower than in the Al-B-Cu composites for the same casting parameters (casting time, rotational speed and pouring temperature of the melt). Conversely, at 60 mm, the hardness values of the Al-B-Mg composites are higher than that of the Al-B-Cu composites for the same casting parameters.

Additionally, it was observed that the range of superficial 15T Rockwell hardness in the Al-B-Mg composites along the main axis of the castings varied widely, from 40.02 to 78.76. The range of 15T hardness values measured along the Al-B-Cu composite castings was: 54.45 – 60.72.

Table 6.7 presents 3-dimensional plots of the experimental data points of the superficial Rockwell hardness values as a function of centrifugal casting parameters along centrifugal force direction of castings (Al-B-Mg and Al-B-Cu composites) and their linear regression model.

SR = superficial Rockwell hardness, CT = Casting time, D = Distance along cast, S = Rotational speed of mold and T = pouring temperature of melt.

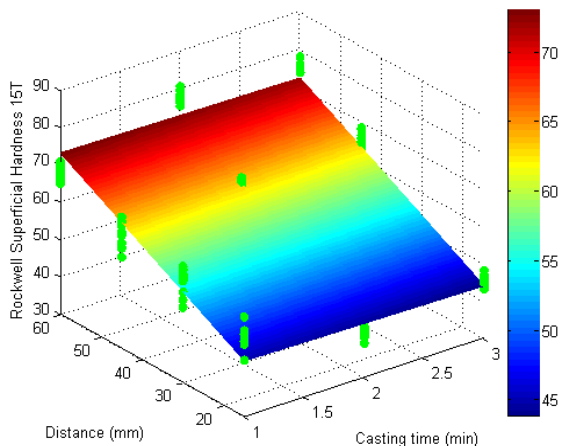
Table 6.7 3-Dimensional plots of experimental data

Functionally graded Al-B-Mg composites

Linear regression model:

$$SR = 36.0344 - 0.51 * CT + 0.6246 * D$$

$$R^2 = 0.916533$$

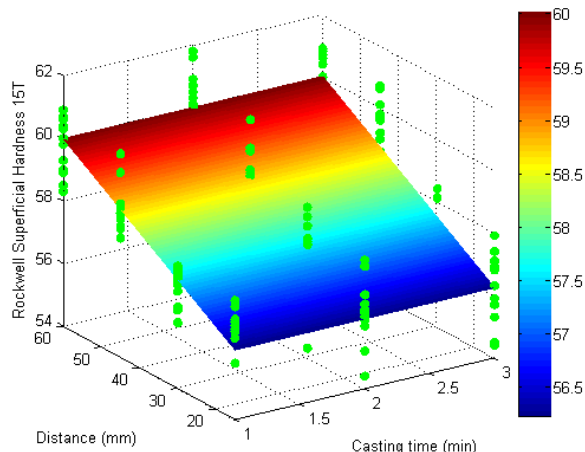


Functionally graded Al-B-Cu composites

Linear regression model:

$$SR = 54.9506 + 0.0108 * CT + 0.0838 * D$$

$$R^2 = 0.710651$$

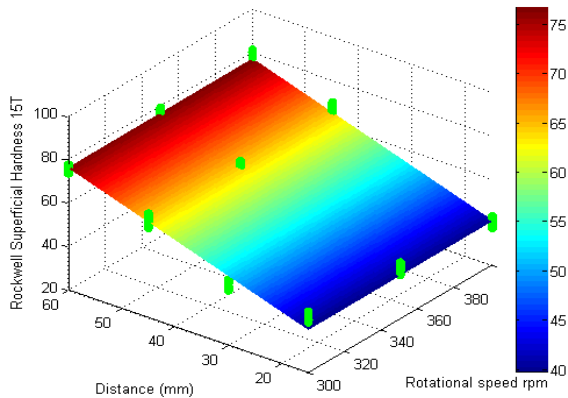


Effect of casting time

Linear regression model:

$$SR = 26.3259 + 0.0046 * S + 0.8078 * D$$

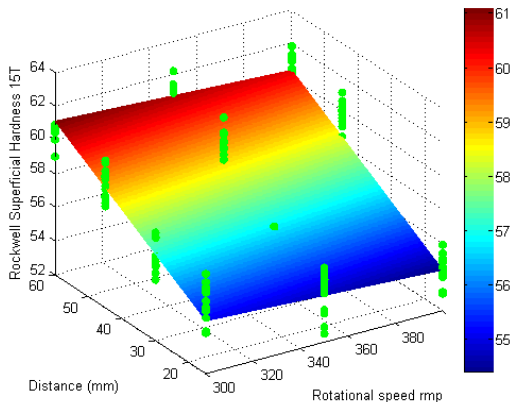
$$R^2 = 0.949874$$



Linear regression model:

$$SR = 55.2622 - 0.0071 * S + 0.1327 * D$$

$$R^2 = 0.780440$$



Effect of rotational speed

Linear regression model:

$$SR = 33.2129 + 0.0081 * T + 0.5176 * D$$

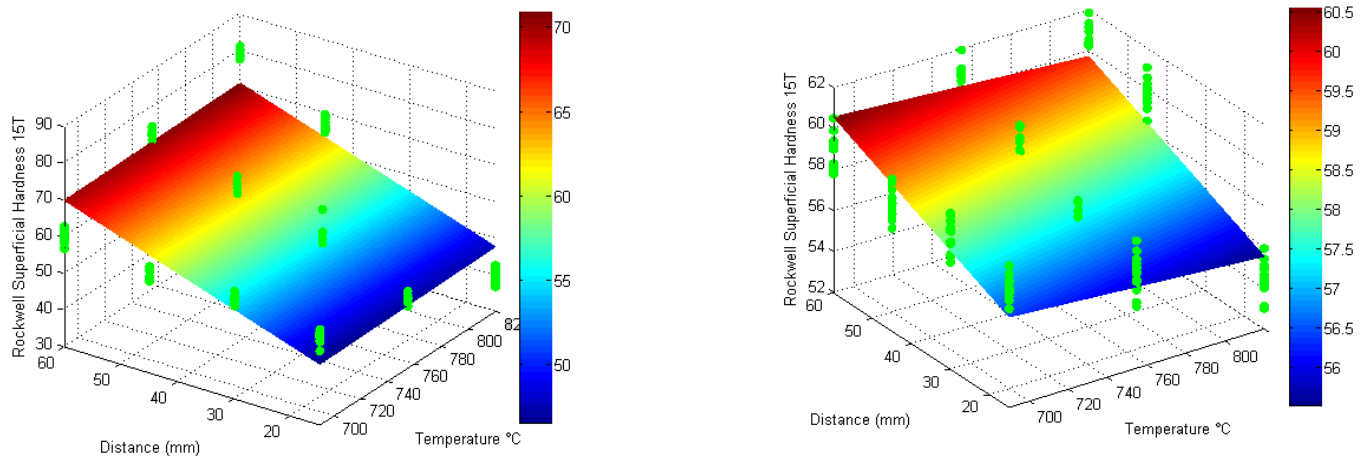
$$R^2 = 0.948375$$

Linear regression model:

$$SR = 59.636 - 0.0067 * T + 0.0924 * D$$

$$R^2 = 0.788615$$

Adelakin Kingsley Tunde, Masters Thesis, UPRM 2009



Effect of pouring temperature

As a concluding remark on the effect of the casting parameters (casting time, rotational speed and pouring temperature) on the redistribution of the reinforcement particles during centrifugal casting of both the Al-B-Mg and Al-B-Cu composites, the impact of the pouring temperature was the most significant parameter affecting the redistribution of reinforcement particles followed by the effect of the casting time. While the rotational speed appears to be the least influential parameter in this investigation. This trend is also observed on the hardness values of the composites. The introduction of the effect of viscosity could be tied to the dispersion of data obtained in the Al-B-Cu composite melts.

7 CONCLUSIONS AND SUGGESTIONS FOR FUTURE WORKS

7.1 *Conclusions*

- (1) A centrifugal casting methodology for the production of functionally graded aluminum based metallic matrix composites was successfully developed.
- (2) Results obtained from this centrifugal casting method show that this technique is able to produce functionally graded aluminum matrix composites with different chemical compositions (Al-B-Mg and Al-B-Cu) reinforced with co-existing aluminum diboride and aluminum dodecaboride particles.
- (3) It was observed that the magnesium addition aided the transformation of the AlB_{12} particles into AlB_2 reinforcement particles. This phase transformation is further enhanced by the various casting parameters. The AlB_2 particles tend to segregate more effectively at the external zone of Al-B-Mg centrifugal castings under the optimum value of the centrifugal casting parameters considered in this investigation.
- (4) For the Al-B-Mg specimens magnesium diffused into the AlB_2 to form a ternary diboride $Al_xMg_{1-x}B_2$.
- (5) In the Al-B-Cu specimens copper did not form any ternary compound with the dodecaboride.
- (6) The steepest compositional gradient observed at the external zone (60 mm) in this work came from the Al-B-Mg composites. While the steepest compositional gradient at the 15 mm is from the Al-B-Cu composites. This corroborated the Mg effect on the melt viscosity at various operating temperatures due to its high solubility level in the aluminum melt.
- (7) Mechanical properties such as superficial hardness and microhardness of both functionally graded Al-B-Cu and Al-B-Mg composites are influenced by the

Adelakin Kingsley Tunde, Masters Thesis, UPRM 2009

microstructure gradient. In effect, higher volume amount of reinforcement particles resulted in larger hardness values measured along the main axis of the cylindrical castings.

- (8) The calculated viscosity of the composites helped explain some discrepancies observed in the expected distribution of particles along the main axis of the centrifuged specimens.
- (9) The difference in volume percent of particles obtained between the 15 mm and 60 mm distances of the Al-B-Cu specimens was lower compared to those measured at the same distances in the Al-B-Mg specimens.
- (10) Reinforcement particles morphology (sizes of particles) distribution as a function of the centrifugal casting parameters along cast specimens (Al-B-Mg) during transformation of AlB_{12} into AlB_2 was very difficult to study due to the irregular shape of the dodecaborides that decomposed and also due to the fact that some of the AlB_{12} particles were observed to be attached to some of the AlB_2 particles.
- (11) SEM/EDS analysis demonstrated the affinity of magnesium towards AlB_2 particles. Also this characterization technique revealed that both copper and magnesium did not dissolve in the AlB_{12} particles.
- (12) A qualitative model for the transformation kinetics of the AlB_{12} particles into AlB_2 particles during centrifugal casting was proposed.

7.2 Suggestions for future work

- (1) This study has been able to manufacture aluminum-boron-magnesium and aluminum-boron-copper composites reinforced with AlB_{12} and AlB_2 , and AlB_{12} and Al_2Cu respectively. However, it is desirable to measure more accurately the solidification rate, cooling rate and direct measurement of viscosity for a better monitoring of the mechanical properties of the composites for different applications. Therefore, it is recommended the use of directional solidification technique for the fabrication of the mentioned composites.
- (2) A thermal characterization technique such as differential scanning calorimetry (DSC) analysis is proposed. DSC analysis would furnish information on heat of transformation of phase heat capacity and the transformation kinetics of phases aided by the addition of magnesium, such as AlB_{12} into AlB_2 as found in the Al-B-Mg composites. DSC could also be employed to provide in-depth understanding of metastable phase transformation as they appear during centrifugal casting of Al-B-Cu composites.
- (3) To further understand the mechanical behavior of the fabricated composites it is recommended to perform impact, tensile, wear and fatigue test of these composites.
- (4) Determination of the kinetics of phase transformation of the AlB_{12} into AlB_2 via the addition of magnesium through numerical modeling is suggested.
- (5) X-ray diffraction could help study the crystal structure of AlB_2 , AlB_{12} and Al_2Cu in the composites.

8 REFERENCES

- [1] Fukui, Y. Fundamental Investigation of Functionally Graded Materials Manufacturing System using Centrifugal Force. *JSME Int. J Series III* 1991, 34, 144-148.
- [2] Lajoie, L.; Suery, M. In *Cast Reinforced Metal Composites*: S. G. Fishman, A. K. Dhingra, Proceedings of the International Symposium on Advances in Cast Reinforced Metal Composites, Chicago, USA, 1988, 15-20.
- [3] Suárez, O. M. Mechanical Properties of a Novel Aluminum-Boron Composite Containing Boron. *Journal of Mechanical Behavior Materials* 2001, 12, 225-237.
- [4] David, R. *Handbook of Chemistry and Physics*, CRC press, Boca Raton, FL, 1998, 185-189.
- [5] Higashi, I. Crystal Chemistry of α -AlB₁₂ and γ -AlB₁₂. *Journal of Solid State Chemistry* 2000, 154, 168 – 176.
- [6] Rai, A.; Lee, D.; Park, K.; Zachariah, M. R. Important of Phase Change of Aluminum in Oxidation of Aluminum. *Journal of Physical Chemistry* 2004, 108, 14793-95.
- [7] Melgarejo, Z. H.; Suárez, O. M.; Sridharan, K. Microstructure and Properties of Functionally Graded Al-Mg-B Composites Fabricated by Centrifugal Casting. *Composites A: Applied Science and Manufacturing* 2008, 39A, 1150–1158.
- [8] Rodriguez-Castro, R.; Wetherhold, R. C.; Kelestemur, M. H. Microstructure and Mechanical Behavior of Functionally Graded Al-A359/SiCp Composite. *Journal of Materials Science A* 2002, 323, 445-456.
- [9] Tunde. K. A.; Suarez, O. M.; Gutierrez, G. "Influence of Centrifugal Casting Processing Parameters on the Distribution of Reinforcement Particles in Aluminum Matrix Composites". *Supplemental Proceedings: Volume 2: Materials Characterization, Computation and Modeling (The Minerals, Metals and Materials Society)*, 137th Annual Meeting and Exhibition. TMS 2008, 2, 99-104.

Adelakin Kingsley Tunde, Masters Thesis, UPRM 2009

- [10] Tetsuro, O.; Yoshimi, W.; Hisashi, S.; Ick-Soo, K.; Fukui, Y. Theoretical Study on Fabrication of Functionally Graded Materials with Density Gradient by a Centrifugal Solid-particles Method. *Composites* 2006, 37, 2194-2200.
- [11] Kang, C. G.; Rohatgi, P. K. Transient Thermal Analysis of Solidification in a Centrifugal Casting for Composite Materials Containing Particle Segregation. *Metallurgical and Materials Transactions B* 1996, 27B, 277-285.
- [12] Duschanek H.; Rogl, P. The Al-B (Aluminum – Boron) system. *Journal of Phase Equilibria* 1994, 15, 543-551.
- [13] Hirai, T. Functional Gradient Materials. *Processing of Ceramics*, Richard J. Brook, et al., eds, Weinheim, New York, NY, 1996, 17B, 293-341.
- [14] Andrew, R.; Sun, D. Functionally Graded Materials (FGMs) and their Production Methods. *The AZO Journal of Materials* online 2000-2008.
- [15] Suresh, S.; Mortensen, A. *Fundamentals of Functionally Graded Materials: Processing and Thermo-Mechanical Behaviors of Graded Metals and Metal-Ceramics Composites*. IOM Communications Ltd: London, 1998.
- [16] Miyamoto, Y. W. A.; Rabin, B. H.; Kawasaki, A.; Ford, R. G. *Functionally Graded Materials: Design, Processing and Applications*. Kluwer Academic Publisher: Boston, 1999.
- [17] Jeong. H.; Paulino, G. H. The Interaction Integral for Fracture of Orthotropic Functionally Graded Materials: Evaluation of stress intensity Factors. *International Journal of Solid and Structures* 2003, 40, 3967-4001.
- [18] Kieback, B.; Neubrand, A.; Riedel, H. Processing techniques for functionally graded materials. *Materials Science and Engineering A* 2003, A362, 81–105.
- [19] Gasik, M. Micromechanical Modeling of Functionally Graded Materials. *Computational Materials Science* 1998, 13, 42-55.
- [20] Neubrand, A.; Rodel, J. Gradient Materials: An Overview of a Novel Concept, *Zeitschrift für Metallkunde* 1997, 88, 358-371.
- [21] Dragana, J. I. Self Formed Cu-W Functionally Graded Materials Created via Power Segregation. *Universidad des Saarlandes. Master of Science Thesis* 2007.

Adelakin Kingsley Tunde, Masters Thesis, UPRM 2009

- [22] Schoutens, J. E.; Tempo, K. Introduction to Metal Matrix Composite Materials. DOD Metal Matrix Composite Information Analysis Center, 1982.
- [23] Emila, P.; Dipak, M.; Mehrotra, S. P. Mathematical Modeling of Particle Segregation during Centrifugal Casting of Metal Matrix Composites. Metallurgical and Materials Transactions A 2006, 37A, 1675-1687.
- [24] Materials for Metal Matrix Composites 2007 <<http://www.acgroupinc.com>>.
- [25] Design of Metal Matrix Composites 2007 <<http://www.composites-by-design.com/metal-matrix.htm>>.
- [26] Melgarejo, Z. H. Fabrication and Characterization of Functionally Graded Al/AlB₂ Matrix Composites for High Wear Aerospace Applications Using Centrifugal Casting. University of Puerto Rico, Mayaguez, Master of Science Thesis 2006.
- [27] Srivatsan, T. S.; Ibrahim, I. A.; Mohammed, F. A.; Lovernia, E. J. Processing Techniques for Particle – reinforced Metal Aluminum Matrix Composites. Journal of Materials Science 1991, 26, 5965–5978.
- [28] Xia, X.; McQueen, H. J.; Zhu, H. Fracture Behavior of Particle Reinforced Metal Matrix Composite. Applied Composite Materials 2002, 17–31.
- [29] Altinkok, N.; Demir, A.; Ozsert, I. Processing of Al₂O₃/SiC Ceramic Cake Preforms and their Liquid Al melt Infiltration. Composites 2003, 34A, 577–582.
- [30] Zhou, W.; Xu, Z. M. Casting of SiC Reinforced Metal Matrix Composites. Journal of Materials Processing Technology 1997, 63, 358– 63.
- [31] Pai, B. C.; Geetha, R.; Pillai, R. M.; Satyanarayana, K. G. Role of Magnesium in Cast Aluminum Alloy Matrix Composites. Journal of Materials Science 1995, 30, 1903 - 1911.
- [32] Geng, L.; Yao, C. K. SiC – Al Interface Bonding Mechanism in a Squeeze Casting SiC/Al Composite. Journal of Materials Science Letters 1995, 14, 606–608.
- [33] Xiaoming, W. The Formation of AlB₂ in an Al-B Master Alloy. Journal of Alloys and Compounds 2005, 403, 283-287.
- [34] Boron Minerals, Boron Information and Boron Properties 2007. <http://www.mineralszone.com/minerals/boron.html>.

Adelakin Kingsley Tunde, Masters Thesis, UPRM 2009

- [35] Totten. G. E.; Mackenzie, D. S.; Dencker, M. Physical Metallurgy and Processes Handbook of Aluminum Inc, New York, 2003, 77, 339
- [36] Murray, J. L. The Al-Mg System: National Bureau of Standards. Bulletin of Alloy Phase Diagrams 1982, 3, 1.
- [37] Sandra, R. P. T. Studies on Directional and Rapid Solidification of Al-B-Cu Composites. University of Puerto Rico, Mayaguez, Master of Science Thesis 2007.
- [38] Van Horn, K. R. (Ed.). Aluminum Copper Phase Diagram. American Society for Metals 1967, 372.
- [39] Gao, J. W.; Wang, C. Y. Modeling the Solidification of Functionally Graded Materials by Centrifugal Casting. Materials Science and Engineering A 2000, A292, 207-215.
- [40] Ho, J.; Lavernia, E. J. Thermal Residual Stresses in Functionally Graded and Layered 6061 Al/SiC. Metallurgical Materials Transactions A 1996, 27A, 3241-3249.
- [41] Watanabe, Y.; Fukui, Y. Microstructures and Mechanical Properties of Functionally Graded Materials Fabricated by a Centrifugal Casting Method (Review), Recent Research Developments in Metallurgical and Materials Sciences 2000, 4, 51-93.
- [42] Watanabe, Y.; Fukui, Y. In Current Issues on Multidisciplinary Microscopy Research and Education, eds A. Mendez-Vilas and L. Labajos-Broncano, FORMATEX, Badajoz 2004, 189.
- [43] Bonollo, F.; Moret, A.; Galo, S.; Mus, C. Cylinder liners in Aluminum Matrix Composite by Centrifugal Casting. La Metallurgia Italiana 2004, 6, 49-55.
- [44] Brinkman, H. C. The Viscosity of Concentrated Suspensions and Solutions. Journal of Chemistry and Physics 1952, 20, 571-581.
- [45] Yunudu, A. C. Heat Transfer: A Practical Approach, Second Edition, Published by McGraw-Hill New York, NY, 2003, 209–220.
- [46] DoITPoMS Teaching and Learning Packages 2008.
<<http://www.doitpoms.ac.uk/tlplib/casting/printall.php>>.
- [47] ASM: Metals Handbook, 9th ed., Vol. 9, Metallography and Microstructures, American Society for Metals, 1985: p. 124.

Adelakin Kingsley Tunde, Masters Thesis, UPRM 2009

- [48] Roger .I. Tanner. Engineering Rheology, 2nd Edition; Oxford Engineering Science Series: New York, 2000, 52-55.
- [49] Rajan, T. P. D.; Pillai, R. M.; Pai, B. C. Functionally Graded Al-Al₃Ni in situ Intermetallic Composites: Fabrication and Microstructural Characterization. Journal of Alloys and Compounds 2008, 453, L4-L7.
- [50] Assael, M. J.; Kakosimos, K. B. R.; Michael, B. J. E.; Quested, P. N.; Mills, K. C.; Nagashima, A. S. Y.; Wakeham, W. A. Reference Data for the Density and Viscosity of liquid Aluminum and Iron. Journal of Physical and Chemical Reference Data 2006, 35, 285-300.
- [51] Watanabe. Y.; Yamanaka, N.; Fukui, Y. Fukui, Control of Composition Gradient in a Metal-Ceramic Functionally Graded Material Manufactured by The Centrifugal Method. Composites Part A 1998, 29A, 595-601.
- [52] Wang, Y.; Wu, Y.; Bian, X. Composition Dependence of Viscosity for Al(1-X)Mg(0≤x≤0.10) Alloys. Chinese Science Bulletin 2007, 52, 1441 – 1445.
- [53] Dindsdale, A. T.; Quested, P. N. The Viscosity of Aluminum and its Alloy – a Review of Data and Models. Journal of Materials Science 2004, 39, 7221-7228.